MSc Mechanical Engineering - Design & Manufacturing

Effects of Er and Eu addition on the fluidity of an A356 alloy in an improved permanent fluidity test mold

J. Veenhuis

FOSECO

October 2024

Department of Design,
Production and Management
Faculty of Engineering Technology

Graduation committee:
dr. ir. T. Vaneker
dr. D. Jafari
dr. F. Liu
dr. D. Dispinar

UNIVERSITY OF TWENTE.

Contents

Abstract

Due to electrification of the automotive industry, the structural parts of cars need to be lighter to achieve the highest possible range on a single battery charge. Therefore, more car manufacturers are turning to aluminum castings to achieve complex high-volume parts with excellent performance at a lower mass. Aluminum has only good mechanical properties when alloyed, with example, Si, Mg, Zn, Cu, Mn. To further increase mechanical properties, the microstructure can be altered by grain refinement of the primary Al matrix and/or modification of secondary eutectic phases of Si. Ti and B are efficient grain refiners and are widely used in industry. For modification of the eutectic Si phase, Sr and Na are used. Recently, more research has been conducted on the addition of rare earth elements to increase the performance of grain refinement and/or modification of the eutectic Si. Er and Eu are potent grain refiner and modifier, respectively. However, it is known that the castability of an alloy can differ greatly when grain refiners and/or modifiers are introduced to the melt. In gravity and low-pressure die casting, castability is often limited by fluidity, especially in thin-walled castings. Therefore, this study focuses on investigating the effects of the addition of Er and Eu on the fluidity of a common foundry alloy A356.

To this end, all the parameters that influence the fluidity have been investigated. From which two improved permanent fluidity test molds have been designed to minimise the variability in the input parameters such that the addition of Er and Eu is the only variable. These molds have been produced and fluidity experiments have been conducted on four compositions; the base alloy (A356), 0.1wt% Er, 0.2wt% Eu and 0.1wt% Er + 0.2wt% Eu addition. Lastly, the microstructure of the samples have been investigated to see the influence of these additions to the microstructure of the alloy and explain the results obtained by the fluidity tests.

The results show no statistically significant in- or decrease in fluidity after the addition of Er and/or Eu to the A356 base alloy. From the results of the reduce pressure test samples, taken before and after the trials, it was found that the melt cleaning treatment was not successful resulting in extremely poor melt quality (bifilm index $>$ 200mm). The bifilm index was found to decrease during the trials, which was not expected. Moreover, Er was unable to grain refine the microstructure, which was attributed to the nucleation of Er on the oxide bifilms which settled to the bottom of the crucible, disabling the $ErAl_3$ as heterogeneous nucleation sites and simultaneously cleaning the melt. After examination of the microstructure of the castings it was found that the eutectic Si of the base alloy was already modified before any addition, which could not be explained by the knowledge currently present in the field. However, the eutectic could be modified even further when Eu was added to the melt, the fluidity decreased, but the effect remained minimal. A Gage R&R study was conducted on the mold and test procedures and it was found that they are capable of measuring fluidity in a repeatable and reproducible way.

Keywords: Fluidity, Erbium, Europium, Melt cleanliness, Grain refinement, Modification, Intermetallics, Permanent mold, Gage R&R

1. Introduction

Aluminum is the most abundant metal in the world, accounting for 8.2% of the earth's crust. It is mostly found in its more stable oxide forms. When purified, it possesses great properties that make it very suitable for industrial use, especially when alloyed. Such as being lightweight, electrical and thermally conductive, corrosion resistant, malleable and has high specific strength and stiffness [1]. Furthermore, aluminum is good castable which makes it suitable for complex shapes and/or large production volumes. Therefore aluminum castings can be readily found in the automotive and aerospace industry [2, 3].

Aluminum is already widely alloyed with Cu, Si, Mg, Zn and Sn. To further increase the mechanical properties of the alloy grain refiners and/or modifiers of eutectic Si can be used. Grain refiners increases the number of grains and thus decrease grain size which improves the strength of the material. Modifiers of eutectic Si change the morphology of eutectic Si from sharp platelets, which act as stress concentrations, to a more finer fibrous structure, which enhances the ductility of the material. In industry, Ti and B are widely used as grain refiners and Sr and Na as modifiers [4, 5].

The increasing demand for cost-effective solutions in the automotive and aerospace industries has led to the search for better grain refiners and modifiers. Lately, research has been conducted on the addition of rare earth elements (REE) to aluminum foundry alloys, to increase the grain refinement and/or modification efficiency. More efficient grain refiners and/or modifiers mean that less needs to be used, which could provide a more cost-effective solution. It was found that the REE scandium (Sc) is a very potent grain refiner but is not widely used because of its high cost. Er is also found to have good grain refinement ability, at a fraction of the cost. The price of Sc is more than two orders of magnitude higher per kg compared to Er [6]. This is why Er has recently been the subject of many research papers. Eu has proven to be an effective modifier and might be the next step in industrial modification of Al-Si alloys [7]. Mechanical properties were verified to increase with the addition of Er and/or Eu [8, 9].

Although much attention has been paid to the mechanical benefits of REE additions, their impact on casting performance, particularly fluidity, has yet to be fully understood. Fluidity is a critical parameter in ensuring the production of defect-free castings. It is known from other alloys that the castability can be altered quite dramatically by the type and amount of alloying elements, grain refiners and/or modifiers added to the melt [10]. To be able to use REE in an industrial setting the parameters that influence the casting process need to be well understood and controlled. The castability of an alloy depends on several phenomena but is often limited by fluidity, especially in thin-walled castings [11]. Fluidity is important for gravity and low-pressure die castings, where flow velocities are low ($<$1 m/s) and pressures are near ambient.

Fluidity in the foundry industry is measured by the length traveled in mm of the metal, through a constant cross-sectional mold cavity, before it is stopped by solidification [12]. Insufficient fluidity can lead to several defects such as incomplete mold filling, cold shuts, shrinkage defects, and poor surface quality [11]. Since most fluidity tests are performed in gravity sand castings, there is not yet a reliable dataset to understand the fluidity behavior in gravity permanent die castings. Fluidity molds and measurements have been notorious for being non-repeatable. When using a permanent mold, more fluidity tests can be performed from the same mold, increasing the test rate and thus has the potential for higher statistical accuracy.

Next to the addition of grain refiners and/or modifiers, fluidity can be heavily influenced by the melt cleanliness by the introduction of so-called bifilms [13]. These bifilms are folded surface oxides that are entrained in the bulk of the melt, which can hinder the flow to a considerable extent [14]. Therefore, the cleanliness of the melt should be increased before trials and measured during experiments.

Therefore, the goal of this work will be to investigate the effects of the addition of Er and Eu on the fluidity of the common foundry alloy A356 (Al-7wt% Si-0.3wt%Mg). A356 is selected since it is the most widely used aluminum casting alloy in the automotive and aerospace industry. Because fluidity is sensitive to many hard-to-control parameters, a test method is needed which reduces the variability in the input parameters. Therefore, a more repeatable permanent fluidity test mold will be designed, simulated, and produced. Validation criteria according to the Gage R&R will be formulated to investigate whether mold and test procedures can be considered a capable measurement system. Subsequently, fluidity experiments will be performed with additions of Er and Eu. Lastly, the microstructure and melt cleanliness will be investigated in detail to provide valuable insights into the importance of melt cleanliness on the Er and Eu additions and their effects on fluidity.

1.1 Problem statement

Foseco Vesuvius is a company that specializes in the development and production of consumables for the foundry industry, such as filters, feeders, binders, coatings and fluxes. The non-ferrous metal treatment (NFMT) is one of the departments within Foseco, which focuses on developing equipment and products to prevent casting defects in non-ferrous castings. Non-ferrous castings are mainly aluminum, magnesium and copper, of which aluminum contributes the majority since it is already widely used in the automotive industry.

The fluxes Foseco produces are used for cleaning the melt, grain refinement and/or modification of eutectic Si. Foseco is constantly investigating new and better recipes for their fluxes; to this end, Foseco experimented with Er- and Eu-containing fluxes. However, in the literature, there is no data on the effects of Er and Eu addition on fluidity. Moreover, the fluidity tests currently in the field are prone to human error and lack repeatability, making it difficult to obtain reliable results. Therefore, the main goal of this work is (1) investigate the effect of Er and Eu additions on the fluidity of an A356 aluminum alloy and (2) develop a reliable, less labor-intensive permanent mold and testing procedures to reduce human error and improve the repeatability and reproducibility of the fluidity measurements.

Foseco can use the knowledge obtained about Er and Eu to determine if these elements might be suitable for industrial adoption. Moreover, Foseco can use the permanent fluidity mold for other element additions to investigate the effects on fluidity. This can help Foseco provide their clients with better solutions to achieve higher-quality melts and improved casting performance.

1.2 Objectives and research questions

This work contains two research objectives which are interdependent since research objective 1 needs the mold and test procedures which is the result of research objective 2.

Objective 1: Investigate the effect of the additions of Er and Eu on the fluidity of the commercially available aluminum alloy, to determine whether Er and/or Eu can be viable alternatives for current grain refiners and/or modifiers of eutectic Si. The research questions which need to be answered to achieve this goal:

- Which commercially available aluminum alloy, provides an appropriate base for evaluating the effects of Er and Eu additions?
- Which addition ratios of Er and Eu can best be used for the fluidity trials to provide valuable information for industry?
- What is the expected impact of Er and Eu additions on the fluidity and solidification behavior of A356 alloy, based on prior research?
- How do Er and Eu influence the microstructure of the A356 alloy during the casting process, and what are the implications for casting performance?

Objective 2: Develop a less labor-intensive, repeatable, and reproducible permanent mold to measure the fluidity of aluminum alloys, ensuring consistent results across tests.
To achieve this goal, the following questions research need to be answered:

- What is fluidity, and why is it critical in the casting process?
- What methods have traditionally been used to measure fluidity?
- What fluidity test mold designs have been implemented in previous studies and what are their limitations?
- Which parameters (e.g., temperature, mold material, alloy composition) most significantly influence fluidity, and how can they be controlled during testing?
- How should the parameters be controlled during the test?
- What criteria will be used to validate the repeatability and reproducibility of the newly designed molds?

1.3 Outline of conducted research

Figure 1.1 gives an overview of the steps needed to achieve the research objectives. Within this thesis, two separate components can be distinguished; the first part is the design part with an analysis of previous designs, simulations and a method to validate the design. The second part has a more conventional structure with a literature review, method, results and discussion. After the fluidity experiments, the samples taken during the experiments are analysed to explain the results obtained by the fluidity test, and see if it is in accordance with the knowledge present in the literature.

In chapter 2; Literature review, the background is given on aluminum alloys and casting processes. Afterwhich, the methods of measuring and estimating fluidity are then discussed and, lastly, the parameters affecting fluidity are discussed in detail. Chapter 3; Mold design, focuses on mold design by analysing previous fluidity molds. After which, the rationale about technical features of the mold is given, in order to keep input parameters constant, and this chapter ends with a method to validate the molds. Chapter 4; Experimental Design, discusses the selected addition ratios based on previous work and describes the method used to measure the fluidity and prepare the samples for examination. Chapter 5; Results and Discussion, gives the results obtained by the fluidity tests and discusses possible explanations for these results based on the microstructures of the samples. Chapter 6; Conclusion and Prospective, sums the most important findings of the work and provides suggestions for further research.

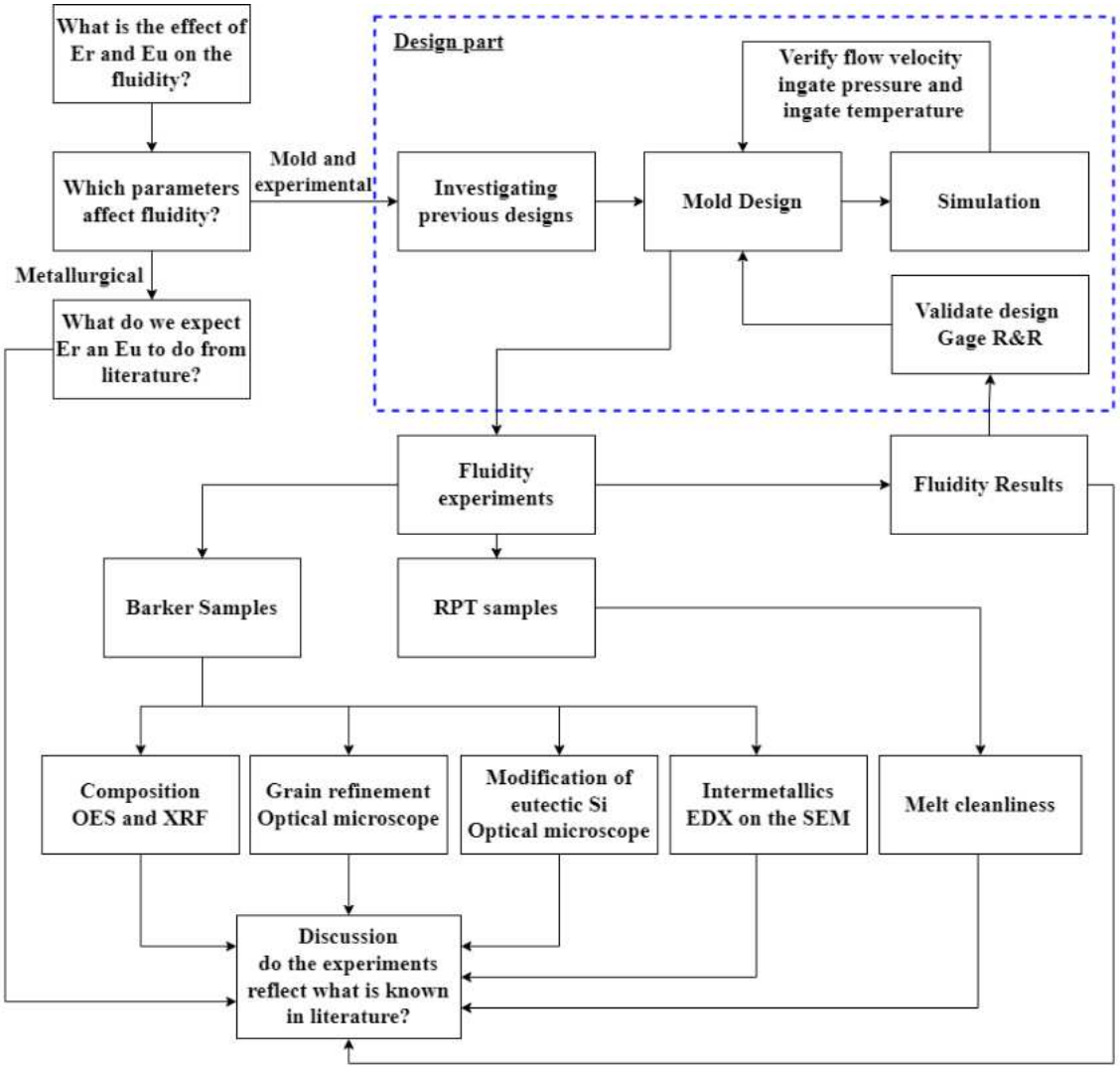

Figure 1.1: Research overview with two separate components

2. Literature Review

In this chapter, a short introduction is given to aluminum alloys and the most common casting processes. The most common defects in castings are discussed, with an emphasis on insufficient fluidity. Methods of measuring and mathematically estimating fluidity are presented. Lastly, all the metallurgical, mold and experimental parameters which influence fluidity are discussed in detail.

2.1 Aluminum alloys

Aluminum is the most abundant metal in the Earth's crust and the second most used engineering material after steel. Aluminum is used because of its good corrosion resistance, high specific strength (when alloyed), and good recyclability. In 2018, 64 million tons of aluminum were produced worldwide, and this number is expected to increase by 6% annually [15]. Aluminum is made from bauxite (an ore containing 15-20% aluminum) in a complex and energy-intensive process. The last step of this process is to cast the aluminum in billets, these billets are used in a cast house to add alloying elements resulting in the desired grade [16]. However, it was only from 1866 on that aluminum was industrially adapted due to the invention of the modern smelting process. This is extremely recent compared to bronze, copper, lead, and iron, which have been around for thousands of years. Nowadays, aluminum is by far the most widely used non-ferrous metal [17]. Aluminum alloys can be divided into two categories; casting and wrought alloys.

Cast aluminum alloys

Cast alloys generally have a higher alloy content than wrought alloys. Cast alloys are used for casting process were complex parts and/or large production volumes are needed. The designation system for cast aluminum alloys, by The Aluminum Association (AA), consists of three digits with an optional prefix letter and a suffix decimal digit. For example A356.1. The first digit gives information about the main alloy element, as shown in Table 2.1. The second and third digits further specify the alloy and are unique, but they are not coupled to certain elements.

Table 2.1: Aluminum Association (AA) casting alloy designation system

1xx - Pure Al (99%+)	6xx - Unused
2xx - Cu	7xx - Zn
3xx - Si with Cu and/or Mg	8xx - Sn
4xx - Si	9xx - Other elements
5xx - Mg	

The letter (A,B,C, etc.) in front of the numeric designation indicates a slight deviation, but not enough to appoint a unique alloy. Lastly, it is possible to have a .0, .1 or .2 behind the numbering which denotes the product form. 0 means a casting, 1 means standard ingot, and 2 means ingots with smaller composition ranges than 1 [18]. The 3xx series (Al alloyed by Si with Cu and/or Mg) is responsible for 85-90% of all aluminium casting produced [5].

Wrought aluminum alloys

Wrought aluminum alloys get there enhanced mechanical properties from work hardening and are produced into billets or bars which are intended to be processed by one or multiple forming steps, such as rolling, forging, drawing, and/or extrusion [18]. If the wrought alloys are cut and/or machined into their final shape, the bar or billet will be already rolled by the cast house, as shown in Figure 2.1.

Wrought alloys are generally made with lower alloy content compared to casting alloys. Therefore, they are softer and weaker before the forming step, but after work hardening during the forming process, the alloy has more strength than a comparable casting alloy.

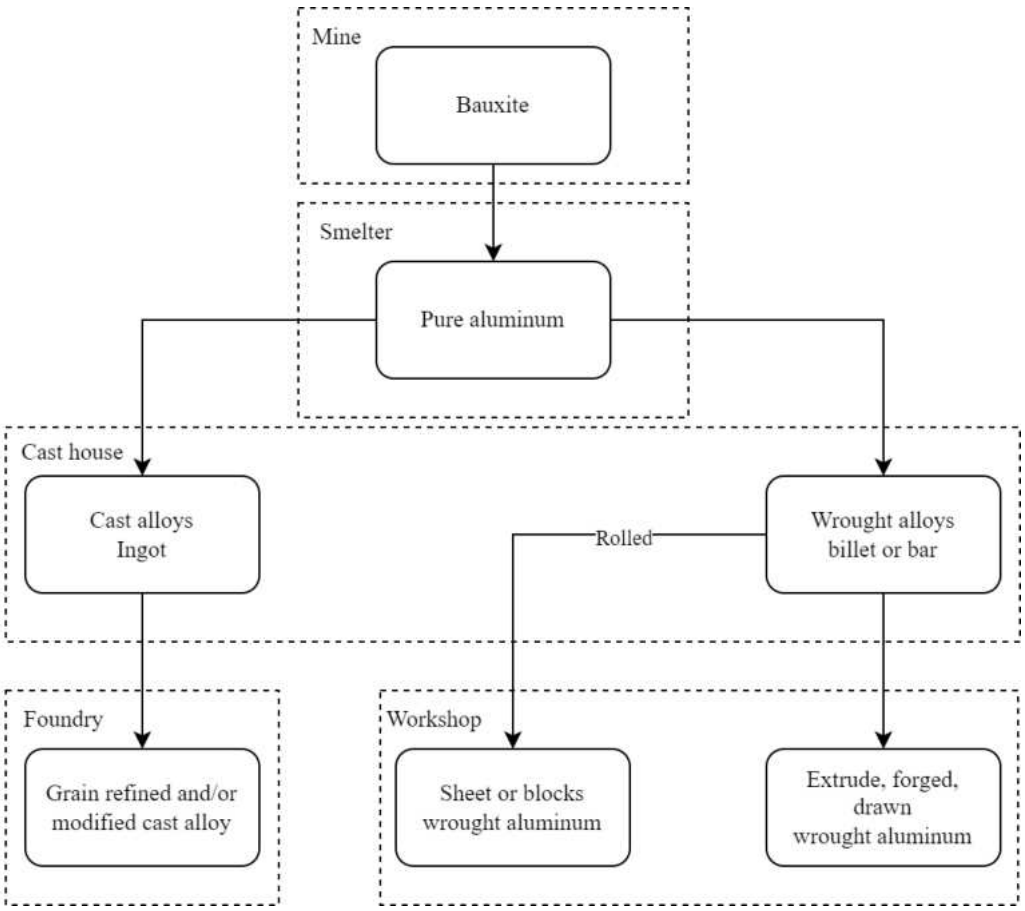

Figure 2.1: Schematic overview of production of cast and wrought alloys

Moreover, the wrought alloys are produced by a direct-chill process which solidifies the billet or bar in a very controlled way. This ensures that there is no porosity in the billet or bar. In contrast to casting alloys, where microporosity is inevitable. Therefore, wrought alloy products have often higher strength.

2.2 Casting processes

Now the different casting alloys are known, the different casting methods will be discussed. Casting involves pouring molten metal into a cavity and letting it solidify to obtain the desired geometry. Casting processes are suitable for producing complex shapes in large quantities. The most widely used casting processes are discussed in the following sections.

2.2.1 Gravity casting

Gravity casting uses, as the name suggests, gravity to generate metallostatic pressure to force the molten metal into the cavity. Therefore, the point where the metal enters the mold needs to be higher than the cavity. Within gravity casting two methods can be distinguished; sand casting and permanent mold casting.

Sand casting

Within sand casting, the mold material is sand and is an expendable item. The mold, in Figure 2.2, is made out of two parts; the cope and the drag, which are the top and bottom part respectively. To create the form of the cavity (negative shape of the final product) a pattern (positive shape) is used to mold the sand around. Sometimes hollow sections are desired within the part, for which cores can be used. They are placed within the mold prior to casting and will be removed after casting. Since the casting shrinks while solidifying, the casting needs to be supplied with more molten metal to maintain the geometry of the cavity, for this risers or also called feeders can be used. The molten metal is poured into the pouring basin and moves down the sprue, loses velocity in the well, to prevent turbulence, and continues through the runner system, into the cavity [19].

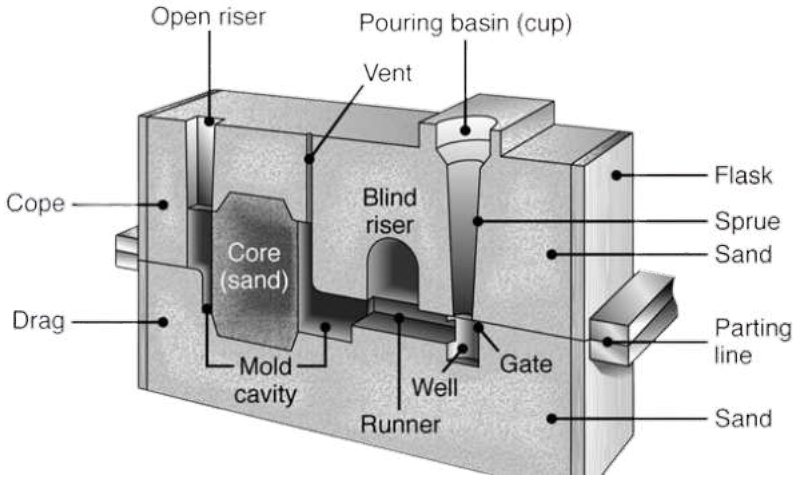

Figure 2.2: Mold nomenclature for sand casting [19]

Permanent mold

Permanent mold also called a die, uses often steel mold halves in which a cavity is milled into, as depicted in Figure 2.3. All the above mentioned geometry can also be found in permanent molds. The advantage of permanent molds that they can be used many times before any rework needs to be done on the die. This process is suitable for quite large production quantities (250-50k per year), with relative thin wall sections (3-4mm) and has reasonable dimensional accuracy (±0.4mm) [20]. Moreover, the heat extraction from the melt is faster than in a sand mold, since steel has a higher thermal conductivity. This faster cooling results in smaller grains and, therefore, in a higher strength of the product [21]. Because aluminum has the tendency to stick/solder to the die a coating can be applied to prevent this from happening.

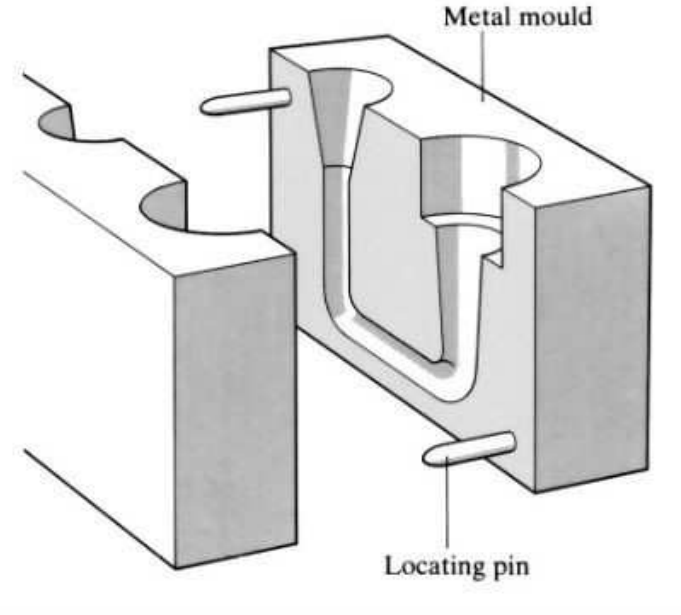

Figure 2.3: Permanent mold [22]

2.2.2 High pressure die casting

High pressure die casting (HDPC) is the process were molten metal is poured into a shot sleeve and this melt is forced under high pressure (20bar [23]) into the mold, see Figure 2.4. Because this process is fairly violent, surface turbulence is inevitable and oxide inclusions tend to end up in the cast product, which increases scrap rate [24]. The process is suitable for extreme high quantities (2k-500k annually), thin wall sections (1-2mm) and has very good dimensional accuracy (±0.1mm) [20].

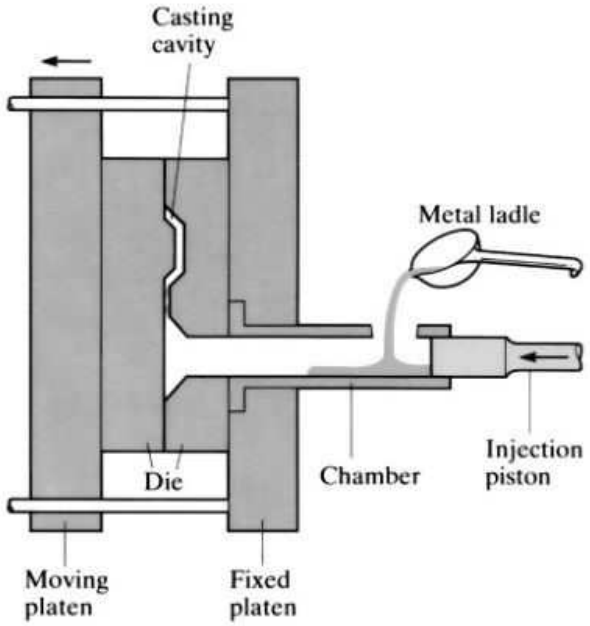

Figure 2.4: High pressure die casting setup [22]

2.2.3 Low pressure die casting

Low pressure die casting (LPDC) uses a pressurised (inert) gas to push the liquid metal from the crucible into the mold, as shown in Figure 2.5. This ensures a controlled filling of the mold and reduces the risk of casting defects. Therefore, LPDC is suitable for critical components such as wheel rims. However, the cycle time of LPDC is around 4-6 times longer than that of HPDC [25]. Therefore, LPDC is be used for lower production runs compared to HPDC.

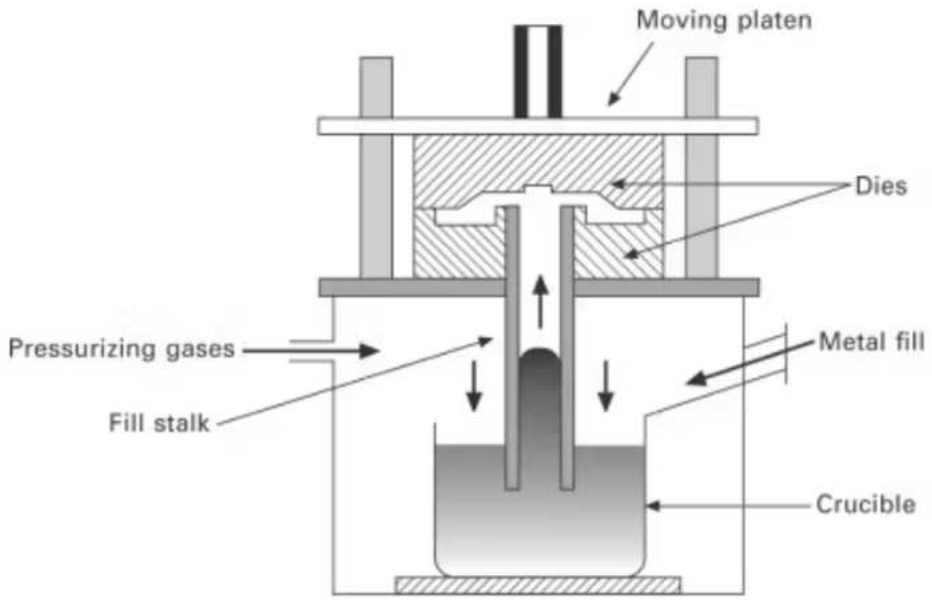

Figure 2.5: Low pressure die casting setup [26]

2.3 Castability and casting defects

The success-rate of the casting process is dependent on the process settings and the castability of the selected alloy. Castability is the ability of an alloy to produce defect-free castings with the desired properties [27]. The most important casting defects include; porosity, hot tearing, macro segregation and insufficient fluidity [28]. These casting defects and how they occur are discussed in the following.

2.3.1 Porosity

Porosity is often the result of the combination of shrinkage of the part, high gas content in the melt, and the presence of folded oxide films (bifilms). As the melt cools, the solubility of the dissolved gases (most importantly hydrogen) drops and diffuses into the pockets formed by the folded oxide films [29]. The inability of the liquid metal to feed the shrinking casting can also lead to porosity, but a non-metallic inclusion or oxide film is always needed to start pore formation and cannot occur in the bulk of the (clean) melt [28]. Pores decrease the mechanical properties of the casting and can be the size of a few micrometers to several centimeters in large castings. Melt cleanliness should be controlled to minimise porosity.

2.3.2 Macro segregation

Macro segregation is the phenomenon of spatial segregation of the composition over several millimetres, centimetres or even meters, within large castings [30]. This segregation occurs due to the relative movement of solids or liquid during the solidification process. This is caused by one or more of the following flow streams [11]:

- Solidification shrinkage feeding flow
- Buoyancy induced flow because of thermal or solutal gradients
- Flow due to capillary forces
- Flow induced by gas bubbles

These flows can take, already nucleated, equiaxed grains (same dimensions, in all directions) and transport them to other parts of the casting where they can accumulate. Furthermore, inclusions can also float or settle depending on their relative density compared to the melt [27].

To mitigate macro segregation the casting should not be too long in the liquid state when the cavity is already filled to minimise the time for the relative motion within the casting to occur. Cooling rate uniformity should be controlled to avoid the solidification shrinkage feeding flow.

2.3.3 Hot tearing

Due to solidification shrinkage and thermal contraction, cracks on the surface can occur in the casting if the interdendritic feeding cannot compensate for the volume loss and the dendrite network is strong enough to stop the flow, but still too weak to handle the thermal stresses. Hot tearing takes place just before the casting fully solidifies when the dendrites already impinged up one another but there is still a liquid metal film on the grain boundaries [28]. Once again cooling uniformity should closely be controlled to mitigate this casting defect.

2.4 Insufficient fluidity

Fluidity in the foundry industry is measured by the length traveled (in mm) of the metal through a constant cross-sectional mold cavity until it is solidified [12]. Lately, Durmus et al. [31] introduced a more general metric which is called the fluidity index (FI) for molds with multiple channels of different channel heights. The FI is formulated as the sum of fluidity length per channel divided by its channel height, as stated in Equation 2.1, giving a higher weight to the fluidity lengths in thinner channels as these are the hardest part of the mold to fill. Insufficient fluidity can lead to several defects such as incomplete mold filling, cold shuts, shrinkage defects, and poor surface quality [11].

$$FI = \sum_{i=1}^{n} \frac{L_{fi}}{h_i} \tag{2.1}$$

It must be noted that fluidity in the foundry industry differs from the definition found in physics, where fluidity is the inverse of viscosity. Paradoxically, viscosity plays no significant role in alloy fluidity, as defined in the foundry industry [27]. A more detailed description of the influence of viscosity on fluidity will be given in section 2.5.1.

2.4.1 Measuring fluidity

In the past, several tests have been designed to compare the fluidity of different alloys, and/or to see the effects on fluidity of different process settings. In this section, the most commonly used tests are discussed. This section is used to answer research questions one and two of Objective 2 from section 1.2.

Vacuum mold

The vacuum test, also called the Ragone test, is one of the first fluidity tests. By which a narrow quartz tube is put into the molten metal and sucked into it by employing a partial vacuum, as can be seen in Figure 2.6. The fluidity length is simply the length the metal has travelled inside the tube.

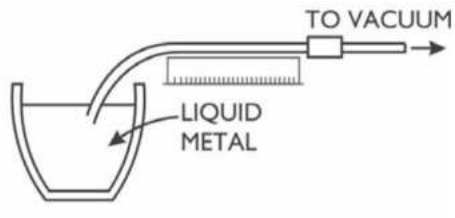

Figure 2.6: Vacuum fluidity test [32]

Spiral mold

In the spiral test, the metal is poured into the sprue and the metal follows the spiral-shaped cavity. This test is shown schematically in Figure 2.7. The advantage of this test is its compact nature, with a small-sized mold it is possible to measure significant fluidity lengths.

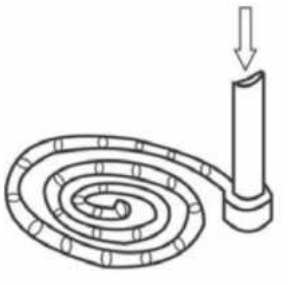

Figure 2.7: Spiral fluidity test [32]

Octopus mold

The octopus design was proposed by Colak et al. [12]. The design, in Figure 2.8, has a runner system that supplies the melt to all channels. The idea of the eight channels with different heights is to observe the filling behavior of smaller channel sections. To ensure both sides of the sprue are filled at the same time, the four arms to the right side of the sprue have the same volume as the four arms to the left side of the sprue.

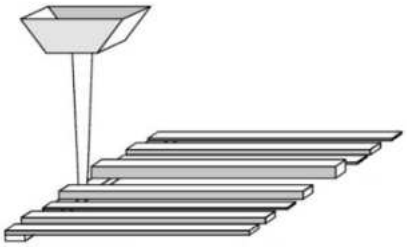

Figure 2.8: Octopus fluidity test [12]

Star mold

The star fluidity test, displayed in Figure 2.9, works by pouring the molten metal into a central hub where it spreads in the different channels. This ensures the same experimental parameters for all channels e.g. ingate metallostatic pressure, superheat and melt cleanliness.

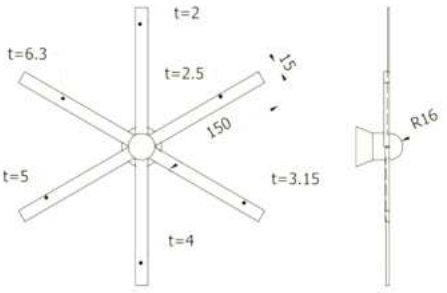

Figure 2.9: Star fluidity test [33]

2.4.2 Mathematical background on fluidity

The trial-and-error approach to see if there is enough fluidity, to fill the mold, is time- and resource-consuming. Therefore, researchers have tried to find analytical and numerical solutions to estimate fluidity, unfortunately, with limited success.

Analytical methods to estimate fluidity

One of the first equations comes from Flemings et al. [34]. Which state that, for pure metals and eutectics, the distance travelled by the melt is equal to the flow velocity multiplied by the solidification time, as shown in Equation 2.2. These metals have a solidification point and not a solidification range and therefore almost constant flow velocity until they solidify. However, in reality the flow velocity decreases when the solidification process starts. Therefore this expression overestimates the fluidity length.

$$L_f = V \cdot t_s \tag{2.2}$$

A few decades earlier Chvorinov (1940) [35] found a relation between solidification time and mold cavity geometry. The mold cavity geometry is quantified by the solidification modulus (M), which is, the ratio between the casting volume (V) to the effective cooling portion of its surface (S). For a constant cross-sectional area channel, the modulus can be written as the cross-sectional area over (A) the channel circumference (C). The solidification modulus was described in Chvorinov's rule, and reads:

$$t_s = C_m M^n = C_m \left(\frac{V}{S}\right)^n = C_m \left(\frac{A}{C}\right)^n \tag{2.3}$$

Where t_s is the solidification time, C_m mold constant and n is an exponent usually between 1.5 and 2. The mold constant C_m should be found experimentally. Combining Equation 2.2 and Equation 2.3 gives the following simple expression for fluidity, for a pure metal or eutectic through a constant cross-sectional area channel:

$$L_f = V \cdot C_m \left(\frac{A}{C}\right)^n \tag{2.4}$$

However, almost all commercially used foundry alloys are long freezing range alloys, which will be explained in section 2.5.1. Therefore, Equation 2.2 needs to be elaborated to accommodate for more complex solidification behavior:

$$L_f = \frac{A\rho V_0(f_{scr}D_h + C_pD_T)}{hC(T - T_0)}(1 + K/2) \text{ in which } K = \frac{h\sqrt{\pi\alpha\Delta x}}{k'\sqrt{v}} \tag{2.5}$$

The explanation of the variables, in Equation 2.5, are stated in Table 2.2.

Table 2.2: Variables used in the mathematical model of Flemings et al. [34]

Symbol	Meaning	Symbol	Meaning
A	Mold cross-sectional area	h	Heat transfer coefficient melt to mold
ρ	Density of the liquid	C	Mold channel circumference
f_{crit}	Critical solid fraction	T	Pouring temperature
D_h	Heat of fusion	T_0	Room temperature
c_p	Specific heat of the melt	K	Constant dependent on h
D_T	Superheat	α	Thermal diffusivity of mold
Δx	Length Δx in Figure 2.12	k'	Thermal conductivity of mold

This model is based on the following assumptions;

- The flow velocity is constant until the flow stops
- Solid particles will form on the flow front and flow with the stream
- The flow stops when the critical solid fraction is reached f_{crit}

In reality however, flow velocity decreases when coming close to the critical solid fraction f_{crit}. Therefore this equation also overestimates the fluidity length. This equation is reasonable in accordance with reality for Al-4.5wt%Cu [34]. When applying this mathematical model to A356 alloy the model overestimates the fluidity drastically [36]. Moreover, for Al-SiC composites the model significantly underestimated the fluidity [37], and for other alloys some of these parameters might not be known by the foundry. This means that this model is fairly limited in describing the fluidity of aluminum alloys. Therefore, the use of this expression in industry has been limited.

Numerical methods to estimate fluidity

To accommodate for more complex mold geometries, Odorizzi et al. [38] used the MagmaSoft commercial package to predict fluidity of A356 foundry alloy. MagmaSoft is a Finite Difference Volume (FDV) method and uses the Navier-Stoke equations to model the filling process, Fourier equations to model the solidification and cooling behaviour and finally the thermodynamic and kinetic equations to model the solid-state transformations. To verify the prediction the authors did ten spiral tests at three different temperatures and compared the results. This comparison can be seen in Table 2.3.

Table 2.3: Simulated vs. experimental results from ten fluidity tests of A356 foundry alloy, at three different temperatures [38]

Temperature [$^{\circ}C$]	**Simulated fluidity length, $\bar{x}$ [mm]**	**Experimental fluidity length, $\bar{x} + \sigma_m$ [mm]**	**Difference experimental vs simulated, $\bar{x}$ [%]**
700	550	460 ± 10	-19.6%
715	620	542 ± 7	-14.4%
730	645	630 ± 10	-2.38%

The authors state that the simulations fits the experimental results. However, there are significant differences between simulation and the experiments, especially, at lower pouring temperatures. Bazhenov et al. [39] conducted simulations, in Procast 2016, on the fluidity of A356 alloy in which the authors fitted the interface heat transfer coefficients to the experimental data. The critical solid fraction was expected to be between $f_{crit} = 0.1$ and 0.15 . In Table 2.4 the simulation is compared to the experimental values.

Table 2.4: Simulated vs. experimental results. Simulated with different critical solid fraction [39]

Pouring temperature [$^{\circ}C$]	**Spiral length [mm]**		
	Experimental	Simulation $f_{crit} = 0.1$	$f_{crit} = 0.15$
670	381 ± 56	349	468
740	735 ± 66	622	752
810	925 ± 26	917	1010

From the table it can be seen that the fluidity is very sensitive to the criticalsolid fraction. It has been shown that modelling the solidification process is difficult due to the lack of reliable data for all the parameters necessary as input for the model [40]. Therefore, the use of numerical methods to predict fluidity has not been widely adopted in industry.

2.5 Parameters effecting fluidity

To understand why it is so hard to predict fluidity, the parameters which affect fluidity should be well understood. These parameters can be divided into three groups; Metallurgical, Mold and Experimental as shown in Table 2.5. In this section, all relevant parameters will be discussed in detail and will be used to answer research questions three from Objective 2, from section 1.2.

Table 2.5: Parameters that influence fluidity, divided into three categories

Metallurgical	Mold	Experimental
Solidification behavior	Cavity geometry	Flow velocity
Specific heat capacity	Thermal conductivity	Ingate pressure
Latent heat	Mold temperature	Superheat
Viscosity	Mold wettability	Melt cleanliness

2.5.1 Metallurgical parameters

Solidification behavior

The solidification behavior of a molten metal depends mainly on the size of the freezing range and the formation of primary and secondary phases. The freezing range is the temperature difference between the liquidus to the solidus line. For casting purposes (depending on alloy composition) two types can be distinguished; long and short freezing range alloys, as shown in Figure 2.10. The addition of grain refiners and/or modifiers can greatly impact the solidification behavior of the primary and secondary intermetallic phases.

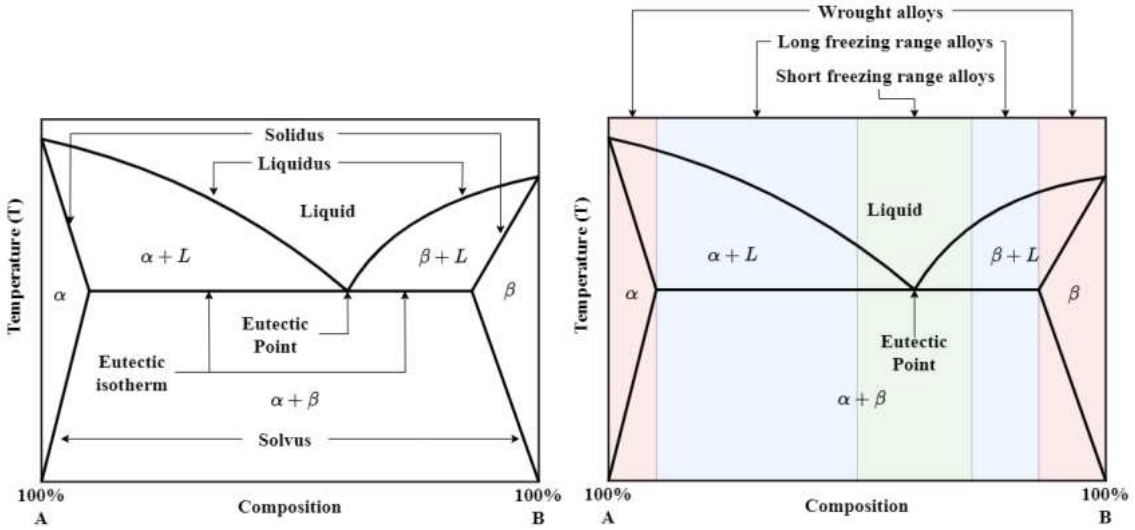

(a) Nomenclature (b) Alloy regimes

Figure 2.10: Generic binary alloy phase diagram

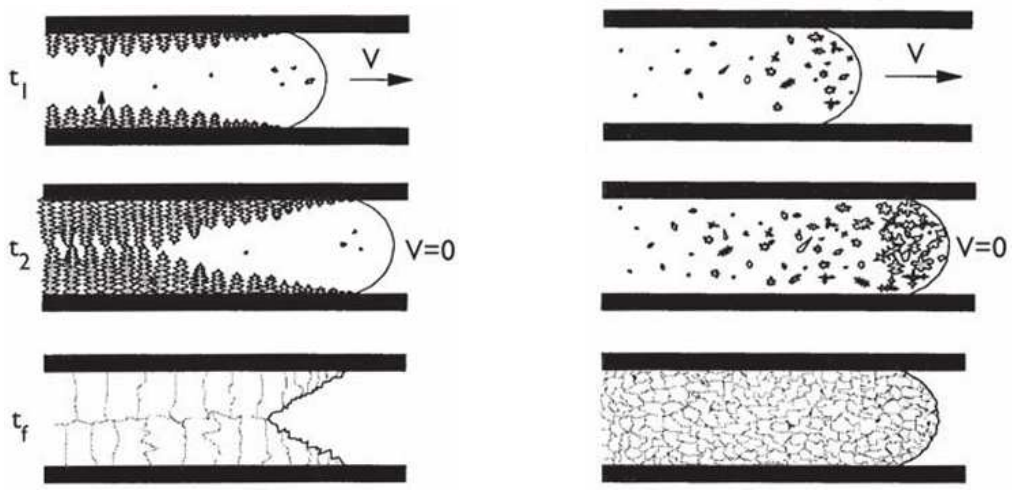

(a) Short freezing range solidification mode [41] (b) Long freezing range solidification mode [41]

Figure 2.11: Solidification modes

The first mode, which corresponds to the short freezing range alloys, in Figure 2.11a is mainly influenced by columnar dendritic growth where the nucleation process starts on the wall of the mold. After which, the dendrites grow to the center of the mold, where they eventually block the flow of the molten metal. This solidification behavior occurs in (almost) pure metals and alloys with compositions close to the eutectic composition, as shown in Figure 2.10b. It must be noted that the columnar dendrites remelt as a result of the supply of molten metal and the release of latent heat during the solidification process. Therefore, this freezing area will move with the flow front, as illustrated in Figure 2.12.

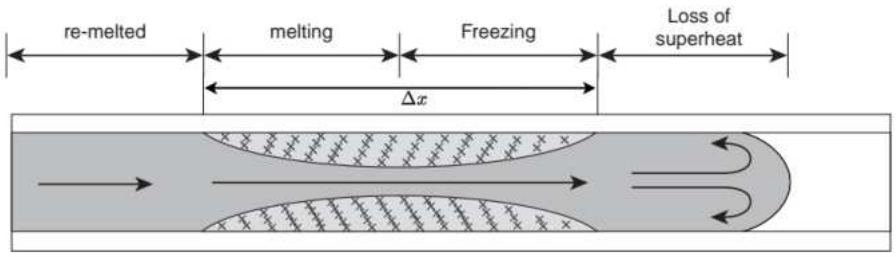

Figure 2.12: Re-melting of the columnar dendrites [29]

The second mode, which corresponds to the long freezing range alloys, is mostly influenced by equiaxed (having approximately equal dimensions in all directions) dendrites, shown in Figure 2.11b. In this mode independent crystals grow in the bulk metal liquid due to constitutional supercooling [32] and are dragged along in the flow. When the flow exceeds a critical solidification threshold (commonly between 20 and 50% solidification [42]) the dendrites get impinged on one another and stop the flow. Therefore, the fluidity of short freezing range alloys can be 2 to 5 times that of long freezing range alloys, which seems to hold for all alloy systems [42].

The temperature at which the dendrites impinge on each other is called the dendrite coherency point (DCP). The solid fraction is also used to indicate the dendrite coherency point. This phenomenon can be found in the long freezing range alloys, where the distance between the liquidus and solidus line, in Figure 2.10a is relatively large. Almost all commercially used Al-Si casting alloys are long freezing range alloys. The DCP can be measured by a rheology meter, as shown in Figure 2.13, where a paddle is stirred at constant RPM and the applied torque is measured. When the dendrite coherency point is reached the torque suddenly increases sharply since it must overcome the strength of the dendrite network [43]. Other methods are based on detecting thermal events in cooling curve to determine the DCP.

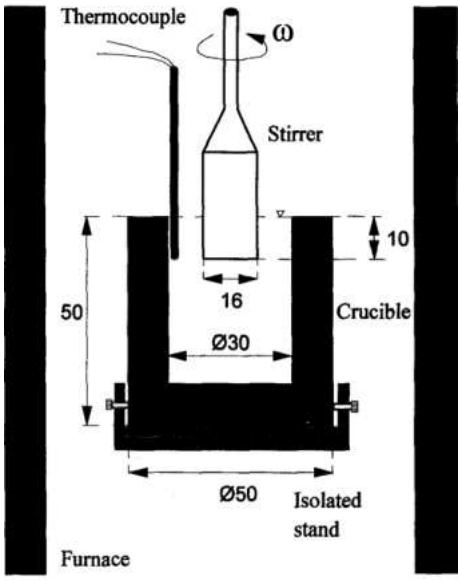

Figure 2.13: Rheology setup to measure dendrite coherency point [43]

Alloy content The composition of the alloy can significantly influence the solidification behavior of an alloy and thus the fluidity. Silicon is the most common alloy element of aluminium and greatly enhances the fluidity therefore the 3xx and 4xx series are used for complex cast geometries. Composition can change parameters such as; solidification mode, viscosity, and surface tension [11].

The relation between composition of a binary alloy system and fluidity is visualized in Figure 2.14. It can be clearly seen that fluidity increases when solidification ranges decreases. Furthermore, the peaks in fluidity-composition diagrams can be very steep, an example is given for an Al-Zn alloy in Figure 2.15. This means, that fluidity is quite sensitive to composition changes. This might be one of the explanations for why fluidity tests are criticised for not being reproducible [29].

The fluidity of the eutectic, in Figure 2.15, is higher than the fluidity of the constituents, in pure form. This is due to the laminar intermetallic crystals which are smoother than the dendritic structure of the constituents. These smoother crystals obstruct the flow less, resulting in even higher fluidity [29].

Since this study will focus mainly on Al-Si alloys, it is good to know that eutectic compositions are alloys with 11-13wt% Si. Alloys with less than 11wt% are considered hypoeutectic and above 13wt% are considered hypereutectic. However, the eutectic composition is not fixed at a certain Si content. For example, the additions of Na can shift the eutectic composition to higher Si content [45].

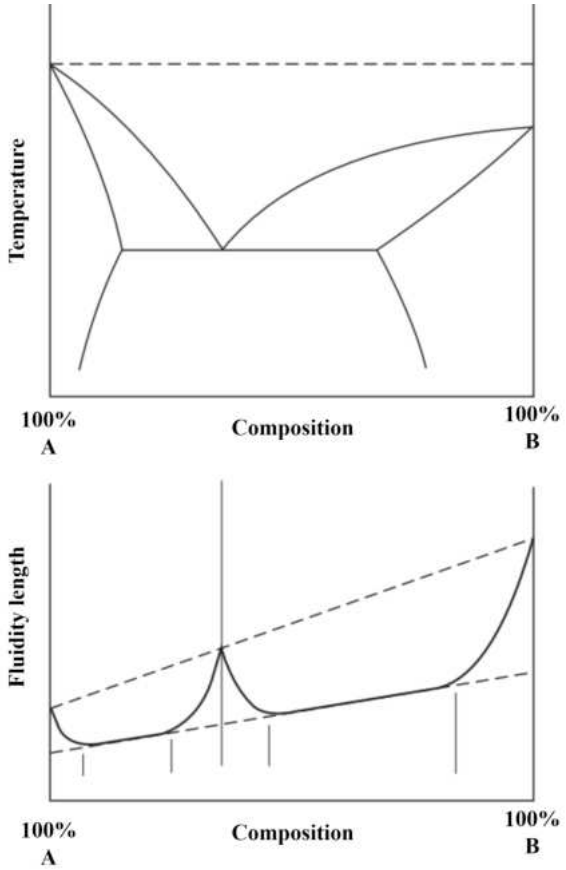

Figure 2.14: Influence of composition on fluidity, poured at zero superheat [29]

Grain refiner Grain refinement is the process of producing smaller equiaxed (equal dimensions in all directions) grains from, otherwise, large columnar grains to increase yield strength and toughness. Moreover, if there are more and smaller grains the secondary phases are more evenly distributed around the grain boundaries [10].

For solidification to occur, two requirements need to be met; undercooling also known as supercooling and the presence of nuclei. Undercooling occurs when a liquid is colder than its freezing point without turning into a solid. This difference between the melting point of the metal and the temperature of the melt is the driving force which is needed to start solidification. However, undercooling is needed; it is not sufficient to start solidification, the melt also needs nuclei to connect the atoms to grow the crystal. This nucleation can happen in two ways; homogeneous and heterogeneous. Homogeneous means that the atoms of the melt itself start forming crystals and heterogeneous means that the atoms of the melt connect to a different particle. Heterogeneous nucleation is always more energy-favorable than homogeneous nucleation, which means that this will happen at lower undercooling because it needs less undercooling to start solidification [46].

To refine the grain and thus create more grains, heterogeneous nucleation sites can be introduced into the aluminum melt. Usually, this is done by introduction of master alloys, where rods or powders with high levels (concentrated) of grain refiners are added to the melt, for aluminium alloys this is often TiB_2 and/or $TiAl_3$ [4]. These TiB_2 and/or $TiAl_3$ particles act as starting point for the Al-matrix to grow on.

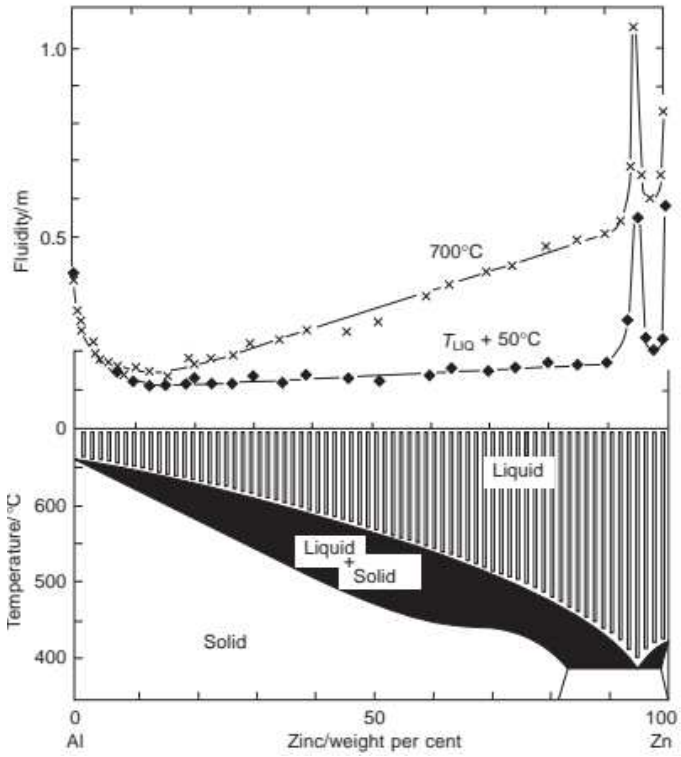

Figure 2.15: Influence of composition on fluidity of an Al-Zn alloy [44]

In melt with a Si content above 2wt% (which are most casting alloys), Si can have a poisoning effect on grain refinement by partially inhibiting grain refinement. This poisoning effect means that an unwanted shell of Ti_5Si_3 grows around the TiB_2 and/or $TiAl_3$ particles inhibiting the potential nucleation site for the Al-matrix. TiB_2 is less prone than $TiAl_3$ to poisoning, as Ti_5Si_3 growing onto TiB_2 is less chemically stable than its counterpart. The poising effect is easily mitigated by adding some extra grain refiner [4].

Another phenomenon that can occur is the fading effect. When a master alloy is added to the melt, the solid TiB_2 or $TiAl_3$ particles are more dense than the surrounding melt. This means that these particles slowly sink to the bottom of the crucible [48]. If the operators wait too long with casting, less of the grain refiners will be in the casted piece, increasing the grain size and thus decreasing the mechanical properties of the casting.

In the literature, research has found that grain refinement has a positive influence on fluidity. Kwon et al. [14], found an increase in fluidity when adding Ti and Al-5Ti-B to Al-4.8Cu-0.6Mn, as shown in Figure 2.18. The authors contributed this behavior to the decrease in the size of the dendrites at the flow front, which would increase the critical solid fraction. The reduced difference in fluidity between the grain-refined alloy and the non-grain-refined alloy at higher superheats would be the result of the larger dendrites breaking up during the filling process and therefore having almost the same size as the grain-refined alloy.

Prukkanon et al. [49] added 0.1, 0.3, 0.5 and 0.7wt% Ce to A356 alloy. The grain size decreased until an addition ratio of 0.3wt% Ce after which the grain size increased with

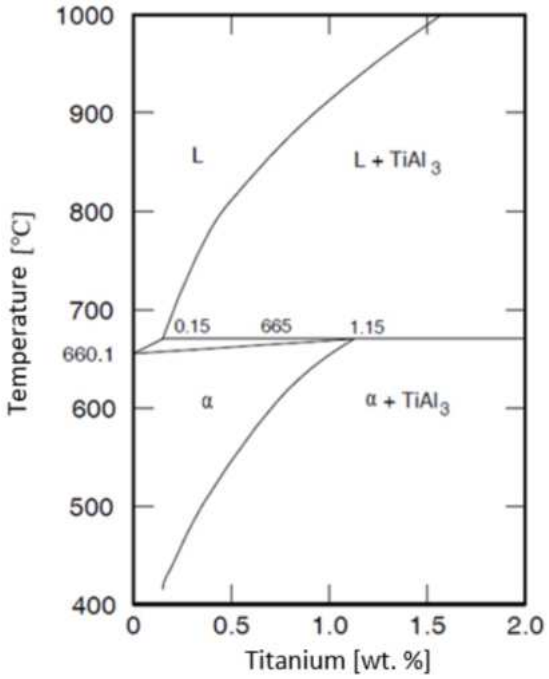

Figure 2.16: Al-Ti binary phase diagram [47]

higher levels of Ce, as shown in Figure 2.17a. In Figure 2.17b, the corresponding effect of Ce addition on fluidity can be seen. When the grain size starts to increase, after 0.3wt% Ce, the fluidity starts to decrease. Giving a strong relationship between grain refinement and fluidity.

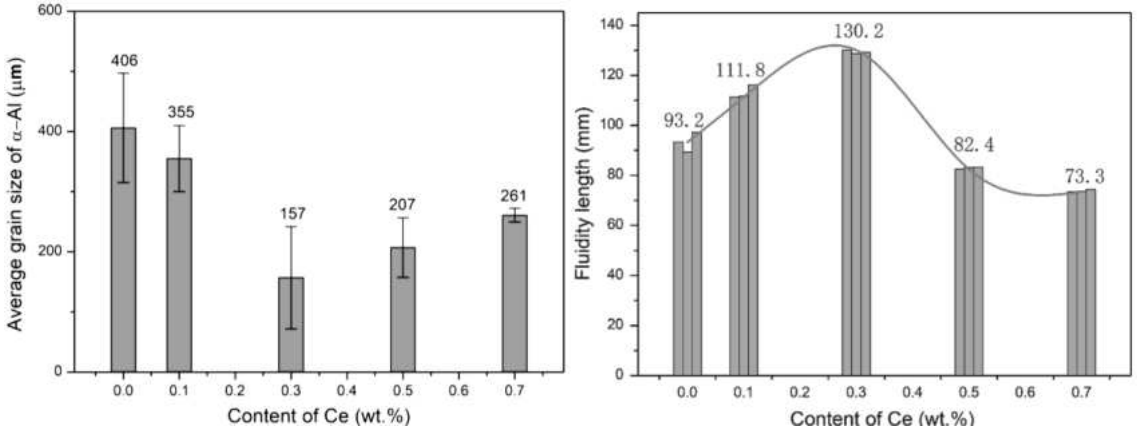

(a) Grain size dependent on Ce addition [49] (b) Fluidity length dependent on Ce addition [49]

Figure 2.17: Effects of Ce addition to an A356 alloy

Dahle et al. [43] found that for A356 the fluidity first decreases with addition of Ti below 0.12wt% Ti and increases after this point. No explanation was found to explain the initial decrease in fluidity. The subsequent increase in fluidity was attributed to a postponed dendrite coherency point in the grain-refined samples. From Figure 2.16, it can be seen that the L + $TiAl_3$ regime starts from 0.15wt% Ti therefore little to no grain refinement can be expected before 0.15wt% Ti. Bazhenov et al. found that the addition of Ti and

B, by means of Al-5wt%Ti5-1wt%B master alloy, to A356.2 alloy had no effect on fluidity [50]. Lang et al. [44] found a large increase in fluidity when grain refined with solely B, at weight percentages of 0.04-0.07wt% B to several Al-Si alloys. However, according to Greer [51] the differences found in the literature can be explained since the effect of grain refinement on fluidity depends on a lot of factors such as: the type and amount of grain refiner, alloy composition, holding time and temperature in the furnace. Therefore, it is believed that grain refinement has a positive influence on fluidity.

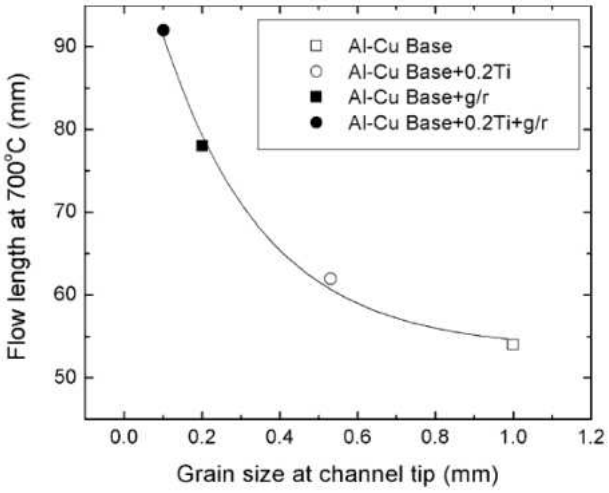

Figure 2.18: Flow length depending on grain size poured at 700°C [14]

Modifiers for eutectic Si In Al-Si alloy system; the coarse plate-like eutectic silicon particles can be modified (in a similar fashion graphite can be modified in cast iron) into fine fibrous silicon, which is clearly illustrated in Figure 2.19 and 2.20. This is advantageous since pure silicon has a diamond-like structure and is thus very brittle. Moreover, the sharp points of these plates act as stress concentrations when the part is loaded in tensile, acting as crack initiation points in the material. Therefore, modifying silicon into a more fibrous morphology greatly improves the strength, but mainly the ductility of the material [52].

The restricted growth theory and the restricted nucleation theory are the two main mechanisms proposed to explain the modification of the eutectic Si [54]. The restricted growth theory states that the preferred growing direction of the silicon is inhibited, i.e. preventing the growth of the plate-like structures. The restricted nucleation theory explains that Sr deactivates AlP by forming a Al_2Si_2Sr layer around it. Therefore Si can neither form plates nor precipitate in its primary forms. This lowers the solidification temperature, as shown in Figure 2.21 which means the melt can flow further before it solidifies, hence improving fluidity [55].

The change in the structure of the silicon to fibrous can also be achieved by rapidly cooling (quenching) or by the addition of certain elements such as Sr, Na, Eu, Sb, Ba, Ca, Y, Yb [52, 56]. Of which Sr, Na en Sb are only commercially used [5], the advantages and disadvantages of the modifiers are shown in Table 2.6.

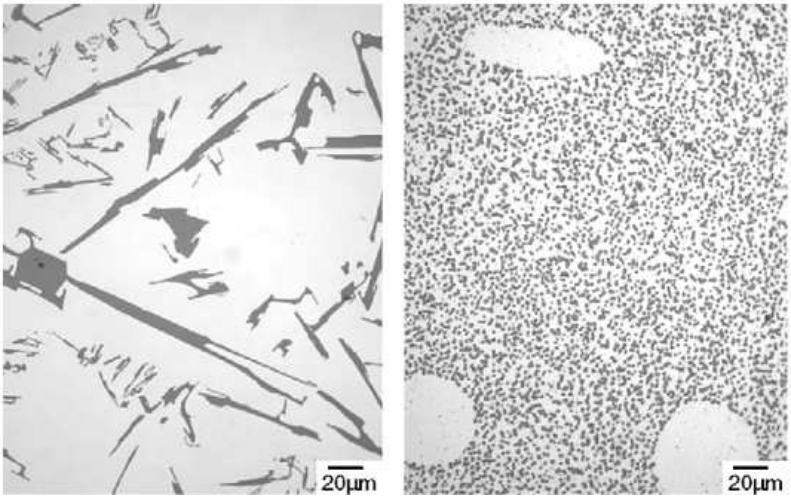

Figure 2.19: Eutectic Si modification with Sr (300ppm) before and after addition, respectively [53]

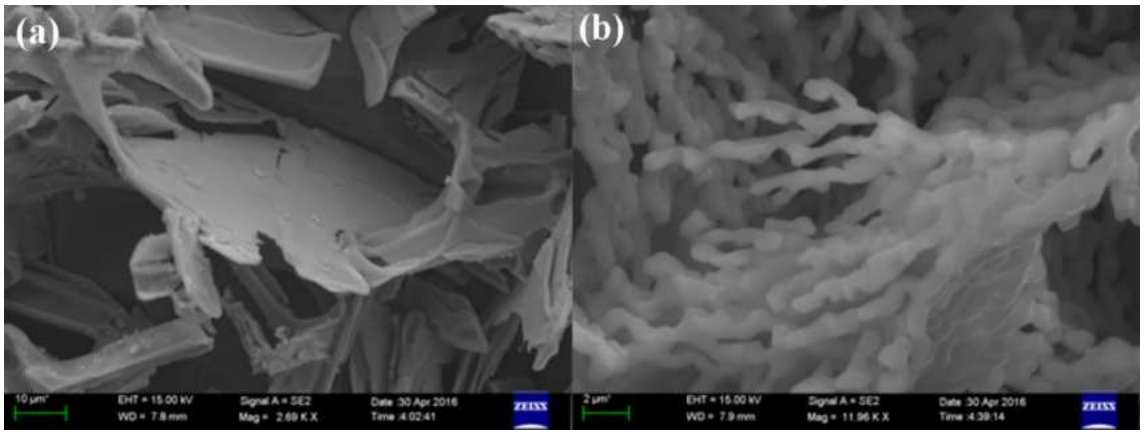

Figure 2.20: Eutectic Si (a) before and (b) after modification with 0.3wt% Eu [54]

Theoretically, elements with an atomic radius 1.65 times larger than that of Si are the most potent for modification, according to the restricted growth theory. Yb and Eu have an atomic radius ratio of 1.66 and 1.70, respectively. This means that Eu is a good candidate as a modifier of eutectic Si. It was found that Yb has less modification capability than Eu, despite its more ideal atomic radius. This implies that the modification capability does not depend solely on the atomic radius of the modifier [56].

Because fluidity is related to the initial stages of the solidification process. The modifiers of eutectic silicon are not expected to have a significant influence on fluidity, since the formation of the eutectic phase occurs at the end of the solidification of the alloy [11]. Bazhenov et al. [50] found that adding the Sr modifier, in the form of Al–10wt% Sr master alloy, does indeed not affect fluidity. Since the rather coarse crystals Al_4Sr, which are present in the master alloy, are fully dissolved and when the alloy subsequently solidifies, a much more compact Al_2Si_2Sr phase is formed which hardly hinders the flow. However, Mollard et al. [57] concluded that modification of eutectic Si by 0.3wt% Sr decreases fluidity at maximum 10% when the introduction of oxide films into the melt is minimised, since Sr

Table 2.6: Advantages and disadvantages of commercially used modifiers [5]

Modifiying agent	Si morphology achieved	Advantages	Disadvantages
Na	Fine fibers	No incubation time Mild sensitive to cooling rate	Rapid fade due to evaporation Low revocery rate Difficult to add Porosity redisribution Overmodification
Sr	Fine fibers	Melts not easy to over-modify Durable effect, easy addition and good recovery	Incubation period Relative high cooling rates favoured Porosity redistribution
Sb	Fine lamellae	Durable and modification effect remains even after remelting	Generation of harmful gas during additon Only refined lamellar structure achieved

forms larger intermetallics with Ti and B. Purkkanon et al. [49] investigated the effects of the addition of Sc to the A356 alloy on fluidity, Sc is an excellent grain refiner and efficient modifier of eutectic Si. It was found that with an increasing degree of modification, the fluidity increases at all pouring temperatures, as shown in Figure 2.22. The improvement in fluidity was expected to be the result of the grain refine ability of Sc.
Therefore, it seems that the modification of eutectic Si cannot significantly change fluidity. If fluidity is decreased, it is often because larger intermetallics have formed with the modifying element that impedes the flow, or the modifier poisoning the grain refiner, increasing the grain size. If fluidity increases, it can be attributed to a decrease in the solidification temperature or the grain refinement ability of the modifier.

Intermetallic Intermetallics are metallic compounds consisting of two or more (semi)metals, these metals often have extremely strong chemical bonds between them, which means that they are often hard, strong but also brittle [58]. Iron (Fe) is the most common impurity in Al-Si alloys and can form multiple intermetallic phases with several elements such as Al_3Fe, Al_6Fe, Al_8Fe_2Si, Al_5FeSi, $Al_8FeMg_3Si_6$ [31]. Some of these forms of intermetallics are larger platelets that harm the ductility of the aluminum alloy and can hinder the flow of the melt during filling, decreasing fluidity [59].

Mg can form Mg_2Si with Si levels above 2wt%, which appear as small dots in the matrix but will not form large needle-shaped shards. These Mg_2Si particals will not cause harm to the ductility of the matrix and/or hinder the flow at low levels. However, at higher Mg concentrations (>15wt%) larger intermetallics will decrease fluidity [60]. Several different intermetallics can be formed between different elements within the alloy. It can be expected that large intermetallics hinder the flow and thus have a negative effect on fluidity.

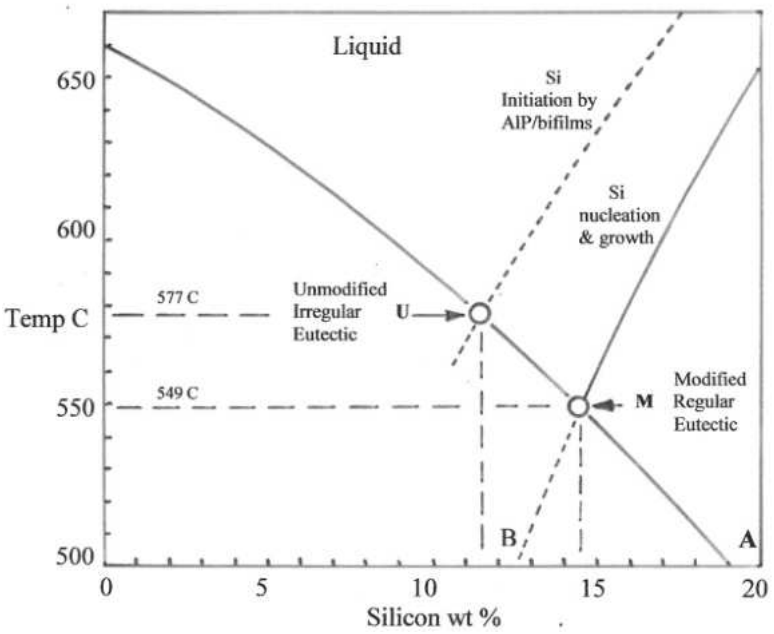

Figure 2.21: Lowering of the solidification temperature by restricting nucleation [55]

Specific heat capacity

Specific heat capacity (C_p) is the energy needed for 1kg of substance to raise its temperature 1K. It is expected from Equation 2.5 that fluidity will increase linearly with increasing C_p. This is logical since the flow has more energy which needs to be dissipated before the flow solidifies. However, C_p is alloy dependent and thus not a parameter which can be adjusted independently. The C_p is not expected to change significantly when small amounts of elements are introduced into the melt.

Latent heat of fusion

Latent heat of fusion, or heat of fusion (HoF) is the amount of energy produced by converting 1mol of material from liquid to solid state. One of the reasons why the Al-Si alloy system has such high fluidity can be partly contributed to the high HoF of primary silicon, which is 3.7 to 4.5 times that of aluminum [61]. This effect starts to be significant at high levels of Si (>10wt%). This means that the Al-Si alloy has more stored energy, and thus will remain longer in the liquid phase, which increases fluidity.

Viscosity

Viscosity does not significantly change with temperature and thus can be considered constant [29]. Ealier formulation of Equation 2.5 contained a viscosity term but later formulations dropped this terms since the effect of the (change in) viscosity is significantly smaller than the experimental scatter [62]. Furthermore, viscosity is difficult to measure accurately; this explains that there is a 400% difference in the reported viscosity of Al alloys.

Viscosity is heavily influenced by melt cleanliness, this means that a dirtier melt has a higher viscosity. Therefore, it is assumed that the lowest reported viscosity (cleanest melt) is the most accurate, which is 1 to 1.4 $mPa \cdot s$, roughly the same viscosity as water at

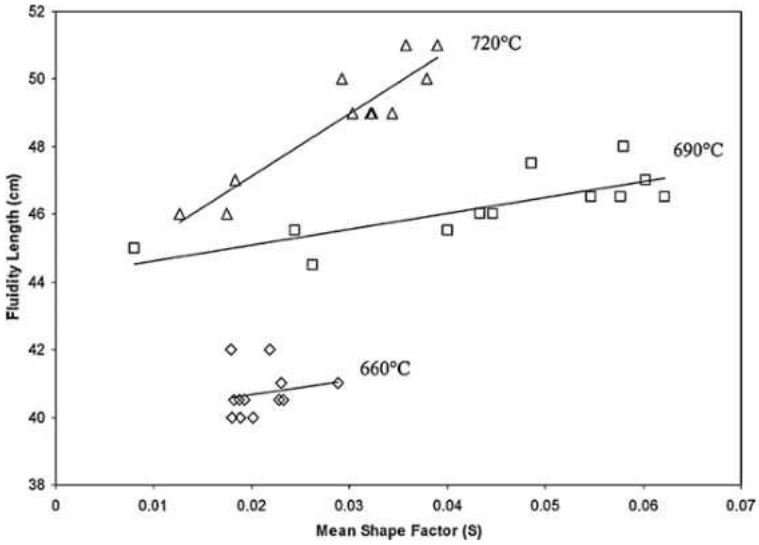

Figure 2.22: Fluidity of A356 alloy dependent on shape factor (higher shape factor means finer modification) of eutectic silicon and casting temperature [49]

room temperature. Furthermore, it can generally be said that for Al alloys the viscosity increases when including Ti; Ni; Cu; Cr; Mn; and decreases with the addition of Si [63].

2.5.2 Mold parameters

Cavity geometry

The geometry of the mold cavity and gating system determine the filling behavior of the mold and should be designed in such a way as to quickly fill the mold cavity, without creating turbulence in the flow. Furthermore, air entrapment should be minimised to decrease back pressure and avoid porosity [64]. The orientation of the cavity also determines the metallostatic pressure available to overcome capillary repulsion and fill the small features of the mold.

Furthermore, the solidification modulus (M) is very important for the solidification time of the gate/mold geometry. The solidification/section modulus is the ratio between the casting volume (V) and the effective cooling portion of its surface (S). The solidification modulus was described in Chvorinov's rule from 1940 [35], and reads:

$$t_s = C_m M^n = C_m \left(\frac{V}{S}\right)^n \tag{2.6}$$

Where t_s is the solidification time, C_m mold constant and n is an exponent usually between 1.5 and 2. C_m should be found experimentally. It must be noted that the solidification time is exponentially dependent on the section modulus, this is one of the reasons the filling of thin-walled sections is difficult. Since fluidity is the distance traveled by the melt before it is stopped by solidification, solidification time is directly proportional to fluidity length.

Thermal conductivity

Thermal conductivity of the mold determines how fast the temperature drops in the molten metal, and thus solidifies. Permanent molds, usually made of steel, conduct significantly more heat away than sand molds. Therefore, coatings can be applied to decrease the heat transfer to the mold. A mold with a higher thermal conductivity will decrease fluidity.

Mold temperature

Another method of decreasing the heat flux to the mold is to increase the mold temperature before casting. This decreases ΔT between the molten metal and the mold. This is done only in permanent molds, at temperatures between 200 and 500°C [29]. Also, the size of the mold can influence the heat extraction; a bigger mold has a higher thermal capacity, and thus can extract more heat from the melt.

Mold wettability

In permanent mold casting, it is undesirable to have the molten aluminum in direct contact with the steel mold. This will lead to the soldering of the steel mold which makes the cast product stick to the mold. This results in faulty products and down-time to clean the mold. To prevent this, coatings and release agents are used to decrease the wettability of the mold.

If the wettability is decreased, the metal flow front will experience capillary repulsion (P_{CR}). This back pressure needs to be overcome to fill the smaller sections of the mold. In gravity casting, this capillary repulsion needs to be less than the metallostatic pressure (P_{HS}) to be able to fill smaller features of the mold. Therefore, the following condition needs to be met.

$$P_{HS} > P_{CR} \Rightarrow \rho g h > 2\gamma(\frac{1}{r} + \frac{1}{R}) \tag{2.7}$$

In which ρ, h, γ, r and R are the density of the molten metal, metal head above the area that needs to be filled, surface tension, and characteristic radii respectively. Since the most difficult parts of the mold are in thin-walled sections, such as structural or cooling ribs as shown in Figure 2.23, $r << R$ or vice versa. Therefore, the expression in Equation 2.7 becomes:

$$\rho g h > \frac{2\gamma}{r} \tag{2.8}$$

An increase in the surface tension of the alloy decreases the mold wettability, making it harder for the alloy to flow into the mold and thus decreasing fluidity. The effect becomes significant in extremely thin-walled castings ($<$ 1mm). But for the majority this effect remains minimal and can be neglected [11].

2.5.3 Experimental parameters

Flow velocity

To increase the fluidity length, the flow velocity can be increased or the solidification time can be prolonged, which makes intuitive sense. This relation, in Equation 2.9, was first stated by Flemmings et al. [66].

Figure 2.23: Structural ribs in casting, where the thickness to height ratio is small [65]

$$L_f = V \cdot t_s \tag{2.9}$$

However, there are clear limits to the velocity that can be used to keep sound mechanical properties in the final casting. The velocity can not be too high which results in surface turbulence, this will lead to surface oxides entrapments (also called bifilms) of which the effects will be discussed in detail in the section melt cleanliness, section 2.5.3.

When a molten metal fills the cavity its flow front reacts with the oxygen in the mold and creates an oxide film. Since the oxide film will get stuck between the flow and the wall the oxide film will tear open and the molten metal reacts, again, with the oxygen in the mold. Creating a continuous process of oxide film production, as can be seen in Figure 2.24.

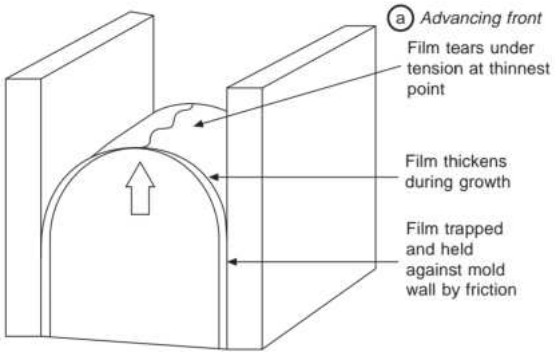

Figure 2.24: Tearing of oxide film on advancing flow front [29]

To ensure that no bifilms are trapped in final casting, cavities are commonly filled from the bottom up, at velocities below the critical speed to prevent jetting, as shown in Figure 2.25. When jetting occurs, the surface tension cannot contain the kinetic energy of flow, which results in surface turbulents.

This critical flow velocity V_{crit}, at the flow front, can be estimated by equating the surface tension, divided by the radius of the flow front to the inertial pressure and writing it in terms of V_{crit}. This equation can also be obtained by using the dimensionless Weber number. The Weber number in Equation 2.10, gives the ratio of fluid inertia to surface

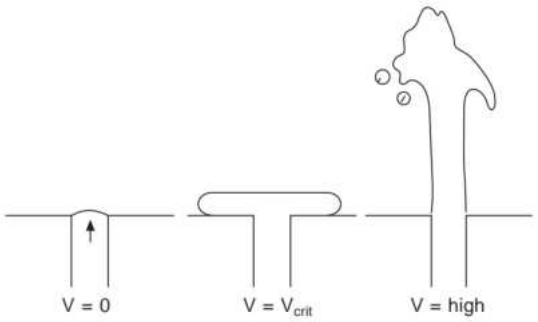

Figure 2.25: Different flow velocities during the mold filling process [29]

tension. U is here the average velocity component, normal to flow front and l will be the smallest dimension of the width or height of the channel. These inertial forces can create surface turbulence, which can create bifilms [42]. If $We > 1$ the flow cannot be confined within the free surface and air and bifilm entrapment within the bulk liquid can be expected [27]. In the case of $We > 60$ the surface will break up into small droplets [67].

$$We = \frac{\rho U^2 l}{\gamma} \tag{2.10}$$

$$\frac{1}{2}\rho V^2 = \frac{2\gamma}{r} => V_{crit} = 2\sqrt{\frac{\gamma}{r\rho}} \tag{2.11}$$

Since the flow also needs to fill large cavities the flow radius can be approximated by its natural flow radius (r in Equation 2.11) in the model of the sessile drop, Figure 2.26. Sessile means sitting and this figure presents a drop on a non-wetting surface. The height h will be determined by the gravity forces pulling the drop flat and the surface tension making the drop as round as possible to minimise surface area.

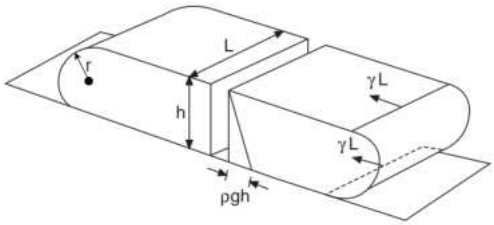

Figure 2.26: Sessile drop analysis to determine natural flow radius [29]

The force pushing the flow front to the sides is the average metallostatic pressure $\rho gh/2$ multiplied by the area hL. We can assume that $h = 2r$. This force needs to be balanced by the surface tension $2\gamma L$, resulting in:

$$\rho g r \cdot 2rL = 2\gamma L => r = \sqrt{\frac{\gamma}{\rho g}} \tag{2.12}$$

Alternatively, the dimensionless Bond number can be used to calculate r. The Bond number, in Equation 2.13, gives the ratio of gravity to surface tension. If the flow front width

l is large and thus $Bo > 1$ the flow front will be flat. If $Bo < 1$ the flow front will have a more spherical morphology [27]. l is the characteristic length, which in this case is the radius r.

$$Bo = \frac{\rho g l^2}{\gamma} \tag{2.13}$$

Using this expression in Equation 2.11 provides a fairly simple but general equation to calculate the critical velocity:

$$V_{crit} = 2 \cdot \sqrt[4]{\frac{\gamma g}{\rho}} \tag{2.14}$$

Since the critical velocity V_{crit} is a function of surface tension γ and density ρ taken to the fourth root, almost all metals have, in their liquid form, a critical velocity of between 0.3 to 0.5 m/s [29], as can be seen in Table 2.7. However, if the melt is heavily oxidated its apparent surface tension can be up to three times its original surface tension [32]. This would increase its critical flow velocity by a factor of $\sqrt[4]{3} = 1.32$. Multiple authors have confirmed that the oxide skin of the melt can greatly affect the flow of the melt [68, 69].

Table 2.7: Critical height and velocity of common casting metals and water for comparison [29]

Liquid	Density kgm^{-3}	Surface Tension Nm^{-1}	Critical height h mm	Critical velocity ms^{-1}
Ti	4110	1.65	12.8	0.50
Al	2385	0.914	12.5	0.50
Mg	1590	0.559	16.0	0.42
Fe	7015	1.1872	10.4	0.45
Ni	7905	1.778	9.6	0.43
Cu	8000	1.285	8.1	0.40
Water	1000	0.072	5.4	0.33

Ingate pressure

The velocity of the melt is, in gravity die castings, a consequence of pressure which is created by the metallostatic pressure. As discussed in section 2.5.1, the flow of molten metal in long freezing range alloys is halted when the dendrites impinge on one another and this network becomes strong enough to resist the metallostatic pressure. If the pressure is higher than the strength of the network, burst feeding occurs, where the dendrites will break and the filling of the mold continues, which is the case in HPDC where pressures reach 20 bar. This is why fluidity is not considered a major factor when selecting the alloy used for HPDC casting.

Superheat

Superheat is the temperature at which the casting takes place minus the melt temperature of the alloy. It is found that fluidity increases linearly with superheat [70]. This is also illustrated well by Evans (1951) [10] in Figure 2.27. This makes intuitively sense, since if more heat is given to the melt it can flow further before it solidifies.

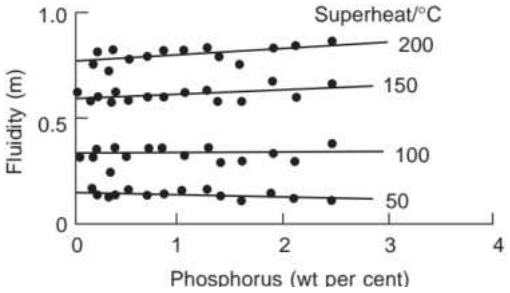

Figure 2.27: The effect of superheat on fluidity at different phosphorus addition ratios [10]

Melt cleanliness

The amount of particles and oxides in the melt determines the melt cleanliness. It was found that folded oxide inclusions within the bulk metal, called bifilms, decrease mechanical properties in the final casting and can reduce fluidity, especially at lower pouring temperatures [14]. This trend can be seen in Figure 2.30. Bifilms are created by turbulence of the melt surface, as shown in Figure 2.28 or by introduction of charge material, alloying elements, or fluxes, as shown in Figure 2.29. Bifilms are inevitable to be created during the casting process by pouring, stirring, fluxing, degassing and/or skimming [13]. The problem with bifilms in aluminum alloys is that they are close to neutrally buoyant, since the oxide skin is denser than the melt but the air inside the bifilm is less dense than the melt, which is combined neutrally buoyant. This is not a problem for ferrous and copper-based alloys, where their oxides are lighter than the melt. On the other side, lithium and magnesium alloys have oxides that are denser than the liquid, causing them to sink to the bottom of the crucible [10].

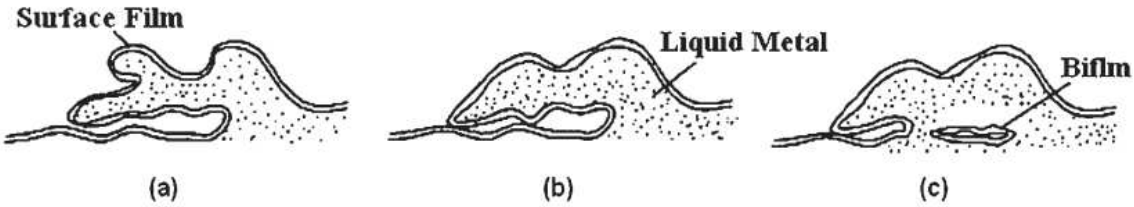

Figure 2.28: Creation of bifilms through surface turbulence [71]

Methods have been proposed to measure the cleanliness of the melt. Such as the Quality Index (QI) by Drouzy et al. [72] who measured the yield strength and elongation at fracture, with these values a score was assigned to the alloy. Erzi et al. [73] also included ultimate tensile strength (UTS), fluidity length and bifilm index. Bifilm index (BI) is a measure of the number and length of the surface oxides which are entrapped within the bulk metal and was first proposed by Dispinar and Campbell [13].

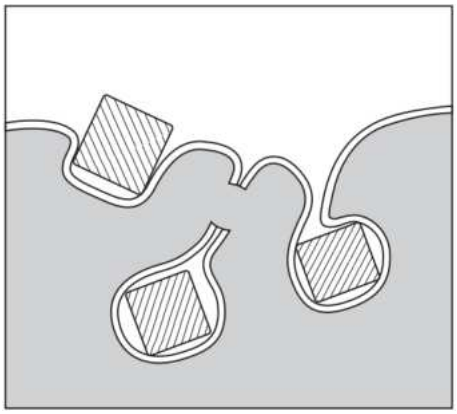

Figure 2.29: Introduction of bifilms into the bulk of the melt by addition of charge material, alloying elements, fluxes and/or older oxides [27]

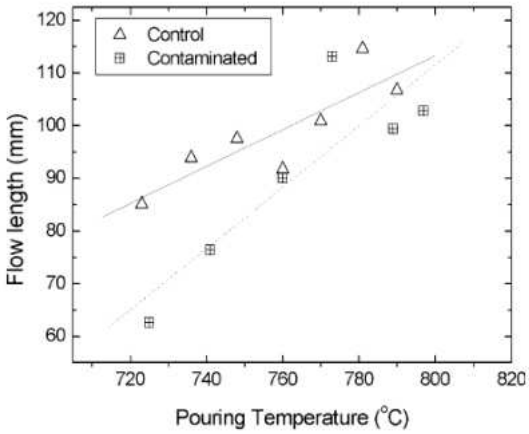

Figure 2.30: Lower fluidity for contaminated A356 alloy melt [14]

Since bifilms can be nanometers thick (and more than 10mm long), this is invisible for most inspection methods. Therefore, the reduced pressure test (RPT) can be used to make these bifilms visible. The RPT works by taking a sample of molten metal and letting it solidify in a partial vacuum environment, usually 80mbar. This expands the air and hydrogen gas, which diffused into the film, creating a larger pore. After solidification, the sample is cut in half and polished. After which, the pore length can be summed, in Equation 2.15, to arrive at the BI with units mm [13]. The BI score and accompanying melt quality definitions are given below: [74]

- $0 \leq$ BI ≤ 10 mm: high-quality melt
- $10 \leq$ BI ≤ 25 mm: good quality
- $25 \leq$ BI ≤ 50 mm: average quality
- $50 \leq$ BI ≤ 100: unacceptable quality
- BI ≥ 100: bad quality that should be avoided

$$BI = \sum (maximum\ pore\ length) = L_p \tag{2.15}$$

The influence of oxide content on fluidity was investigated by Timellio et al. [75] in a spiral sand mold. The shortest spiral, compared to the longest spiral, was found to have a comparable average pore size, but a 72% higher bifilm index, indicating that BI is a better measure for calculating melt cleanliness compared to measuring the average pore size. Five tests were carried out at the same temperature ($700°C$) and the longest spiral had 14.7% better fluidity. Erzi et al. [73] investigated the use of a supplier quality index (SQI) with which they can score the raw materials of different suppliers . This SQI in calculated in the following manner:

$$SQI = (YS + UTS + \%e + F) - (BI) \tag{2.16}$$

In which YS, UTS, $\%e$, F and BI are the yield strength, ultimate tensile strength, elongation at fracture, fluidity and bifilm index respectively. It must be noted that all variables except bifilm index should be as high as possible to come to the highest score.

Such a quality index is not very suitable for day-to-day control of the melt since preparing specimens for a tensile test and polishing samples to measure BI is time-consuming. However, such index can be used when the foundry receives a new batch of raw materials or when changing suppliers.

For a foundry to improve the quality of their melt they can use a degassing operation and/or use salt fluxes to clean the melt. With degassing an inert gas, often Ar or N_2, is fed through an impeller into the melt. The impeller stirs the melt and the bubbles flow through the melt, taking the oxides to the surface where they can be skimmed off the surface [76]. Fluxes can be added to the melt, often in granular form, to react with unwanted elements in the melt. When designed correctly, these reaction products are less dense than or more dense than molten aluminum, resulting in these impurities floating to the surface or settling at the bottom of the crucible. The impurities which float will be skimmed off during the removal of the dross. Dross is an oxidation layer that floats on top of the melt. Fluxes also serve the purpose of creating a layer over the melt such that aluminum does not react with oxygen and creates dross, resulting in loss of usable aluminum, which is undesired [77].

2.6 Summary

In this chapter, an introduction is given to aluminum alloys and the most common casting processes. The most important casting defects are discussed and the importance of fluidity is highlighted. Methods of measuring and mathematically estimating fluidity have been discussed. It was concluded that analytical and/or numerical mathematical models are limited in estimating fluidity, since the parameters involved in calculating the fluidity are often not accurately known and the sensitivity of these parameters to the fluidity is strong. From the parameters that influence fluidity, the solidification behavior has the largest effect and is determined by alloy composition, grain refinement, modification of eutectic Si and the formation of intermetallics. Melt cleanliness, and in particular the presence of bifilms, can have a substantial effect on the fluidity when present in large quantities. Increasing the volume-to-surface ratio of the channels in the mold increases quadratic solidification time and thus increases fluidity. The thermal conductivity of the mold can be altered with coatings, but is mainly determined by the material of the mold. Flow velocity should be controlled ($<$0.5-0.65m/s for aluminum alloys) to prevent major surface turbulence during casting; therefore, pouring from great heights should be avoided. Superheat increases the fluidity linearly while changes in viscosity, latent heat, specific heat capacity and mold wettability have minor effects on fluidity and can often be neglected.

3. Mold Design

From the previous chapter, it is known that solidification behavior and melt cleanliness are the most significant parameters which affect fluidity. In this chapter, new fluidity molds are proposed with the goal of keeping the mold and experimental parameters constant. Such that the change in the metallurgical parameters, due to the different addition ratios of Er and Eu, is the only variable during the experiments. To this end, existing fluidity mold designs from the literature are analysed and their shortcomings are be discussed. After which, the functional aspects of the molds are highlighted and finally the design considerations per mold and experimental parameter are explained. Lastly, a method is discussed to validate whether the mold and test procedures are capable of reliably measuring fluidity. In this chapter, research questions three to six of Objective 2, from section 1.2, are answered.

3.1 Analysis of existing fluidity mold designs

As discussed in subsection 2.4.1, multiple designs have been proposed. However, these designs have some problems to keep the mold parameters and/or the experiment parameters constant, which affects the fluidity measurement.

Vacuum mold

The vacuum mold has some technical limitations. Firstly, the mold i.e. the narrow quartz tube is partially submerged in the metal, consequently heating the tube, this makes the mold temperature dependent on the temperature of the melt and makes it time-dependent. Secondly, if the relative distance from the melt surface to the tube is not constant during and/or between tests, the ingate pressure will not be constant. This can be a consequence of the operator filling the crucible to different levels or the melt level will drop since metal is extracted from the crucible during the test.

Spiral mold

The spiral mold has the problem that the constant curvature of the channel makes the flow velocity in the channel nonuniform along its cross-section. This creates a difference between the cooling rate of the melt on the inside and outside of the curvature. Moreover, during the experiment the melt will enter the mold and heat is extracted, in turn heating the mold. This preheats sections of channel, later in the mold, which locally increases the mold temperature, as shown in Figure 3.1. This can lead to higher fluidity if the melt reaches these preheated areas.
Therefore, the proposed design should have straight channels and the channels should not be able to preheat other channels during testing.

Figure 3.1: Preheating later sections of channel by introduction of melt to the mold

Octopus mold

Although the octopus mold has multiple channels, these channels do not experience the same experimental parameters. The channels furthest from the sprue have less superheat because the mold already extracted heat from the flow, when the melt reaches these channels. In addition, these channels are filled first since the flow is redirected from the well, at the bottom of the sprue, to the sides of the mold. Creating higher dynamic pressure at the end of the runner, which is illustrated by the simulation in Figure 3.2.
Therefore, the proposed design should have a single channel or multiple channels directly connected to the sprue such that the distance from the sprue to the channel is consistent.

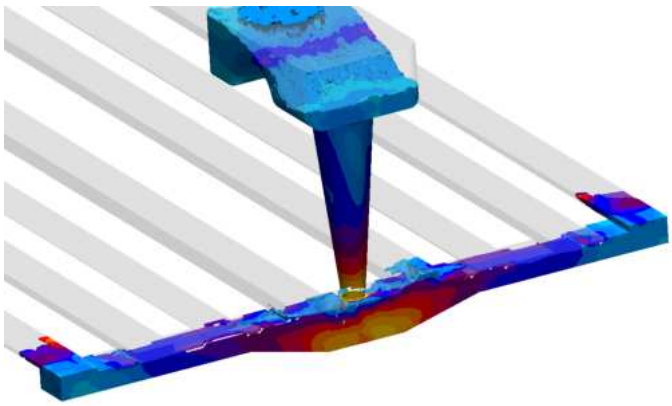

Figure 3.2: Channels furthest from the sprue are filled first due to higher dynamic pressure

Star Mold

The star mold ensures same superheat for all channels. However, the channels are hydraulically connected to the central hub, as shown in Figure 3.3. This makes the ingate pressure depend on the flow rate of the other channels. If a stopper is used and thus the pouring basin is fully filled before the melt is allowed to enter the mold and the volume of the pouring basin >> the casting volume, then it can be assumed that the melt level of the pouring basin remains almost the same, ensuring even pressure during the experiments.

Another problem with this design is the pressure surges caused by a phenomenon called hydraulic transients, also known as water hammer experienced in plumbing. This occurs when an incompressible flow quickly comes to a hold, for example when the aluminum fills

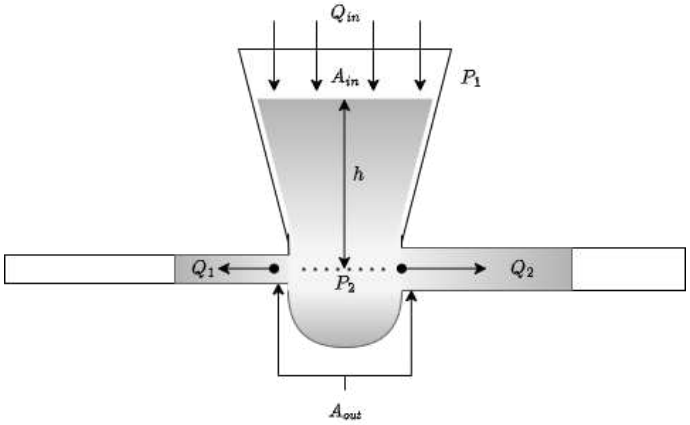

Figure 3.3: Ingate pressure dependency on melt velocity

a channel completely. All the kinetic energy is suddenly converted into a pressure wave which propagates back through the channel. This can fill other channels further which would not be able to do themselves. This can result in higher fluidity for smaller cross-sectional area channels.
Therefore, the proposed design should ensure a large enough pouring basin volume such that the ingate pressure is not dependent on the filling behavior of other channels and the opening to the channels should not be directly inline with other channels to prevent the problem with the hydraulic transients.

3.2 Proposed designs

The proposed designs of the molds are based on existing molds and comply to the requirements described in Appendix 7.3, ensuring both functionality and reliability in fluidity measurement. The Radial Quad mold in Figure 3.4a is an improved version of the Star Mold and the Vacuum mold in Figure 3.4b is an improved version of the existing Vacuum mold / Ragone test. The technical drawings of the Radial Quad and Vacuum mold can be found in Appendix 7.4.1 and 7.4.2 respectively. The Radial Quad mold has four arms which are bolted to a central plate to ensure alignment with respect to each other. Since this molds consists out of four separate arms, the melt from one channel cannot preheat another channel. In the center, a disposable isolating pouring basin is installed in which a conical stopper is placed, where during the experiments melt will enter the mold. The technical drawings of the mold to produce the isolating pouring basin can be found in Appendix 7.4.3. The arm(s) of both molds have three bolts to level the mold before use, such that the metallostatic pressure is constant along the channel. Length indications were engraved on the drags such that reading the fluidity length is easy after casting. The Vacuum mold uses a disposable low-carbon steel bent tube to suck melt from the crucible. This tube is made airtight by two silicone O-rings placed on the outside of the tube. To make the rest of the molds also airtight a silicone (60 Shore A) gasket is used, as shown in blue in Figure 3.4b, and mechanical pressure is applied by four toggle clamps attached to the cope of the mold. The partial vacuum is applied on the rear side of the mold where the tube is attached to a hosetail, a schematic overview of the vacuum setup is given in Figure 3.5.

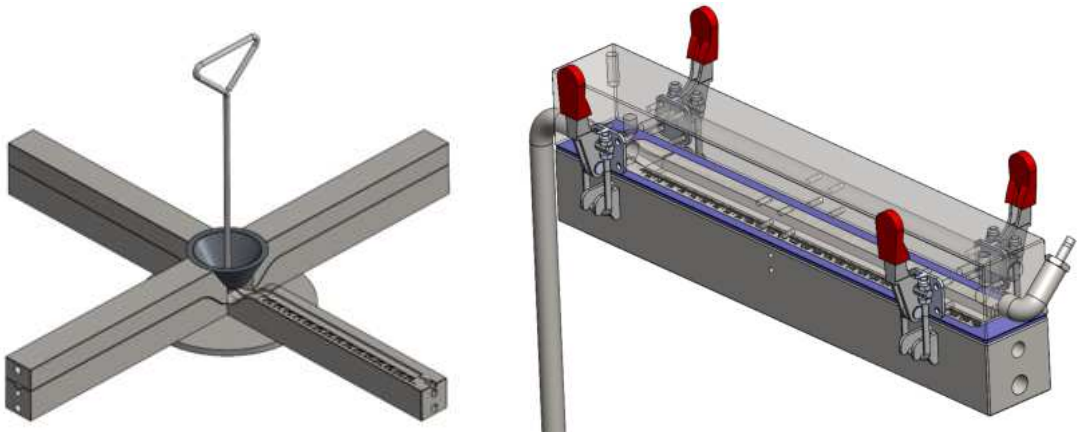

(a) Radial Quad mold (b) Vacuum mold

Figure 3.4: Proposed improved fluidity test mold designs

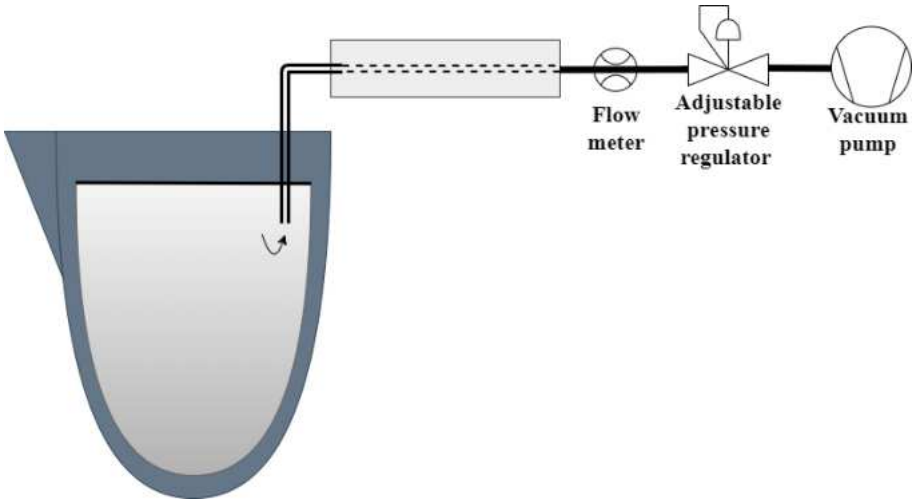

Figure 3.5: Schematic overview Vacuum mold setup

3.2.1 Mold parameters

To ensure constant mold parameters, that is, the cavity geometry, thermal conductivity, mold wettability and mold temperature, it was chosen to design permanent molds. This also meant that multiple results could be obtained quickly from one mold, which eliminates the labor intensive mold-making process in sand castings. The molds were made of stainless steel 1.4401 (X5CrNiMo17-12-2) to ensure that the molds do not corrode during longer storage periods.

Cavity geometry

The idea of having multiple channels of different dimensions, for the Radial Quad design, is to be able to see the difference in flow behavior when the section modulus of the channel changes and to determine the minimal channel height that can be filled with which composition. The dimensions of the channels were based on the literature, which were slightly altered based on the results of simulations. Durmus et al. [31] used a permanent mold with 4 channels with 2,4,6 and 8mm height which were 20mm wide and 300mm long of which the 2mm channel almost never filled. Colak [12], used the octopus design in a sand mold

with channel heights of 0.5,1,2,3,4,5,6 and 8mm which were 20mm wide and 500mm long. The 6 and 8 mm channels always fully filled and the 0.5mm channel never filled in the experiments. Pulivarti et al. [78] used a star shape design in a sand mold with channels of 2,4,6 and 8mm height, 30mm wide and 250mm long.

From the simulations, in Figure 3.6, it was found that the 3,4,5 and 6 mm channels provided a good range for the A356 alloy at a critical solid fraction of 20% [42]. The 3mm channel only filled a little and the 6mm channel got almost fully filled during simulations. Therefore, improvements or degradation of the fluidity could be measured. Because the mold is made from stainless steel the thermal conductivity of the mold is significantly higher than that of a sand mold, therefore, a channel length of 300mm was sufficient. The channel width was set at 15mm to ensure a smooth metal flow front, which made reading the fluidity measurements also easier.

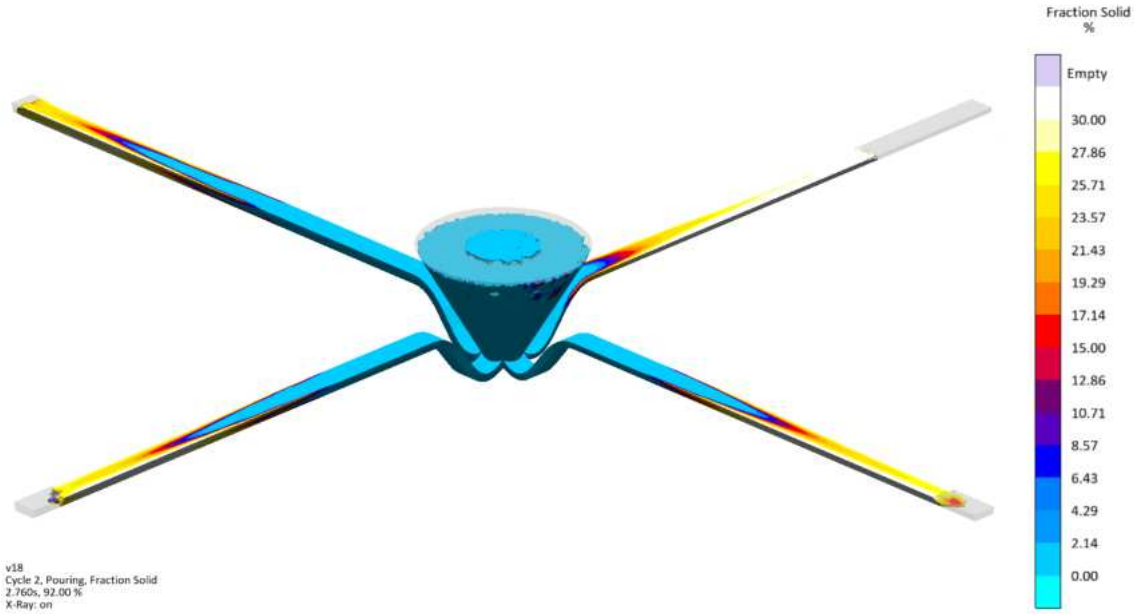

Figure 3.6: Fraction solid simulation with a critical solid fraction of 20%

Thermal conductivity and mold wettability

Since the mold does not change during or between tests, the thermal conductivity can be assumed to remain constant. However, at the start of the trials, the mold was coated with a thin ($< 100\ \mu$m) spray-on boron nitride. This coating ensures that the molten aluminum does not solder to the permanent die. The degradation of this thin layer is not expected to have major influences on thermal conductivity or mold wettability during fluidity tests, because the boron nitride has about 27 times the thermal conductivity of stainless steel (in hexagonal form) [79]. Therefore, the heat conduction from the melt to the mold is limited by the thermal conductivity of the mold itself. As long as a visible layer of boron nitride was on the mold, the mold wettability was assumed to be constant.

Mold temperature

The dies of, both molds, are heated to a common mold temperature of 250°C ±3°C and accurately controlled by the Fitron 8 TP. Heating elements are installed in all copes and drags and thermal couples are located in all drags. For the vacuum mold, the melt is drawn through a single use metal straw. As discussed in section 3.1 the mold temperature is melt temperature dependent. Therefore, to ensure the same conditions throughout the fluidity experiments, a surface-mounted thermocouple was installed on the shorter horizontal part of the straw, shown as a red dot in Figure 3.7. The vacuum was applied to the system when the temperature of the straw reached 250°C.

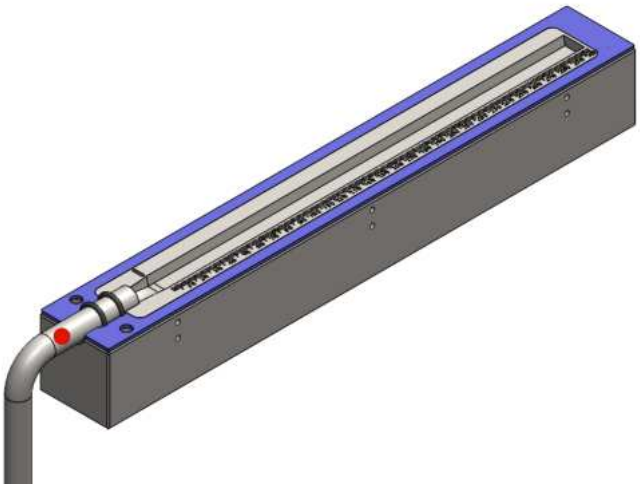

Figure 3.7: Red dot: Location of surface-mounted thermocouple on metal straw

3.2.2 Experimental parameters

Flow velocity

The curvature of the entrance to the channel, indicated in red in Figure 3.8, is designed such that the melt fills the channels of the Radial Quad mold in a slow and controlled manner. When the stopper is removed from the pouring basin the melt experiences a short free fall which greatly increases the flow velocity of the melt. This is unwanted since surface turbulence might occur, therefore the flow is redirected such that the flow is driven by metallostatic pressure instead of the initial dynamic pressure when filling the channels. Because measurement of the melt flow velocity is not practical, due to the high-temperature (>700°C) conditions which are present during fluidity tests, the flow is simulated to check if there will be no significant surface turbulence during the filling procedure. In Figure 3.9, the moment is shown when the melt enters the channel, at about 0.55m/s which is expected to not cause any major surface turbulence. Since there is plenty of oxygen in the mold, an oxide layer will be created increasing its apparent surface tension and increasing the critical flow velocity, as discussed in section 2.5.3.

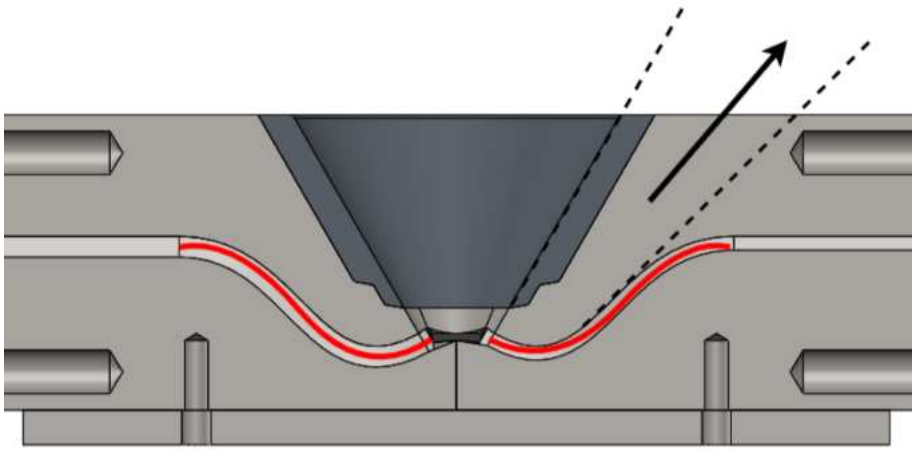

Figure 3.8: Curved entrance to channel for flow control

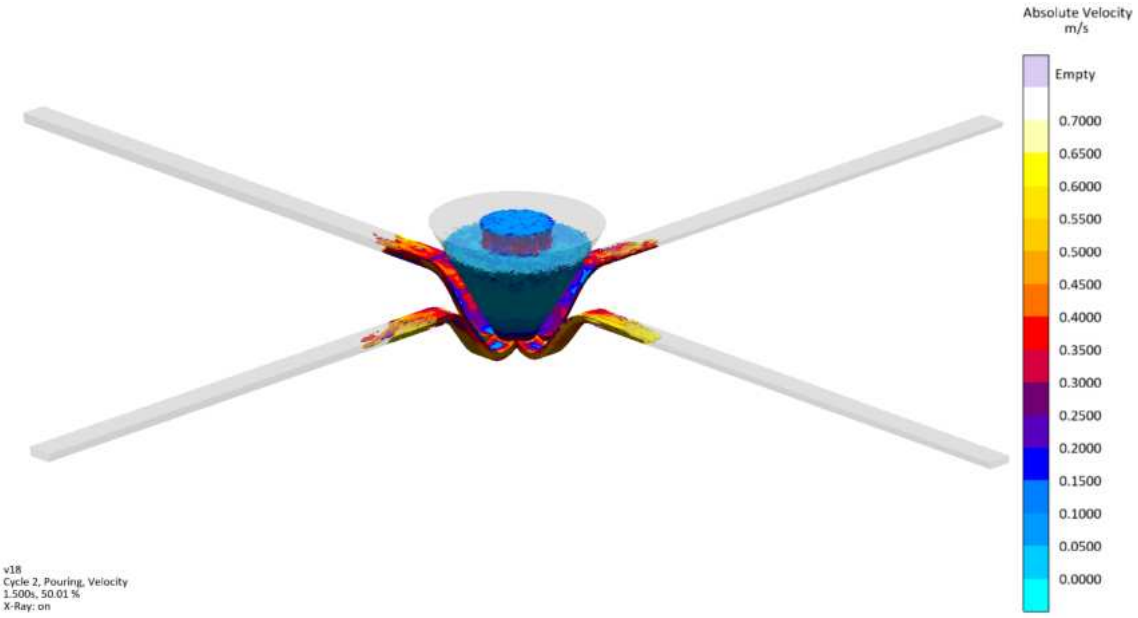

Figure 3.9: Flow velocities about 0.55m/s when entering the mold

For the Vacuum setup, the melt velocity is determined by the airflow rate through the mold divided by the cross-sectional area of the mold. A more complete description and example of the calculation are given in Appendix 7.2.

Ingate pressure

For the Radial Quad mold, the volume and shape of the pouring basin was designed such that it could fill multiple times the volume of the channels, without effecting the level of the melt in the pouring basin significantly when the stopper is removed to ensure a uniform ingate pressure. In addition, the design of the pouring basin, as simulated in Figure 3.11, has an overflow, which ensures that the pouring basin can be filled until melt comes out of the overflow, this ensures constant metallostatic pressure for every test, as shown in the Figure 3.10. Moreover, the possible hydraulic transients, discussed in section 2.4.1, are redirected in the direction of the pouring basin instead of towards other channels, as shown in Figure 3.8.

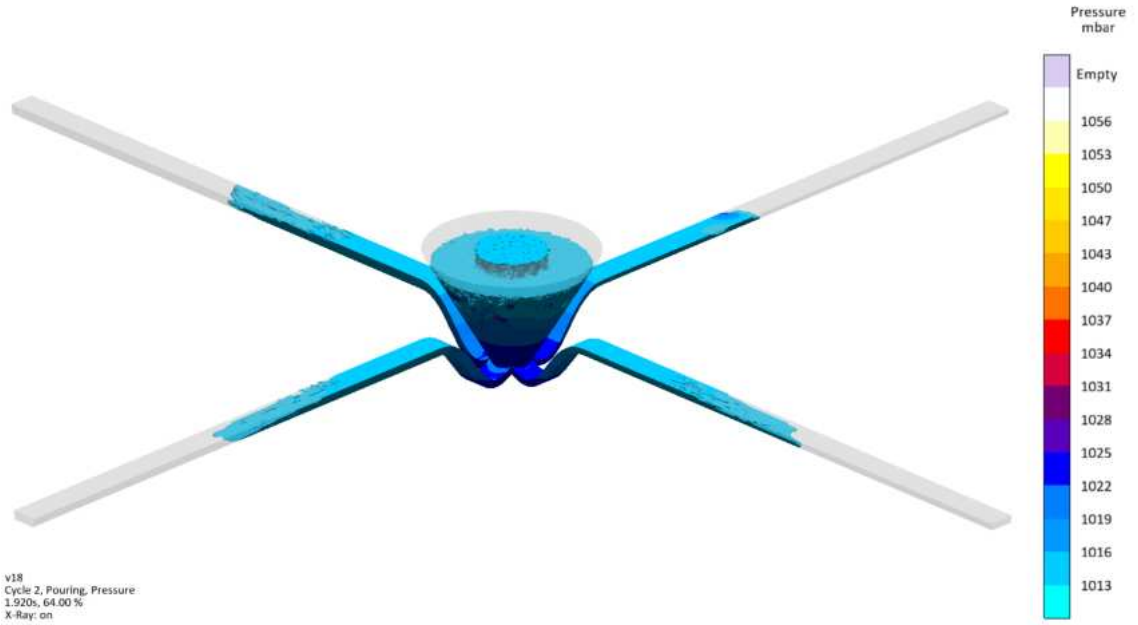

Figure 3.10: Pressure distribution in Radial Quad during filling

For the vacuum setup, the ingate pressure is determined by vacuum level applied to the system. As discussed in section 3.1, the ingate pressure is dependent on the height between the level of the melt and the mold. Therefore, every time at the beginning of a series of fluidity tests, the pressure setting needs to be adjusted accordingly. See Appendix 7.1, for a detailed description of the required pressure setting. This pressure setting can be kept constant during the tests, as the amount of melt sucked from the crucible is negligible compared to the volume in the crucible. Therefore, the melt level will not change significantly. To be able to compare the results of the experiments, the vacuum setting is chosen such that it is equivalent to the metallostatic pressure experienced in the Radial Quad mold, which corresponds to a metal head of 35mm.

Superheat

For the Radial Quad setup, the superheat was controlled by a thermocouple attached to the stopper, which was removed when the temperature reaches $725°C$. The pouring basin was made out of an isolating material such that the melt would not cool too quickly for the operator to react and remove the stopper. The isolating pouring basin can be seen in Figure 3.11.

(a) Isolating pouring basin (b) Cross-section of isolating pouring basin

Figure 3.11: Design of isolating pouring basin with overflow

For the Vacuum setup, the straw is directly inserted into the melt. Therefore, the temperature of the melt is directly correlated with the temperature entering the mold. To have a melt temperature of 725°C when entering the mold, the same as in the Radial Quad setup, a simulation was performed from which it was determined that the furnace temperature should be set to 800°C, as shown in Figure 3.12.

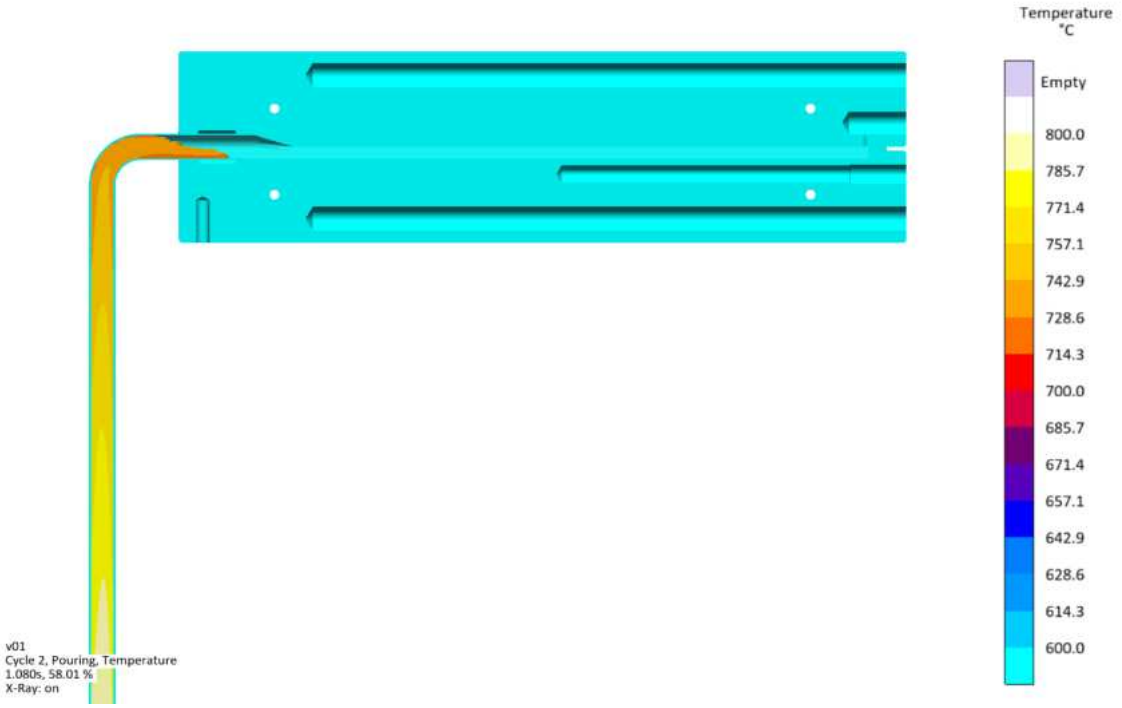

Figure 3.12: Simulation of Vacuum mold (cross-section) with 800°C melt temperature ensures ingate temperature of 725°C

3.2.3 Validation of the mold and test procedures

To test whether the new mold and test procedures can be considered capable measuring systems to measure fluidity, a Gage Repeatability and Reproducibility (Gage R&R) study is conducted. The measurement system is considered capable if the variation in the measurement system is small compared to the variation of the product/process, which in this case is the inherent variation of the fluidity of the alloy. The different sources of variation during an analysis of the measuring system are shown in Figure 3.13, where the variation due to the equipment is called repeatability and the variation due to the appraiser/operator is called reproducibility. The Gage R&R as calculated as follows:

$$GageRR = \sqrt{EV^2 + AV^2} \tag{3.1}$$

Where EV and AV are the equipment and appraiser variation, respectively. EV is calculated by the range (the highest minus the lowest) measurement of a part by the same operator. The variation measured be attributed to the measurement device itself. AV can be calculated by letting multiple operators measure the same parts and with the difference between the averages of the measurements, per operator, the AV can be determined. Lastly, the part-to-part variation (PV) can be calculated by measuring multiple identical parts, multiple times and with the difference between the average measurements, of different parts, part-to-part variation can be established. To see if the measuring system is capable, the GageRR percentage should be calculated of the total variation. To calculate the total variation, the following equation should be used:

$$TV = \sqrt{GageRR^2 + PV^2} \tag{3.2}$$

The measurement system is considered capable if the Gage R&R $< 10\%$ of the total variation. If $10\% <$ Gage R&R $< 30\%$ the measurement system can be used depending on the measurement method, application and the risks involved. Lastly, if Gage R&R $> 30\%$ the system is considered not capable and the system requires improvement. The mathematical calculations are described in detail by Cepova et al. [80]. To collect enough data, three fluidity tests are performed on four compositions by three people, which amounts to 36 castings in total. The fluidity measurements per casting are read twice (on different days) per operator, according to the procedure in subsection 4.4.1.

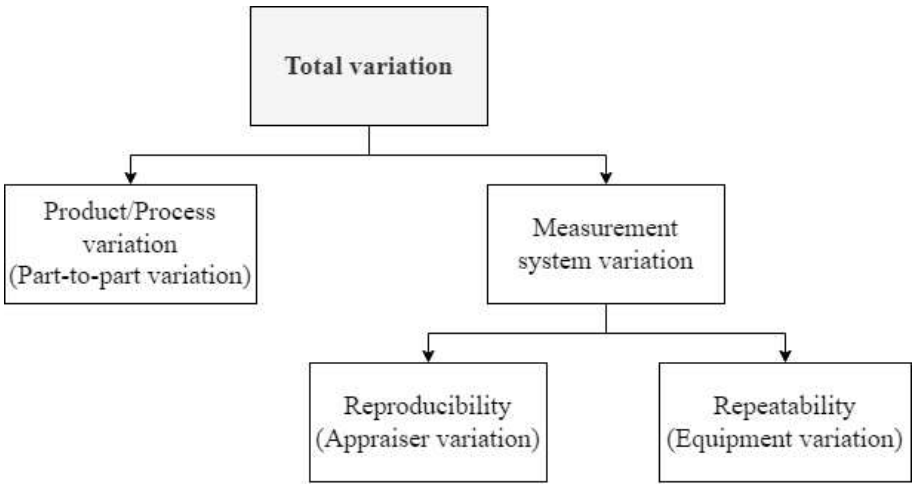

Figure 3.13: Variation types within a measurement system analysis

3.2.4 Summary

In this chapter, existing mold designs have been discussed and their problems in keeping the mold and/or experimental parameters constant have been identified. The spiral mold has non-uniformal cooling across its cross-section and preheats other parts of the mold. The octopus test has different experimental conditions per channel. In the vacuum/Ragone test, the ingate pressure is related to the level of the melt, and its mold temperature is related with the melt temperature. Lastly, the star mold has the problem that the channels are inline hydraulically connected, which might cause problems with hydraulic transients. Improved designs of the Vacuum Mold/Ragone Test and the Spiral Mold have been proposed to mitigate the above-mentioned problems. Design considerations to keep the mold and experimental parameters constant have been discussed. Finally, the Gage R&R method is explained, which is used to validate whether the molds and test procedures are capable of measuring fluidity. This means that the inherent variation of the measurement system is small compared to the variation in the fluidity of the alloy itself.

4. Experimental Design

In this chapter, the proposed molds from the previous chapter are used to measure the metallurgical effects of Er and Eu on the fluidity of a commercially used alloy, directly addressing the research question one and two from Objective 1, from section 1.2. To this end, the base alloy was selected, and the addition ratios of Er and Eu are determined on the basis of the literature. Lastly, the test procedures for performing fluidity measurements and sample preparation are discussed. The samples are used for the analysis of the melt cleanliness and solidification behavior to explain the results from the fluidit tests.

4.1 Base alloy, Er and Eu addition ratio selection

The widely used A356 alloy (Al-7wt% Si-0.3wt% Mg) was selected due to its wide use in the automotive and aerospace industries. The selected addition ratios of Er and Eu for the trials, are based on addition ratios by others who investigate the gain in mechanical properties, when adding Er and/or Eu. A summary of this research is discussed in the following.

4.1.1 Base alloy selection

A356(Al-7wt%Si−0.3wt%Mg) is selected as the base alloy, as it is the most widely used base alloy in the automotive and aerospace industry. Therefore, the knowledge gained on this base alloy has the most industrial relevance.

4.1.2 Er addition

Multiple authors have investigated the effects of Er addition on the mechanical properties on commercially available aluminum alloys. Sahin and Dispinar [8] investigated Er ratios between 0 and 0.3wt% (with and without Eu addition) on A356 alloy, they reported the highest increase in mechanical properties at 0.1wt% Er + 0.3wt% Eu. Peeratatsuwan et al. [81] investigated the addition of Er (0, 0.1, 0.3, and 0.5wt%) to semisolid A356 and found diminishing returns regarding grain refinement and modification of the eutectic Si after 0.1wt% Er. Shi et al. [9] investigated the addition ratio range: 0, 0.1, 0.2, 0.3 and 0.4wt% Er to A356 alloy and found the best mechanical properties at 0.3wt% Er, due to the combination of grain refinement and eutectic Si modification. Lastly, Nie et al. [82] looked at the Al-Mg, Al-Zn-Mg, Al-Zn-Mg-Cu and 1420 Al-Li alloy systems with an addition ratio range of 0 to 0.7wt% Er. They concluded that after 0.1wt% Er, minimal extra grain refinement can be expected compared to the 0.1wt% Er. Ahmad et al. [83] found that the tensile strength and the elongation increased 1.32% and 9.1% with 0.1wt% Er content, respectively. Moreover, the hardness also improved from the addition of 0.1% Er aluminium. From this research, it can be concluded that 0.1wt% Er can be considered optimal. Therefore, this addition ratio was selected for the trials.

4.1.3 Europium addition

As stated above, Sahin and Dispinar [8] found good Si modification at 0.3wt% Eu in A356. Mao et al. [54] considered the addition range Al-7Si-xEu alloys (x=0, 0.04, 0.1, 0.16, 0.22, 0.3wt%) to A356 commercially foundry alloy. Visible modification was observed from 0.16wt% Eu. The grain size, however, increases with increasing levels of Eu. This seems to be the poisoning effect of the Eu on the Ti present in the melt. Li et al. [84] found full modification of the eutectic Si at the addition ratio of 0.05wt% Eu on a high purity Al-5Si alloy. Nogita et al. [56] observed the full modification at an addition of 0.06wt% Eu in Al-10Si alloy. The research of Sahin [8] and Mao [54] were done on A356 base alloy, hence it was chosen to use an average addition ratio of 0.2wt% Eu for the trials as this is likely to provide good modification of the eutectic Si.
To conclude, the effects on fluidity, of the four addition ratios in Table 4.1 to an A356 alloy, were investigated.

Table 4.1: Alloying ratios of Er and Eu used for fluidity experiments

Name	Er wt%	Eu wt%
0.0 (Base alloy)	-	-
0.1 Er	0.1	-
0.2 Eu	-	0.2
0.1 Er + 0.2 Eu	0.1	0.2

4.2 Excluded parameters from fluidity analysis

Some of the parameters that affect fluidity, from Table 2.5, are not used for the analysis of the fluidity results. Mostly, because the change of these parameters, due to the different addition ratios, are not expected to change the fluidity in a significant way.

4.2.1 Specific heat capacity

To check if the addition of Er and/or Eu could have a significant influence on the specific heat capacity (C_p) a calculation was performed in Factsage, which is a chemical thermodynamic database. The conclusion was that the C_p changed from 115.84 J/g K for the base alloy to 115.58 J/g K for the Er + Eu composition which is a difference of 0.2% which is negligible. Therefore, this parameter is not be considered during the analysis of the fluidity results.

4.2.2 Latent heat of fusion

The latent heat of fusion was calculated for the base alloy, 0.1wt% Er, 0.2wt% Eu and 0.1wt% Er + 0.2wt% Eu in Factsage. It was found that the 0.1wt% Er + 0.2wt% Eu composition had around 2.4% lower heat of fusion compared to the base alloy, which is relatively small. Therefore, the change in latent heat of fusion is not considered during the analysis of the fluidity results.

4.2.3 Viscosity

The viscosity was not taken into account, as the effects of the change in viscosity are expected not to influence the fluidity in a significant way, as discussed in section section 2.5.1. Moreover, Foseco does not possess a high-temperature rheology meter, therefore, it was decided to not include it in the scope of this research.

4.3 Hypothesis of the influence of Er and Eu on the fluidity

This section answers research question three of Objective 1 of section 1.2. The addition of Er is expected to increase the fluidity of the A356 alloy. Since Er is a grain refiner and there is strong evidence in the literature that grain refiners improve fluidity. Since grain refiners create smaller dendrites and these dendrites can move more easily pass each other, increasing the critical solid fraction of the melt, increasing fluidity, as discussed in detail in section 2.5.1. The amount of improvement in fluidity is difficult to predict, as it depends on the level of grain refinement achieved, as demonstrated by Prukkanon et al. [49].

It is even more difficult to predict the effect of Eu on fluidity, since the effect of modifiers on fluidity is expected to be small. Because it is not known whether Eu is capable of lowering the solidification temperature by restricted nucleation, it cannot be expected to increase fluidity in this manner. Sahin and Dispinar [8] did not observe major intermetallics formed when added with 0.3wt% Eu. Therefore, it is expected that the formation of intermetallics does not significantly change the fluidity of the A356 alloy.

4.4 Method

Before the trials, both the Radial Quad and the Vacuum molds were levelled using a bubble/spirit level and the bolts on the underside of the mold to ensure the same metallostatic pressure in the channels. The molds are cleaned with a vacuum or compressed air to remove any debris which might hinder the flow of the molten metal. The mold is heated to $110\pm3^{\circ}C$ to remove any moister from the mold. A fine coat of spray-on boron nitride is applied to the mold to prevent soldering of the aluminium to the dies. Finally, the mold is heated to $250\pm3^{\circ}C$ to be ready for the castings.

The isolating pouring basin, for the Radial Quad mold, was made from a Foseco Kalmin alt-6 recipe and cured with CO_2 in the mold, the technical drawings of this mold are shown in Appendix 7.4.3. After which, stored for at least 48h in a, $20^{\circ}C$ and 30% humidity, climate controlled cabinet to fully develop its green strength. And finally, heated to $60^{\circ}C$ in a oven for at least 24h to remove any residual moisture.

The base alloy for the experiments was aluminum alloy A356 (Al-7%Si-0.3%Mg) commercial 131 purity of which 40kg was melted in a SiC crucible at $750^{\circ}C$ with a Nabertherm resistance furnace. Master alloys of Al-10wt%Er and Al-10wt%Eu, in waffle form, were used to acquire the desired compositions for the tests. Degassing was performed with 5L/min Ar for 300s at 250RPM with a XSR ⌀140mm rotor head, based on internally experimental work by Foseco, were BIs of 1-2mm were achieved for pure aluminium. Barker and RPT samples, shown in Figure 4.1, were taken before and after the casting trials. To be used later to investigate the microstructure and melt cleanliness.

Figure 4.1: Left) Barker sample solidified in copper mold. Right) RPT sample solidified under partial vacuum (80mbar) in thin steel mold

Fluidity tests were conducted in the Radial Quad mold, as shown in Figure 4.2, while taking the safety measurements in consideration of Appendix 7.5. The surface of the melt was skimmed to remove any dross (mass of solid impurities and oxides ontop of the melt). The temperature was checked if it had reached the set 750°C. Melt (around 2kg) was taken from the furnace with a spoon, to have more than needed for the fluidity test. The melt was poured into the pouring basin. The stopper was removed by a second operator when the temperature in the pouring basin reached 725 $°C$, read on the thermocouple attached to the stopper. The operator kept filling the pouring basin after the stopper was removed to keep constant metallostatic pressure. If the operator would add to much melt to the pouring basin the excess melt would go through the overflow into a second container. The cope of the mold was removed when the casting fully solidified, and the fluidity length could be read from the integrated ruler engraved on the drag. A description of the fluidity reading procedure is described in more detail in subsection 4.4.1.

The fluidity tests in the Vacuum mold were performed by inserting a straw in the mold and closing the die. The surface-mounted thermocouple (RS PRO K Pipe Clip Surface Temperature Probe 434-2437) was attached to the straw and the temperature was monitored by the digital thermocouple, shown in the blue rectangle in Figure 4.4. In the control panel, a flow sensor (RS LZT-08A01M-V), the yellow rectangle in Figure 4.4, was placed to measure airflow through the system. The pressure regulator (SMC IRV20-C08BG), the red rectangle in Figure 4.4, was used to set the required vacuum level, as described in Appendix 7.2. The partial vacuum is generated by a venturi vacuum generator (SMC ZU05SA) connected to a compressed air line (± 7 bar). When the temperature of the straw reached 250°C the vacuum was applied to the system and held for at least 5 seconds to fully solidify the melt in the mold. After which, the fluidity length could be read from the integrated ruler engraved on the drag, as shown in Figure 4.3. The control panel was captured on camera to analyse the data after the trials.

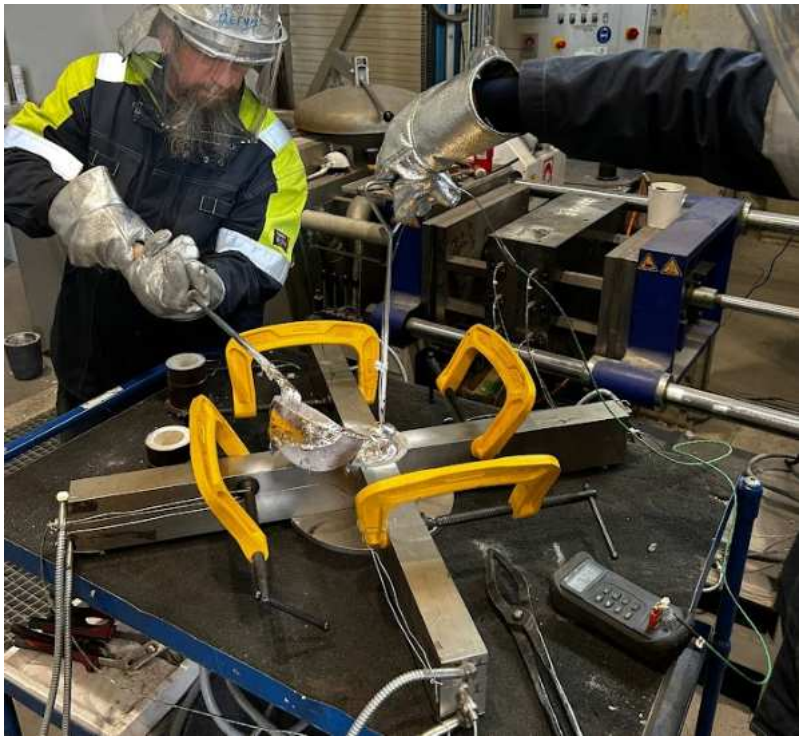

Figure 4.2: Radial Quad setup during fluidity test

4.4.1 Fluidity reading procedure

to account for variations in flow front shapes, fluidity was quantified by averaging the furthest point of flow with the point where it contacted both of the mold walls. In Figure 4.5 an example is given, from the picture it can be seen that the flow front reaches 153mm and the point where the flow front fully touches both sides of the channel is at 147mm. This means that the fluidity reading of this channel is (153+147)/2 = 150mm.

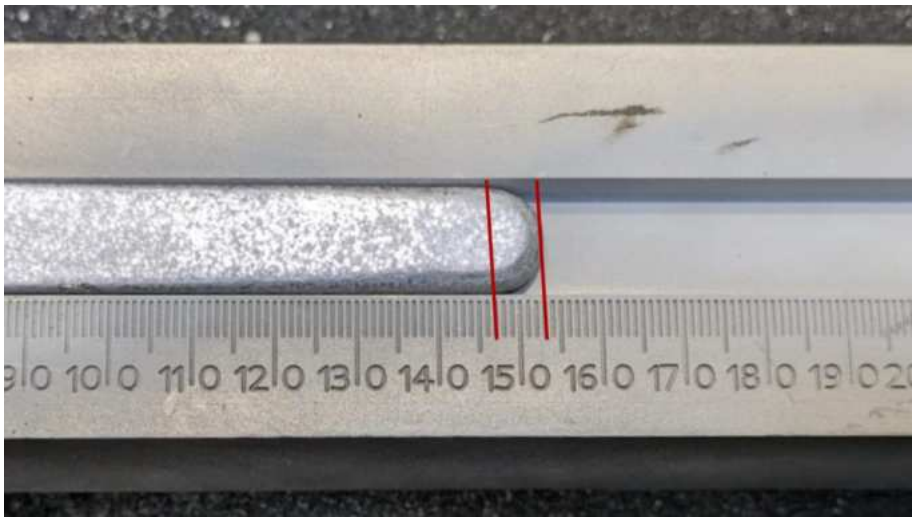

Figure 4.5: Fluidity reading procedure

Figure 4.3: Vacuum setup opened after fluidity test

4.4.2 Composition verification

To verify if the desired addition ratios from Table 4.1, were achieved, the composition was measured with a QUANTOLUX QLX3 Optic 132 Emission Spectrometer (OES). The weight percentages of Er and Eu were taken from the Bruker S6 X-Ray Fluorescence (XRF) spectrometer data since the OES machine cannot detect Er and Eu. Furthermore, the XRF machine was also used to identify possible other modifiers within the base alloy.

4.4.3 Grain size and microstructure of cast pieces

The impact of Er and Eu on the microstructure was analysed to correlate grain size and modification of the eutectic Si with fluidity results, providing insight into how these additions affect the casting performance. The grain size was determined on the Barker sample and the microstructure was investigated by an optical microscope on the same sample. To determine the grain size, a 10x10mm piece of sample was sanded till 2000 grid, polished and edged to see the individual grains under polarised light. Then 50 length measurements, for the grain size analysis, were taken at random to establish an average grain size for each sample. This method is also used by Foseco for all their grain size analyses of aluminum alloys. To verify the measurements, an employee of Foseco redid the measurements and the results were averaged.

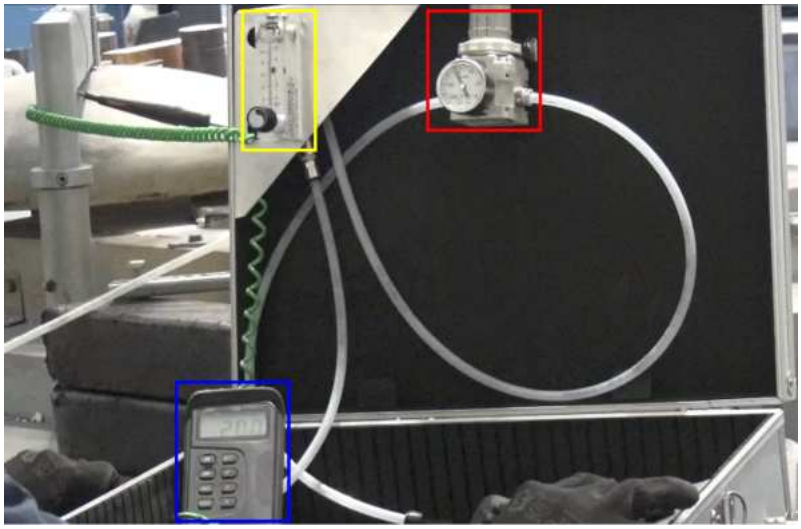

Figure 4.4: Vacuum setup control panel

To see if the grain size of the Barker sample is representative of the grain size in the arms in the channels, the cross-sections of the arms for, every composition, were examined. The arms, of the castings with the lowest and highest fluidity per composition were cut 60mm from the sprue as indicated in Figure 4.6. This was done such that the cross-section was taken at the same place regardless of fluidity length in each channel. Subsequently, the arms were stacked and embedded in a clear resin to make sample handling easier, as shown in Figure 4.7. The bottom side of the sample was ground to a 2000 grid and polished to investigate the microstructure under an optical microscope. After which, the samples were edged and examined under polarised light, as shown in Appendix 7.8. Since the cross-sectional area of the channels is smaller than 10x10mm only 25 measurements per channel were taken. Finally, the average grain size was determined based on the 2x25=50 measurements per channel cross-section, of the same composition.

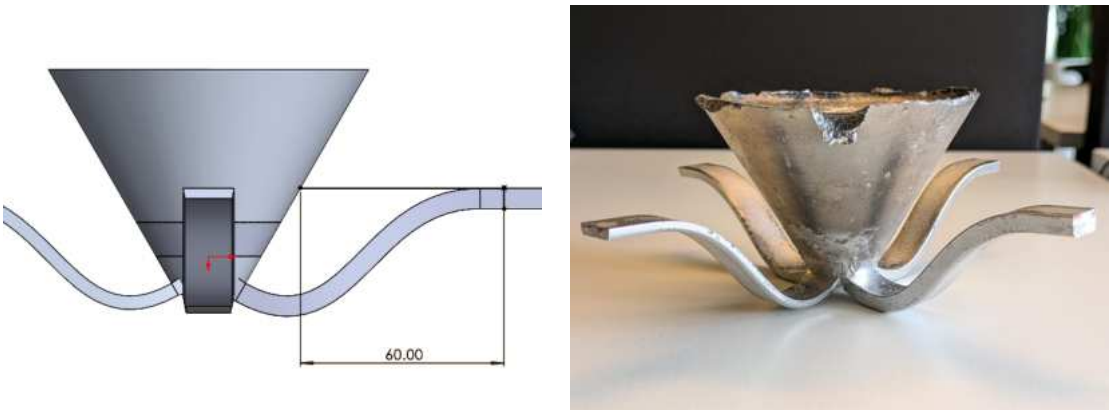

(a) Location were the arms were cut

(b) Arms cut off

Figure 4.6: Location where arms were cut off the pouring basin, to investigate microstructure and grain size

Figure 4.7: Arms of the shortest and longest fluidity casting per composition were embedded for microstructural analysis

4.4.4 Melt cleanliness measurement

The melt cleanliness was determined to correlate the quality of the melt with the results obtained from the fluidity tests. For this, the RPT is used to evaluate the maximum feret length of the pores, the RPT is widely used in industry. The samples were cut in half and ground to an 800 grid such that the cut surface could be scanned and the pores were clearly visible. Subsequently, ImageJ software was used to determine the maximum feret diameter of each pore, and these were summed to obtain the BI of each sample. The threshold of the software was kept just below the point where sanding marks were detected as pores. To verify the results obtained by ImageJ, a manual check was performed by an employee of Foseco by coloring all pores in Paint software after which ImageJ could easily detect the colored pores.

4.4.5 Intermetallics detection

To investigate whether intermetallics have formed during the addition of Er and/or Eu, which might hinder the flow during casting and thus decreasing fluidity, Energy Dispersive X-ray analysis (EDX) was performed (with a Zeiss Sigma Gemini) on the Barker samples.

4.5 Summary

In this chapter, rationale for the selection of the A356 base alloy and the addition ratios of 0.1wt% Er and 0.2wt%Eu is given. An explanation is presented why the specific heat capacity, latent heat of fusion and viscosity do not significantly change the fluidity and therefore are not considered during the analysis of the fluidity results. The hypothesis is formulated that the addition of Er increases the fluidity and that the addition of Eu does not change the fluidity of the A356 base alloy. Lastly, the procedure for performing the fluidity casting trials and the sample preparation was discussed.

5. Results and Discussion

In this chapter, the results of the fluidity measurements are explained with the insights gained from the microstructure of the samples, taken during the casting process, and the BI obtained from the RPT. Moreover, technical difficulties experienced with the vacuum mold are discussed. The results of the fluidity measurements were analysed and the composition, metallography analysis of the grain size, modification of the eutectic Si and intermetallics were performed. Possible explanations were proposed to explain the results obtained from the fluidity tests. Lastly, the validation of the mold and experimental procedures with use of the Gage R&R are performed.

5.1 Technical difficulties with Vacuum mold

During the fluidity tests of the vacuum mold, the straw, which was installed on one side of the mold and the other end submerged into the melt, was not getting up to required 250°C and found an equilibrium around 205°C. This meant that during the testing the melt already solidified in the straw before entering the mold. To mitigate this problem, it was decided to increase the flow velocity to give the melt less time to cool down in the straw before reaching the mold, which seemed to work. The increase in flow velocity might have exceeded the maximum flow velocity to induce surface turbulence. However, all the fluidity tests had smooth and constant flow fronts, indicating that no significant turbulence had occurred.

In addition, a more severe problem was the airtightness of the mold. Several gasket designs, made of different thicknesses and materials (graphite foil) were used. However, the semi-closed design of the gasket (open on the side of the straw, in Figure 3.7) allowed the O-rings to push the gasket to the sides when the cope applied mechanical pressure on the O-rings. An attempt to mitigate this problem was to install pins on both sides of the straw. However, it was found that this was not a reliable method of making the mold airtight. This meant that the required vacuum level could not be reached and melt could not be sucked into the mold. Therefore, no repeatable fluidity test could be performed.

Lastly, the thermal expansion coefficient of the silicone gasket is approximately 10 to 15x higher than that of the stainless steel mold. Therefore, with a mold temperature of 250°C, it meant that even with a thermal expansion compensated gasket design, the gasket could not be properly installed at room temperature and still began to wrinkle at elevated temperatures, making it very difficult to keep the mold airtight during testing. Moreover, manual (re)locating the gasket on a 250°C mold was challenging. This also contributed to the mold not being airtight. Therefore, it was decided that the Vacuum mold measurements results were not repeatable enough and would not be used for the fluidity results.

5.2 Fluidity measurements results

In total 36 fluidity castings, in the Radial Quad mold, were performed divided by three operators, performing three trials per composition for four compositions. To see the effects of the addition to the fluidity the average fluidity lengths per composition, including standard deviations, are shown in Figure 5.1. What can be seen is that the fluidity for 3 mm is around 50mm which is almost the same for all compositions. When going to 4mm channel height, the fluidity almost triples to 145mm after which it seems to increase linearly with 50mm per millimeter of channel height. The nonlinear behavior below the 4mm channel height is contributed to the higher capillary repulsion and the smaller section modulus, which exponentially decrease the solidification time.

Er has a slightly higher average fluidity than others in the 4mm channel and above. In contrast, Eu performs the worst in all channels except the 5mm channel where it reaches 190mm, where the base alloy performs even worse at 180mm. In 4mm channel and above, the Er + Eu composition performs better than Eu but worse than Er. The deviation in the 3mm channels is smaller than in the larger channels, which might be the result of the smaller channels getting heated up less by every casting such that the mold temperature stays more constant than in larger channels. The changes in fluidity by the additions to the base alloy are noticeable but stay minimal.

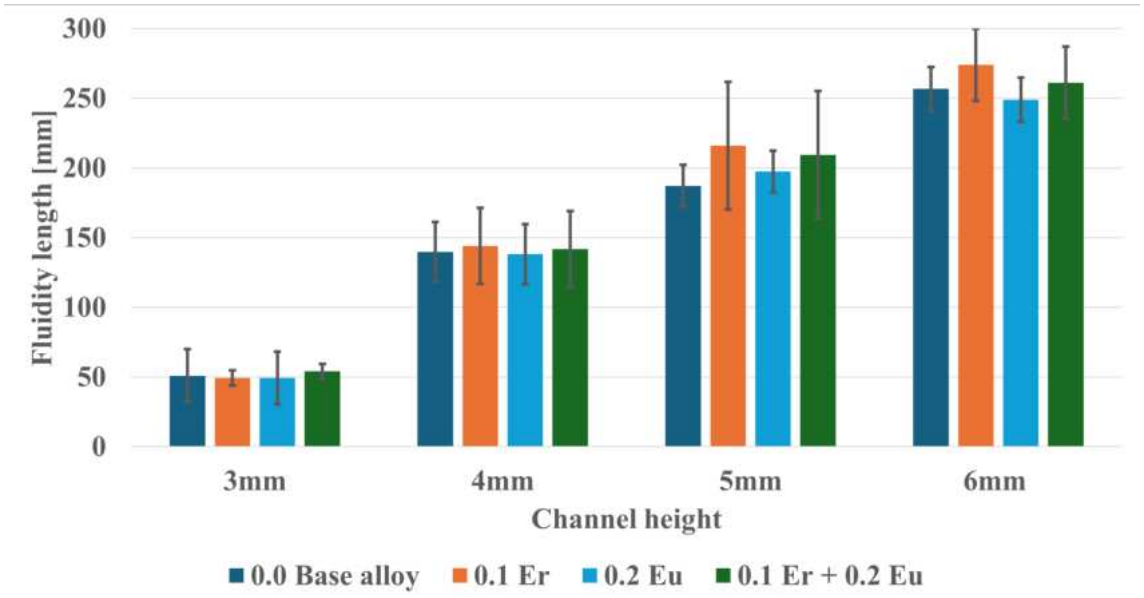

Figure 5.1: Fluidity length of the four channels per composition

To better understand the differences between the base alloy and the additions, Figure 5.1 is normalised to obtain Figure 5.2. Now, it can be more clearly observed that Er has the potential to have the highest fluidity. However, the data could not give enough statistical significance (with a confidence interval of 95%) to be able to state that Er has a higher mean fluidity than the base alloy. Nevertheless, the Er + Eu composition, is in most cases (above 3mm channel height), in between the Er and Eu results. This seems to indicate that Er increases fluidity and Eu decreases fluidity and when both Er and Eu are added to the melt, the performance becomes averaged. However, the microstructures should be examined to support this hypothesis and see if there is evidence which can explain the minimal difference in fluidity.

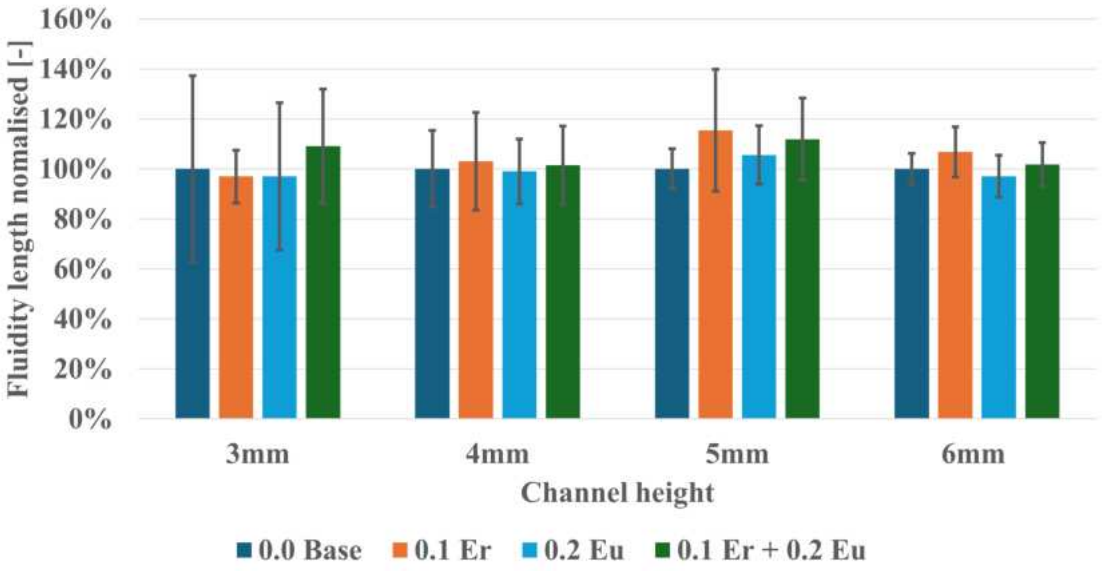

Figure 5.2: Normalised fluidity length of the four channels per composition

5.3 Metallurgical parameters

In this section the metallurgical parameters are discussed which can contribute to a difference in fluidity, to explain the results obtained by the fluidity tests. By investigating these parameters, research question four of Objective 1 is answered, as can be read in section 1.2.

5.3.1 Composition verification

The measured chemical compositions of the desired four addition ratios, are given in Table 5.1. What can be seen is that the Er is within 0.01wt% of its target, which is considered good. However, the Eu content is 0.1wt% higher than aimed for, this is the result of a faulty addition calculation by the author. From the microstructures, it was found that the microstructure of the 0.2 Eu composition (with 0.31wt% Eu) was more and better modified than the microstructure of the 0.1 Er + 0.2 Eu, as will be discussed later in this section. As can be seen from Figure 5.2, the composition of 0.2 Eu performs the worst; therefore, it is expected that the addition of too much Eu has slightly decreased the fluidity.

Table 5.1: Composition of the alloys tested in wt%

Name	Al	Si	Fe	Cu	Mn	Mg	Ni	Zn	Ti	Er	Eu
0.0 (base alloy)	Bal.	7.14	0.45	0.11	0.05	0.29	0.01	0.04	0.02	-	-
0.1 Er	Bal.	7.14	0.46	0.11	0.06	0.28	0.01	0.05	0.02	0.09	-
0.2 Eu	Bal.	7.22	0.44	0.11	0.05	0.30	0.01	0.04	0.02	-	0.31
0.1 Er + 0.2 Eu	Bal.	7.12	0.47	0.11	0.05	0.26	0.1	0.05	0.02	0.09	0.22

5.3.2 Solidification behavior

How an alloy solidifies has the most significant influence on fluidity, as discussed in section 2.5. Therefore, the microstructures of the fluidity casting and Barker samples were examined to determine what the influence of the additions were on grain size, modification of the eutectic Si and formation of intermetallics, and how this could affect the fluidity. For this, Barker samples were used, that were taken before and after additions of Er and/or Eu and before and after fluidity trials.

Grain refinement The results of the grain size analysis are shown in Figure 5.3. The overview images used for the grain size analysis can be found in Appendix 7.6. The grains do not seem to be affected by the addition of Er and/or Eu. In an A356 base alloy the sample is considered grain refined if the grain size of a Barker sample is $\leq 300\mu$m [85]. This means that the addition of Er was unable to refine the grain, which is unexpected.

What should be noted is that the grain size after the casting trials is consistently smaller than before the trials. Due to the bad quality of the melt, which will be discussed in detail in section 5.4, many bifilms are present in the melt. During solidification the dendrites grow and are able to straighten out the bifilms. This creates a large surfaces that inhibits the confection of molten metal, preventing dendrites from being fragmented by other dendrites in the flow, resulting in larger grains. If the quality of the melt increases, after the trials (which was the case, as discussed later), fewer of these bifilms are present which results in more fragmented dendrites, explaining the decrease in grain size [86].

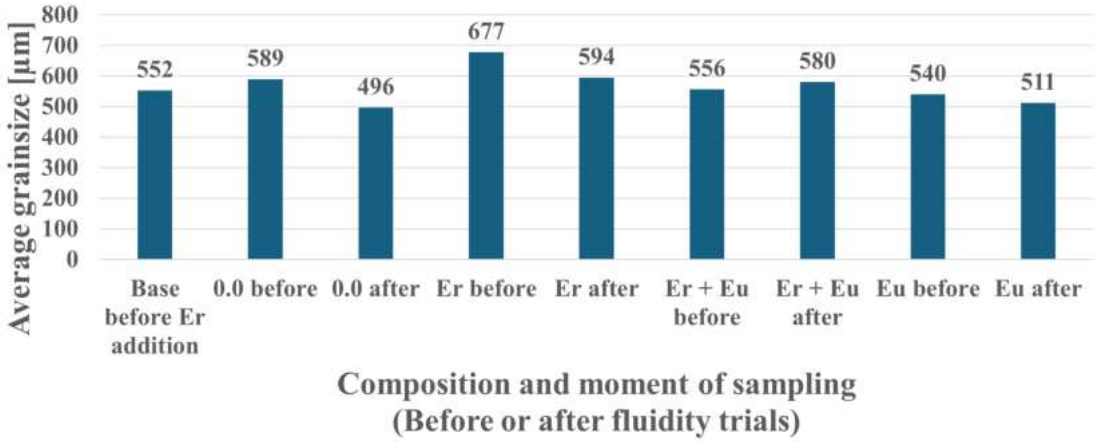

Figure 5.3: Grain size of different compositions before and after the casting trials

The grain size observed in the Barker samples was compared to the grain size in the cross-section of the arms of the casting, the results are shown in Figure 5.4. The images themselves, used for the grain size analyses, can be found in Appendix 7.8. What can be noted is that the grain size in the Barker sample is almost always higher than in the channels. This is logical since the solidification modulus in the channels is significantly lower than in the Barker mold, this increases the cooling rate, which creates smaller grains in hte channels [87]. With the same logic, smaller grains can be observed in the smaller channels. The 3mm channel in the short 0.0 base alloy was over-edged, therefore, grain size analysis was not possible. The grain size in the Barker is not very indicative of the grain size in the channels. This could be the cause of the limited grains that could be measured on the cross-section of the channels. As there is no significant increase and/or decrease in the grain size, due to the different additions to the base alloy, the fluidity could not be influenced too much by grain refinement.

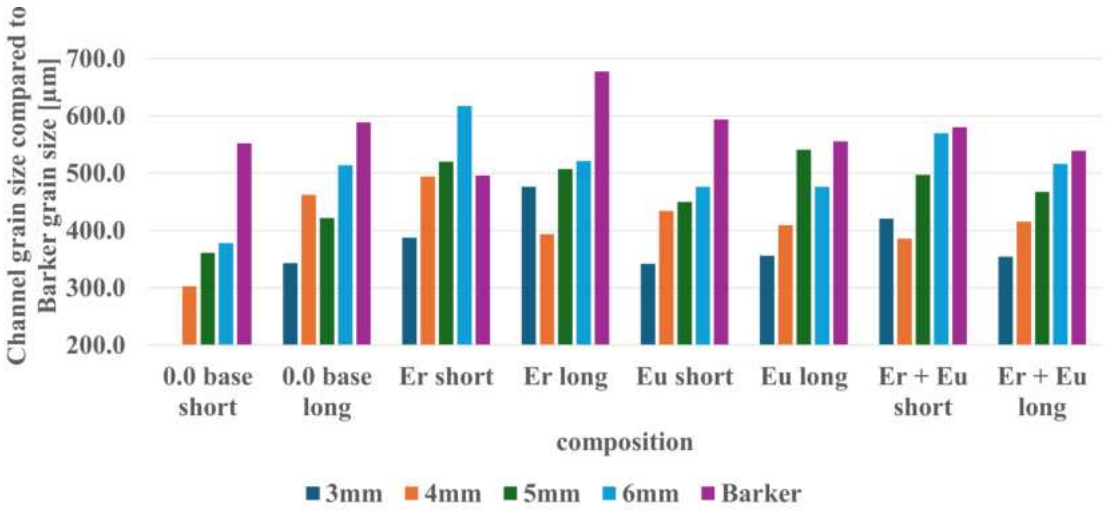

Figure 5.4: Grain size in channel cross-section compared to grain size found in Barker

Modification of the eutectic Si To verify if the eutectic Si is indeed modified by the addition of Eu, the barker samples were observed by the optical microscope. Figure 5.5 gives a comparison between the microstructure of a standard as-cast A356 alloy and the microstructure observed in the base alloy used in the fluidity experiments. What must be noted is that Si is already modified in the 0.0 base alloy, which is extremely surprising and should not be the case. For reference, Figure 5.6 shows two images of unmodified base alloys, at higher magnifications. In the non-modified A356 of Figure 5.6, the Si platelets are about 20 to 40μm where the Si particles in the base alloy used were 5 to 10μm. This means that the effects of the modification of the eutectic Si, by addition of Eu, on fluidity can be more difficult to compare because the differences with the base alloy are less pronounced.

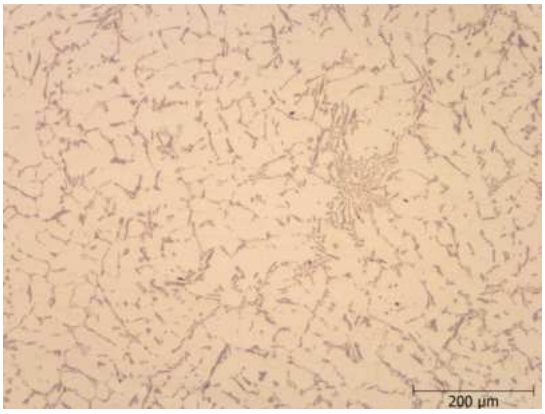

(a) Microstructure of an as-cast A356 alloy (image received from D. Dispinar)

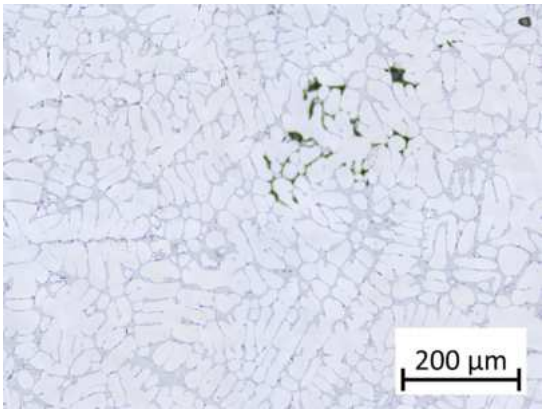

(b) Microstructure of used 0.0 base alloy (A356) is already modified before addition

Figure 5.5: Microstructure of Barker sample

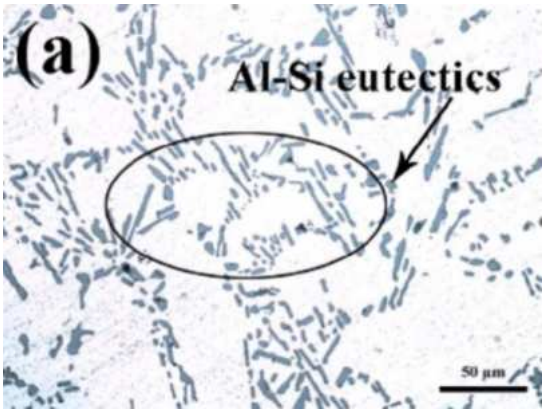

(a) A356 microstructure with plate-like Si [88]

(b) A356 microstructure with plate-like Si [8]

Figure 5.6: Unmodified A356 base alloys under different magnifications

In Figure 5.7, the microstructure of the 0.0 base alloy and the Er + Eu composition are compared, minimal differences can be detected between the microstructures. Although the base alloy was already modified, the addition of only Eu further increased the level of modification, which can clearly be seen in Figure 5.8. The addition of solely 0.31wt% Eu (the 0.2 Eu composition), creates almost perfect distributed and fibrous eutectic Si. From the microstructures of the eutectic Si alone it is hard to predict if fluidity increases or decreases, since the grain size and intermetallic formations are more relevant for the fluidity than the modification of the eutectic Si, as discussed in section 2.5.1.

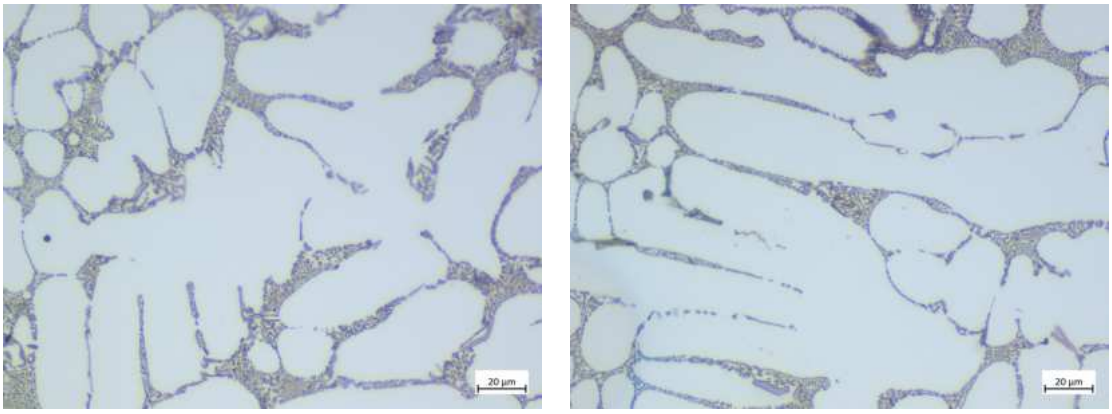

(a) 0.0 base alloy (b) Er + Eu composition

Figure 5.7: Microstructure of Barker samples under 500x magnification

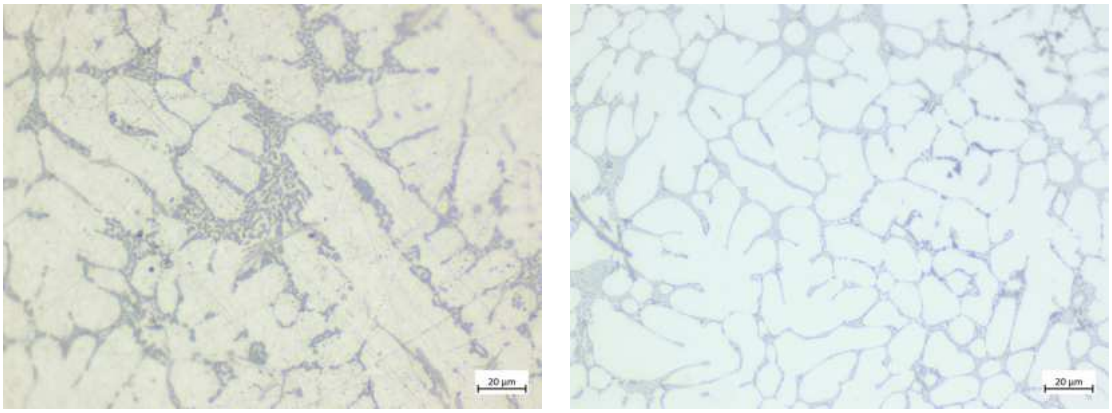

(a) 0.0 base alloy microstructure (b) Eu modified microstructure

Figure 5.8: Microstructure of channel cross-section

Intermetallics From Figure 5.9, it can be seen that the base alloy already has quite some intermetallics present in its microstructure mostly iron (Fe) based. The brighter intermetallics are Fe-based and the dimmer intermetallics are MgSi particles. From Figure 5.10, it can be seen that Er alone creates some small and compact intermetallics that should not cause major problems with fluidity. From the SEM image of the Eu composition in Figure 5.11 it can be seen that there are fewer and smaller intermetallics present, except some small chunky Eu-based intermetallics. It seems that the addition of Eu also modifies the morphology of the intermetallics, which would be beneficial for fluidity. However, from the fluidity experiments it seems that the addition of Eu has an adverse effect on the fluidity. This gives the impression that the size and morphology of smaller intermetallics is not that relevant for the fluidity. Lastly, the SEM image of the Er + Eu composition in Figure 5.12 shows large and long needle-like intermetallics that contain both Eu and a little bit of Er. These intermetallics might explain the reduction in fluidity of the Er + Eu composition.

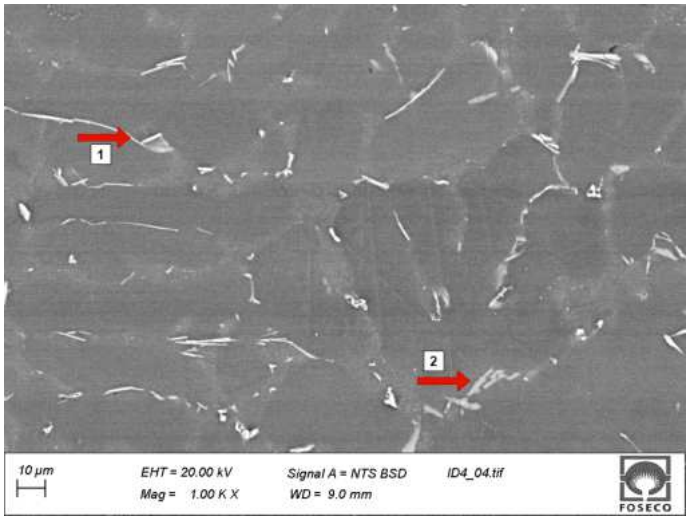

Figure 5.9: SEM image of microstructure of 0.0 Base alloy 1. AlFeSiMn intermetallics are longer and needle-like, 2. MgSi intermetallics are shorter and chunkier, which appear dimmer in the image

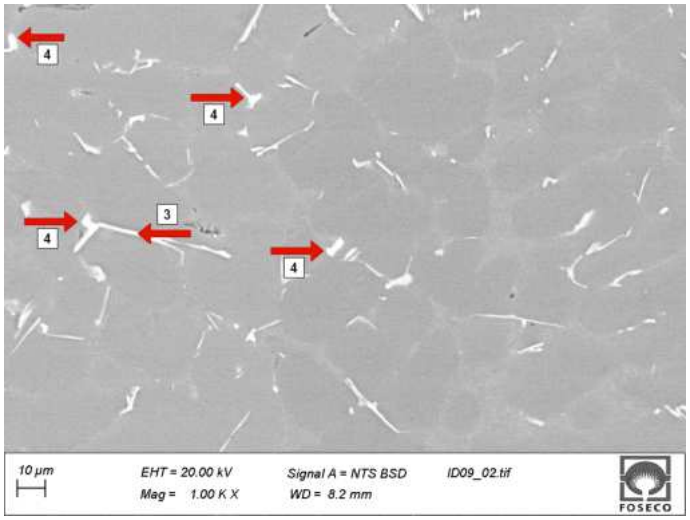

Figure 5.10: SEM image of microstructure Er composition 3. AlFeSiMn intermetallics are longer and needle-like (distributed over the whole image), 4. A few Al, Er(20-27wt%), Si(≈23wt%) and Mg(≈3wt%) rich regions

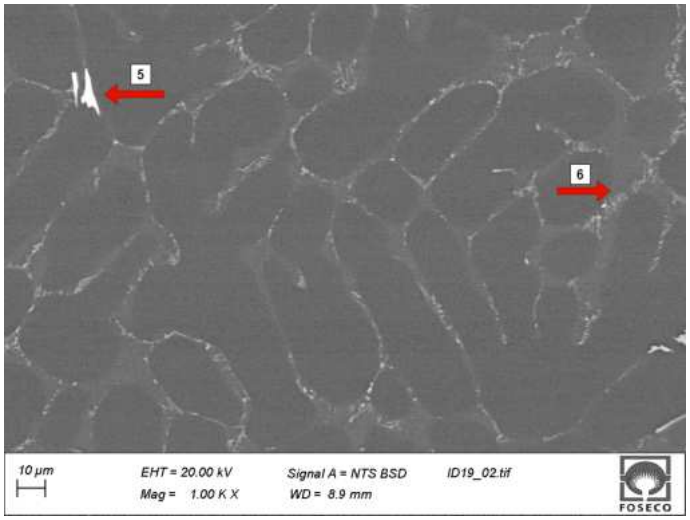

Figure 5.11: SEM image of microstructure Eu composition 5. Al (73wt%), Eu(16wt%), Si(11wt%), 6. Fe and Mg rich regions, possible MgSi and/or AlFeSiMn intermetallics

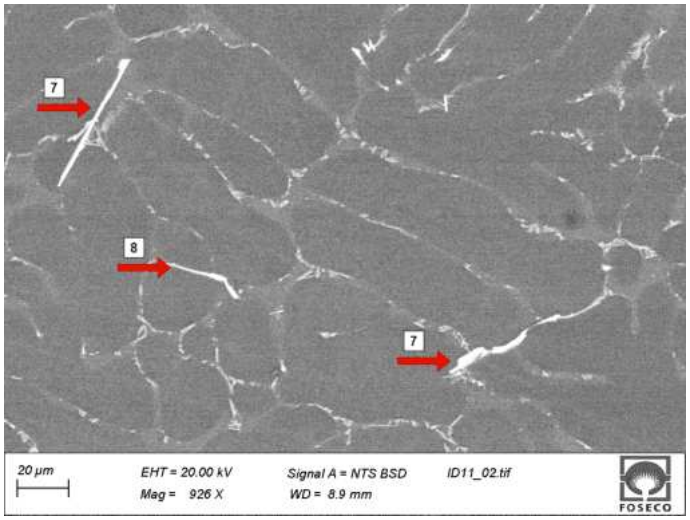

Figure 5.12: SEM image of microstructure Er+Eu composition 7. Intermetallics which consist out of Al(30-50wt%), Eu(30-40wt%), Si(≈20wt%) and Er(≈3wt%) which are long and needle-like, 8. AlFeSiMn intermetallics which are also needle-like (distributed over the whole image)

5.4 Melt cleanliness

The melt cleanliness was determined before and after fluidity casting trials using the RPT, which is widely used in industry. The scans of the cross-section are displayed in Figure 5.15. It can be seen that the pore size increases after casting trials of the base alloy, indicating that the melt quality decreases. Er has visually the highest increase in melt quality after the casting trials. The Eu and Er + Eu composition have a finer distributed pores over the cross-section. The results of the calculated BI by the ImageJ software and the manual check by an employee of Foseco, in Figure 5.13, confirm the visual observations.

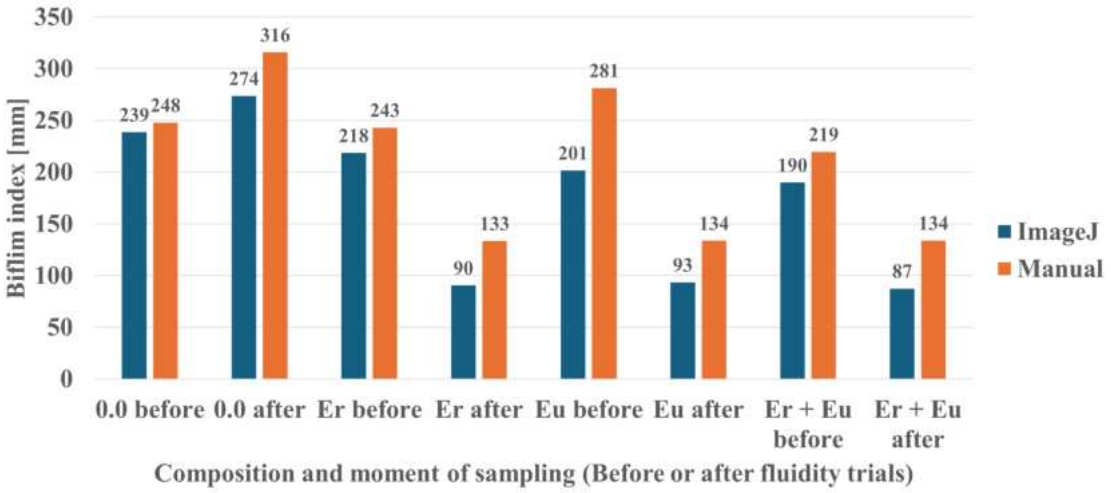

Figure 5.13: Biflim index measured before and after fluidity casting trials

What must be noted is that the quality of the melt was extremely poor since the RPT samples are littered with pores throughout their entire cross-section. As discussed in section 2.5.3 it is known that a BI between 50mm and 100mm is an unacceptable melt quality and above 100mm the melt should not be used. Therefore, such a poor melt quality can have effects on the solidification behavior of the alloy and therefore the fluidity.
In Figure 5.14, the fluidity index of the individual fluidity tests are plotted against the BI of the test. The BI of the base alloy is the worst and is reasonable constant compared to that of the other compositions. Because RPT samples were only taken before and after the trials the BI per test was linearly interpolated, based on the time between trials. However, the data is significantly scattered; a slight trend can be observed at higher BIs a lower fluidity can be expected. The correlation is not strong, but to seem to be in accordance with literature. Timellio et al. [75] performed fluidity tests and found that the castings with the shortest fluidity had 72% higher BI compared to the casting with the largest fluidity, which corresponded to a reduction in fluidity of 13%. Groteke et al. [89] found a 20% improvement in fluidity in a 319 alloy (6wt%Si-3.5wt%Cu-1wt%Fe) when the melt was cleaned by a degassing operation, and thus bifilms were removed.

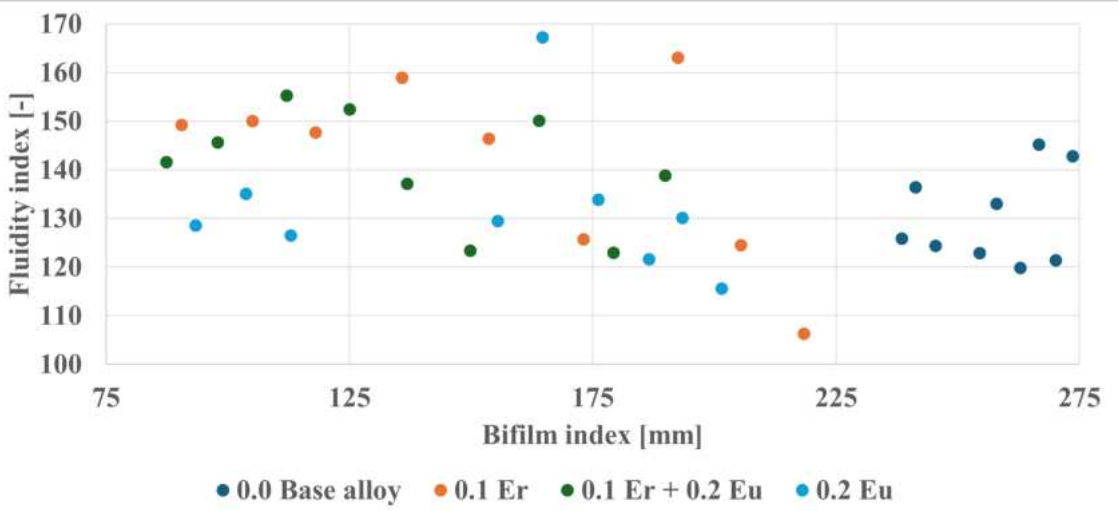

Figure 5.14: Biflim index vs fluidity index

From the BIs of the samples, in Figure 5.13, it can be seen that the quality of the base alloy has decreased from a BI of approximately 240mm to around 275mm after the trial. A decrease is expected because taking melt from the furnace, for sampling, disturbs the surface and entrains bifilms into the bulk of the melt [13]. However, within Er, Eu and Er + Eu compositions, the quality of the melt increases (decreasing BI) after the trials, from a BI of 200mm to around 100mm. It should be noted that although the BI decreased by 50% this is still above the acceptable levels as discussed in section 2.5.3. A decrease in BI after casting tests is unexpected and possible explanations for this phenomenon are given later in this section.

In the Eu and Er + Eu composition, there are many small voids in the samples instead of fewer larger ones. This is in accordance with the observations made by Li et al. [90] who used a CT scan to classify the pore density and pore size. It was found that the addition of Eu (100ppm) and P(10ppm) decreased the pore size and increased the pore density. More and smaller pores are less detrimental for the mechanical properties of the cast part than a few larger pores, this is a positive side effect of Eu. Sr and Na also have the ability to redistribute pores within the casting as earlier stated in Table 2.6.

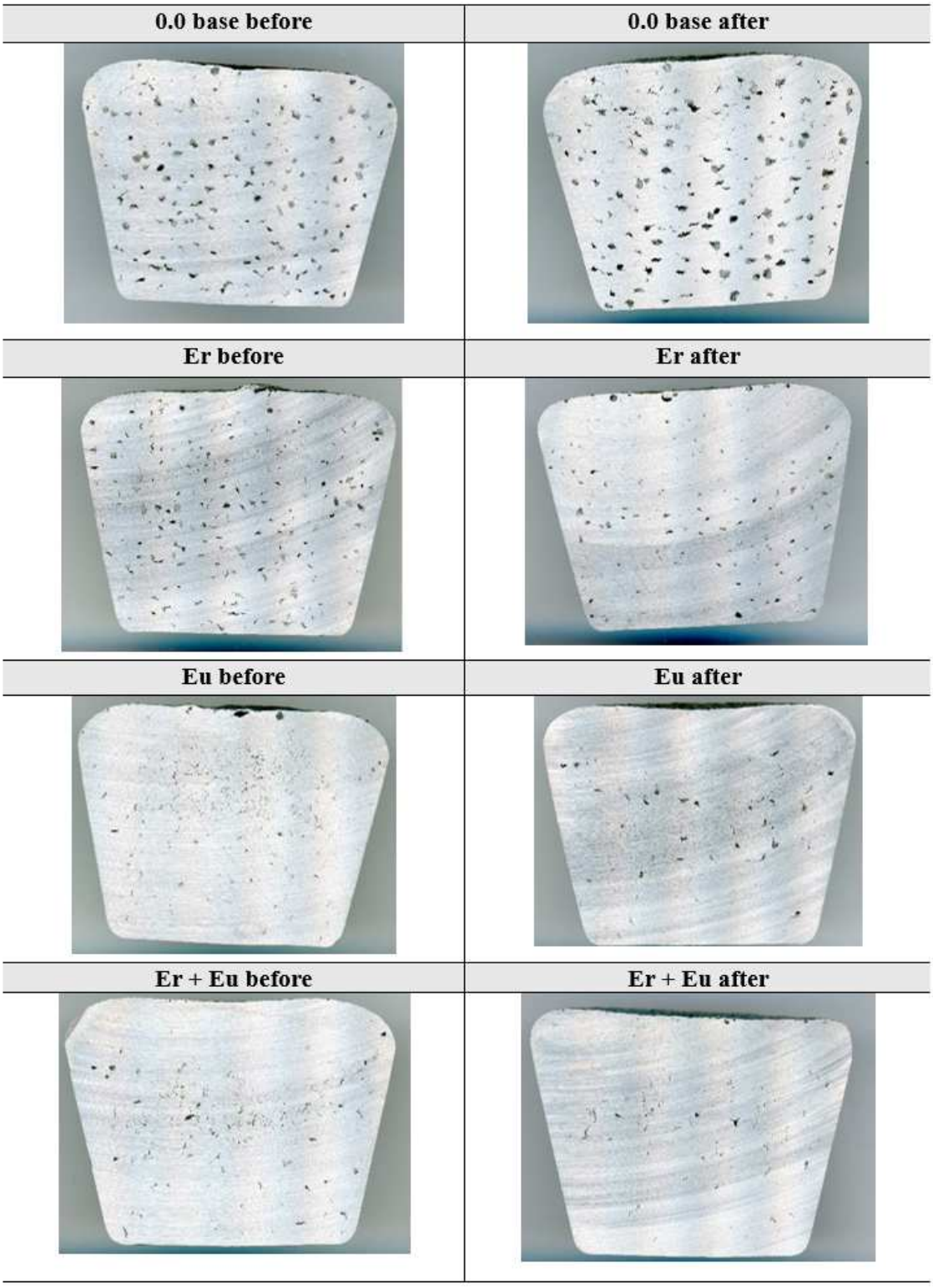

Figure 5.15: Scans of cut and ground RPT samples, left and right are the samples shown before and after the fluidity casting trials, respectively

5.5 Hypotheses for results obtained

Multiple unexpected results were found during the analysis of the experiments. In this section, some possible hypotheses are given to explain the observations. The unexpected results can be stated as follows;

- No grain refinement observed with the addition of 0.1wt% Er with or without 0.2wt% Eu. According to literature 0.1wt% Er should be enough to observe good grain refinement
- An increase in melt quality, which means a decrease in BI, after the fluidity trials for the Er, Eu and Er + Eu composition. Normally melt quality decreases when taking melt from the furnace, due to disturbance of the melt surface
- BI of the melt after the degassing operation was extremely high >200mm. The settings which were used were also used to obtain BIs of 1 to 2mm in pure Al, therefore it was expected that similar results could be obtained for the experiments performed in this work
- Already modified eutectic Si found in base alloy. Base alloy A356 does not have the elements in its compositions which could cause modification of the eutectic Si nor the cooling rate was high enough to cause this morphology
- No significant changes observed in the fluidity between the different compositions. Although the grain refinement of Er would be expected to yield higher fluidity

5.5.1 Decreasing BI after trials and no grain refinement

As discussed in section 2.5.3, the difficulty with bifilms in aluminium alloys is their neutral buoyancy. However, there are two mechanisms that can change the density of the bifilms which makes them sink to the bottom of the crucible, and thus decrease the amount of bifilms in the bulk of the melt, as observed in Figure 5.13. That is, the thickening of the bifilm through further oxidation of the dry, non-wetted inside of the bifilm and the nucleation of intermetallic compounds on the wetted outside of the bifilm which is in contact with the melt [91, 27]. When a bifilm is newly created its oxide layer is thin (few nanometers thick) and flexible. Over time, the air which got entrapped between the dry surfaces of the bifilm is consumed by further oxidation of the oxide layer. The development of oxides thickness is given in Table 5.2. The trials took around one and a half hours per composition; therefore, the thickness of the bifilms could increase by two orders of magnitude, from its original thickness. This makes the oxide layer thicker, denser and more rigid. Firstly, the oxygen gets consumed after which the nitrogen, to form nitrides. However, if there is enough (8mL/kg [91]) hydrogen in the melt the diffusion of the hydrogen into the bifilm is dominant and the young and flexible bifilms get inflated which increases their buoyancy and the bifilms will float to the top of the melt, which is schematically shown in Figure 5.16. Because samples were taken from the top of the melt and the BI decreased with time, it can be expected that the hydrogen content was not high enough in the melt to inflate the bifilms to allow them to rise to the surface.

Table 5.2: Grow process of oxides in liquid aluminum alloys [10]

Growth time	Thickness	Type	Description	Possible source
0.01 to 1 s	1nm to 1μm	New	Confetti-like fragments	Pour and mold fill
10 s to 1 min	10μm	Old 1	Flexible, extensive films	Transfer ladles
10 min to 1 hr	100μm	Old 2	Thicker films, less flexible	Melting furnace
10 hr to 10 days	1000μm	Old 3	Rigid lumps and plates	Holding furnace

From literature it is known that many intermetallics prefer to nucleate on the wetted side of the bifilms which is energetically favorable [71]. Some of these intermetallics are α-Fe (Al_{15}-Fe_3Si_2), β-Fe (Al_5FeSi), Si eutectic and Sr rich phases [92]. Moreover, Er is more physicochemical active than Sr, La and Ce and is confirmed to be able to clean the melt [9], indicating that it is possible for Er to nucleate on the bifilms. This process of nucleation on the bifilm occurs atom-by-atom and creates an even layer around the bifilm, increasing its density until it sinks to the bottom of the crucible [10]. It is expected that Er and/or Eu nucleated on the bifilms as intermetallics which thickens the oxide layer, resulting in a more dense bifilm which sediments to the bottom of the crucible. This also explains why the BI of the base alloy worsens while the BI of the additions of Er and/or Eu decreases. Moreover, the Er nucleated on the bifilm cannot be used effectively as a grain refiner, supporting the observation that no grain refinement was found, thus further strengthening the credibility of this hypothesis.

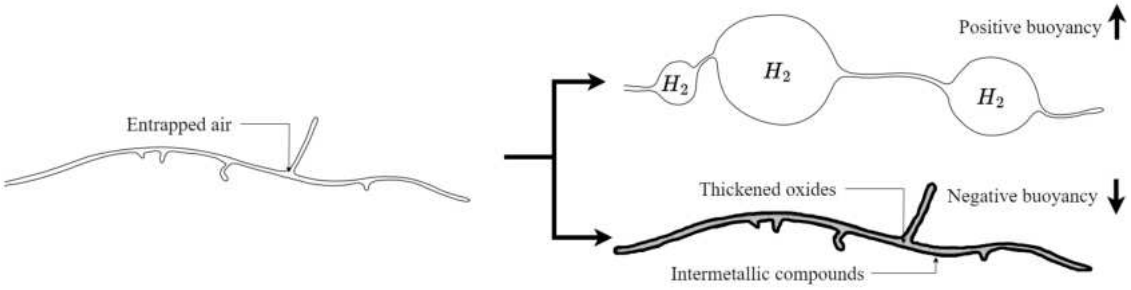

Figure 5.16: Two possible developments of bifilms in the melt (modified figure of [10])

Increasing melt quality after addition of grain refiner is experimentally confirmed by Gyarmati et al. [93] for $AlTi_3$ grain refiner. The authors conducted two experiments in which they investigated the degree of sedimentation of bifilms with the use of $AlTi_3$ grain refiner. In the first experiment, A1 in Figure 5.17 (b), the $AlTi_3$ was fully disolved into the melt at 800°C, according to the stable phase diagram Figure 5.17 (a). It was observed that the Ti nucleated on the bifilms as $(Al,Si)_3Ti$ which made the bifilms sediment. For the second experiment, A2 in Figure 5.17 (c), the $AlTi_3$ was introduced in the melt at 690°C. At this temperature the melt is in the L + $AlTi_3$ regime; therefore, $AlTi_3$ does not fully dissolve. The denser $AlTi_3$ particles start sinking to the bottom of the crucible taking the large bifilms with them, cleaning the melt.

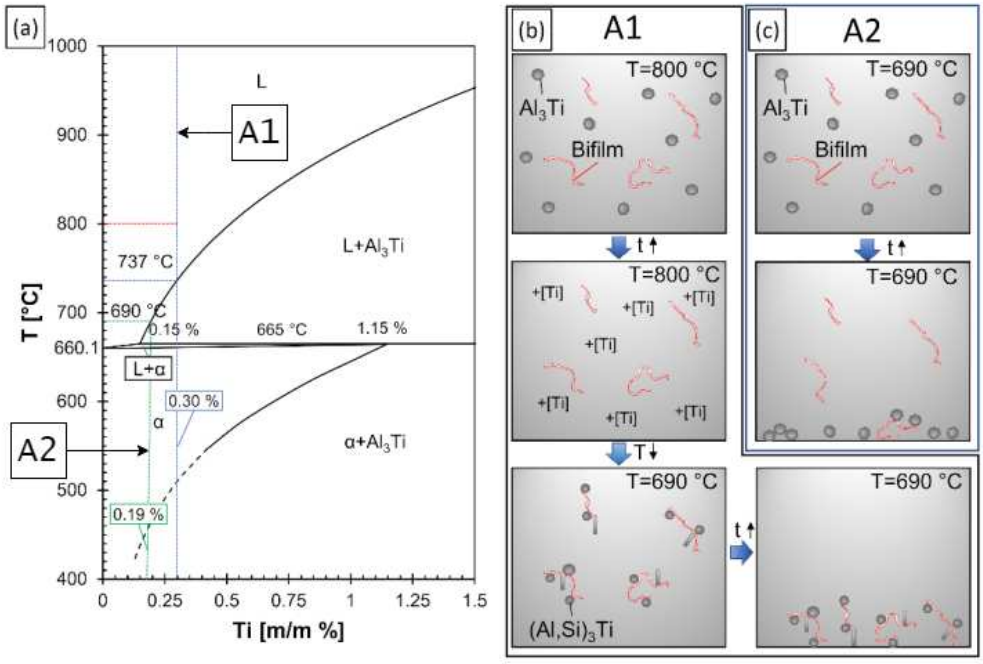

Figure 5.17: Two experiments (A1,A2) conducted on the sedimentation of bifilms with the use of $AlTi_3$[93]

To investigate if Er can undergo these same mechanisms the binary phase diagram of the Er-Al system was calculated in FactSage, as shown in Figure 5.18. The Er master alloy has an Er content of 10wt%, which corresponds to the left side of the diagram. The desired composition of the melt was 0.1wt% Er in the melt, which corresponds close to the right side of the phase diagram. This means that, if the Er master alloy dissolved quickly enough, only the mechanism of experiment A1 (in Figure 5.17) could occur. However, in another experiment by Gyarmati et al. [94] the sedimentation time was investigated and it was found that significant sedimentation occurred after only 10 minutes in the melt. Therefore, it might be possible that the $ErAl_3$ particles of the master alloy already settled to the bottom of the furnace before they had the chance to go into solution. This might be possible because $ErAl_3$ has 1.6 times the density of $TiAl_3$, increasing sedimentation rate. Therefore, both mechanisms; A1 and A2 from Figure 5.17 are assumed to have played a role in the cleaning of the melt.

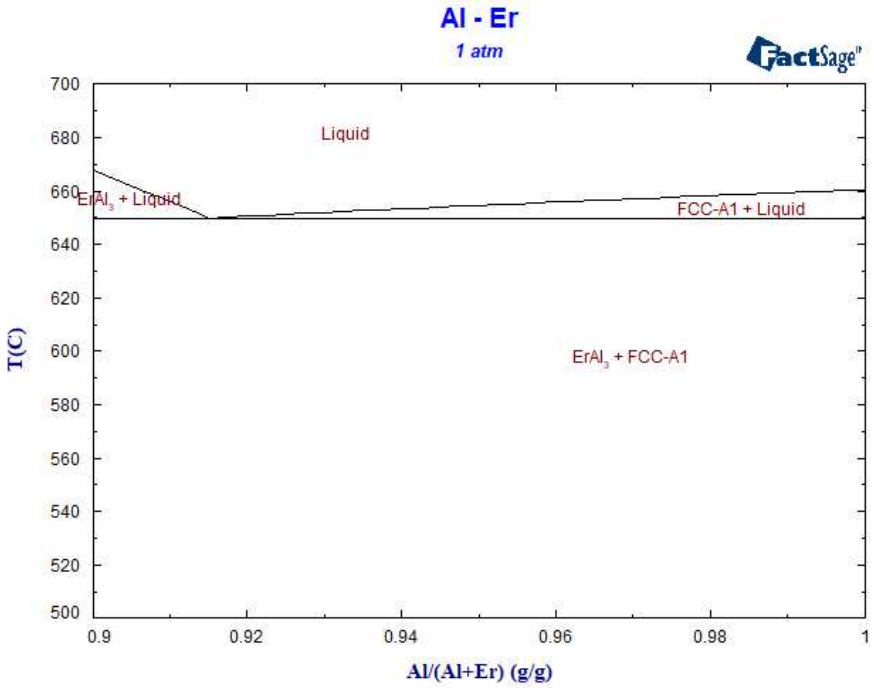

Figure 5.18: Al-Er binary phase diagram Al-rich (90-100wt% Al)

5.5.2 Unsuccessful cleaning of melt

The settings for the degassing operation to clean the melt were taken from the experimental work done internally by Foseco, for the same furnace with the same degassing equipment. However, the alloy used was a commercially pure aluminum alloy. The sensitivity of the degas parameters to melt cleanliness was demonstrated by Dispinar et al. [95] where it was shown that turbulence and the creation of a vortex by the rotary degassing unit increased the BI from 70mm to 120mm after two degassing operations. Thus, it worked counterproductive for the melt cleanliness, however, the hydrogen content did decrease. Therefore, more work needs to be done to find degassing settings which can reliably clean the melt of bifilms.

5.5.3 Already modified base alloy

In section 2.5.1, possible methods to modify the eutectic Si were discussed. Namely, by rapid cooling and/or the addition of modifying elements to the melt. The compositions of the base alloy samples were investigated by OES and XRF to see if any modifying elements were present, which could explain the modified microstructure. However, these elements could not be found or were not present in large enough quantities to cause modification. The measured concentrations are given in Table 5.3. Moreover, the samples were cast in a standard Barker mold, therefore, the cooling rate could not be high enough to modify the microstructure. This means that no conclusion could be reached to explain the modified Si morphology in the 0.0 base alloy. More research is needed to investigate this behavior.

Table 5.3: Concentrations, in wt%, of possible modifiers in base alloy

Sr	Na	Eu	Er	Sb	Ba	Ca	Y	Yb
<0.0001	0.0003	Not detected by XRF	Not detected by XRF	<0.003	0.0008	0.0048	Not detected by XRF	Not detected by XRF

5.5.4 No significant change in fluidity with different additions

It seems that there is strong evidence to support the hypothesis of Er and Eu nucleating on the bifilms and making these bifilms sink to the bottom of the crucible and thus cleaning the melt. This in turn deactivates the heterogeneous nucleation sites of the primary Al matrix, which inhibits grain refinement. Moreover, the base alloy was already modified; therefore, it seems logical that no significant difference in fluidity could be observed. Since the sole purpose of adding Er and Eu is to refine the grain and modify eutectic Si, respectively.

5.6 Validation of mold and test procedures

To evaluate the performance of the mold and test procedures the Gage R&R study has been conducted. As discussed in subsection 3.2.3, there are three sources of variation, namely, equipment, appraiser and part-to-part variation. Which for this experiment, is the variation due to the Radial Quad mold, operator and melt/material, respectively. The results of the Gage R&R per composition are shown in Table 5.4, noting that the variations given are measures of the standard deviation with unit mm. The filled worksheets can be found in Appendix 7.9. What can be noted is that the Appraiser Variation is very small, indicating that the difference between the measurements of different operators is relatively small compared to the total variation. This means that the operator has little influence on the measuring result, which is desired. Moreover, the equipment variation is also relatively small, meaning that the difference between the multiple measurements of the same component, by the same operator, yields almost identical measurements. This indicates that the equipment, i.e. the Radial Quad mold does not contribute significantly to the variation measured during the fluidity experiments. The Gage R&R is calculated to be 11.5% of the total variation, which is slightly above the 10% threshold, which is indicative of a well capable measuring system. When the GRR is between 10-30% it is generally accepted, but the risks associated with the measurements should be taken into consideration. Because fluidity is such a sensitive parameter it is necessary to measure multiple times, before getting any statistical significant data, which averages out the variation due to the operator and/or mold. Therefore, it can be concluded that the Radial Quad mold and its testing procedures can be considered to be a capable measurement system to measure fluidity.

Table 5.4: Results of the Gage R&R of the different compositions given in [mm]

Composition	0.0 base	0.1 Er	0.2 Eu	0.1 Er + 0.2 Eu	Average	% of Total Variation
Equipment Variation (EV)	2.05	0.93	1.17	1.98	1.53	10.4%
Appraiser Variation (AV)	1.17	0.65	0.35	0.60	0.69	4.7%
Gauge R&R (GRR)	2.36	1.14	1.22	2.07	1.70	11.5%
Part Variation (PV)	10.13	18.66	18.29	11.17	14.56	99.1%
Total Variation (TV)	10.40	18.70	18.33	11.36	14.70	

5.7 Summary

In this chapter, the technical difficulties with the Vacuum mold were discussed, which mainly involved the airtightness of the mold. From the fluidity tests, no statistical significant increase or decrease could be detected with the different additions. However, it could be found that Er has the potential for the highest fluidity, Eu seems to decrease fluidity, and when adding Er + Eu the performance is averaged. 3mm seems to be the lower limit for thin-walled features since the fluidity into these parts remained minimal, at about 50mm (in a 15mm wide channel). After 3mm height channel, the fluidity increases by 50mm per 1mm in channel height. The composition analysis showed that too much Eu was added (0.31wt% instead of 0.2wt%) during the experiments, creating an even better and finer distribution of the eutectic Si. Therefore, 0.3wt% can be considered enough to reach full modification. Eu also redistributes larger pores into more smaller pores, which can be beneficial to the mechanical properties of the casting. The addition of 0.1wt% Er was unable to refine the microstructure of the A356 base alloy, it is expected that Er nucleated on the bifilms, disabling the heterogeneous nucleation sites. The decrease in grain size after the casting trials is contributed to the unfurling of the bifilms, which prevents the breakage of dendrites in the flow. Measurement of the grain size in the channels of the Radial Quad mold is difficult due to the small cross-sectional area of the channels. The base alloy was already modified, and no modifying elements could be found in the composition, nor could the cooling rate be high enough to cause this modification. Further research is needed to investigate this phenomenon. Therefore, a minimal difference could be seen between the eutectic Si of the base alloy and the Er + Eu composition, which should have the highest modification. Some intermetallics were found within the base alloy, Er created some smaller intermetallics, Eu seems to also modify the morphology of intermetallics which makes them finely distributed, and the Er + Eu compositions created some longer needle-like intermetallics, but these are expected to not have any major effect on fluidity. The melt was not able to be properly cleaned with the degassing settings, re-emphasising the sensitivity of the degassing parameters on melt cleanliness. The results of the fluidity measurements seem to suggest that an increase in BI decreases the fluidity, which is in accordance with the literature. However, the melt became cleaner after the trials for the Er, Eu and Er and Eu compositions, which also suggests the cleaning of the melt by the addition of Er and Eu. Therefore, the hypothesis is that the Er and/or Eu have nucleated on the bifilms, increasing their density, which caused them to settle to the bottom of the crucible. This cleans the melt and deactivates the grain refiners as heterogeneous nucleation sites for the primary Al-matrix. From the Gage R&R study it was concluded that the variation in the measurement system is small enough, compared to the variation of the fluidity of the alloy, that the mold and test procedures can be considered capable of measuring fluidity, reliable and repeatable.

6. Conclusion and Prospective

In this chapter, the key findings of this work are listed and their implications for the industry are described. Moreover, a reflection on the research objectives is given, which were formulated in section 1.2. Lastly, recommendations are given for further research and suggested improvements are given on the mold design.

6.1 Summary of the key findings

Below the key findings of this work are listed.

- The Ragone test, spiral mold, octopus design and star mold have their limitation in keeping the mold and/or experimental parameters constant. Therefore, repeatable and reproducible fluidity measurements have been difficult to perform
- From the fluidity experiments, no statistical significance conclusion could be drawn on the increase or decrease of the fluidity, by the additions of Er and/or Eu, to an A356 alloy, due to the extremely poor melt quality
- The average fluidity of the compositions, show that Er performs better than Eu and Er + Eu creates an averaged performance. Apparently indicating that Er increases fluidity and Eu decreases fluidity and combined create an average fluidity between the two
- The ±50mm fluidity in the 3mm (15mm width) height channel seems to be the lower limit of the fluidity for the A356 base alloy with and without additions of Er and/or Eu. After 3mm channel height the fluidity seems to increase linearly with 50mm of fluidity per 1mm channel height
- The melt could not be successfully cleaned with the degassing operation. The melt quality had a BI >200mm and decreased by half to around 100 after the casting trials of Er, Eu and Er + Eu compositions. This is, however, still above the acceptable levels for melt cleanliness. The difficulty in cleaning the melt restates the sensitivity for process parameters during the degassing operation
- The decrease in grain size after the casting trials is attributed to less unfurling of bifilms which made the breakage of dendrites possible, resulting in smaller grains
- The addition of 0.1wt% Er did not result in grain refinement since the quality of the melt was extremely poor at BI above >200mm. Therefore it is believed that Er nucleated on the bifilms and thus deactivating the nucleation sites for the primary Al matrix

- The addition of 0.1wt% Er and/or 0.2wt% Eu cleaned the melt of bifilms by precipitating on the bifilms, increasing its density and making the bifilm sink to the bottom of the crucible
- The base alloy used (A356) was already modified before addition of 0.1wt% Er and/or 0.2wt% Eu. No modifying elements were found in the composition and the cooling rate could not be high enough to cause this modification. Therefore, no conclusion could be drawn why the base alloy was already modified
- 0.31wt% Eu created an excellent modification of the eutectic Si and can be considered enough for full modification of the eutectic Si
- A small but noticeable trend could be found which indicates that worst melt cleanliness, and thus higher BIs, would results in lower fluidity
- Er created some smaller intermetallics, Eu alone seems to create smaller and more distributed the intermetallics and Er + Eu created longer-needle like intermetallics which are expected to not cause significant disturbance to the fluidity
- From the Gage R&R study it was found that the variation due to the Radial Quad mold and operator are small enough (GageRR = 11.5%), compared to the inherent variation of the fluidity of the alloy, that the mold and procedures can be considered capable of reliably and repeatably measuring fluidity

6.2 Reflection on research objectives

In this work two research objectives were formulated namely;
Objective 1: Investigate the effect of the additions of Er and Eu on the fluidity of the commercially available aluminum alloy, to determine whether Er and/or Eu can be viable alternatives for current grain refiners and/or modifiers of eutectic Si.

Objective 2: Develop a less labor-intensive, repeatable, and reproducible permanent mold to measure the fluidity of aluminum alloys, ensuring consistent results across tests.

Objective 1 could not be completed as the quality of the melt disabled the effect of grain refinement of Er and the base alloy was already modified, making it even harder to observe the effects of Eu on fluidity. To achieve this objective, the same experiments should be pefromed with a confirmed clean melt on a non-modified A356 base alloy.

However, Objective 2 was successful, with an acceptable Gage R&R score of 11.5% of the total variation. Therefore, the Radial Quad mold and its accompanying testing procedures can be reliably used to measure fluidity. Therefore, Foseco can use this mold and test procedures to redo the fluidity measurements with Er and Eu to successfully complete research Objective 1.

6.3 Implications for the industry

From this work the importance of melt quality has been again highlighted. The large amount of bifilms nullifies the effect of expensive grain refiners and act as crack initiation points in the castings. The data suggest that a worse melt quality decreases fluidity. Therefore, in the best interest of the foundries and casthouses, working with A356 alloy, to first mitigate all melt cleanliness issues before experimenting with grain refiners and/or modifiers of eutectic Si. It has been shown that the melt quality is sensitive to the degas parameters, therefore these parameters should be optimised to reliably clean the melt.

From the Radial Quad test setup, the influence of the operator and the variance of the equipment is small compared to the inherent variation of fluidity experiments, indicating that this mold and procedure are repeatable and reproducible. Therefore, they can be considered to be a capable measuring system for measuring fluidity. Moreover, if foundries want to cast thin sections in a permanent mold, it is advised to have a section height of at least 4mm since the 3mm channel barely filled, regardless of addition ratios. Lastly, excellent modification of the eutectic Si was observed with the addition ratio of 0.31wt% Eu to the A356 alloy, therefore it is recommended to use at least 0.3wt% Eu when modification is desired.

6.4 Improvements on mold design

As for the design of the Radial Quad mold, it would be suggested to incorporate an isolating handle for the operator to remove the cope after casting. Within the experiments, glue clamps were used that were heavy and limited the movement of the operator that needed to fill the pouring basin. Also, a method of holding the heating elements in the mold would be recommended since they will burn up if they come out of the mold while being turned on. Lastly, a second pin and slot would be practical to align the cope and drag between castings.

6.5 Further research

For further research, it would be recommended to redo the experiments but with confirmed clean melts. To this end, research should be conducted on finding degassing parameters which are able to reliably clean the melt. Moreover, it would also be beneficial to measure the hydrogen content before and after fluidity trials to investigate whether enough hydrogen is present to inflate the bifilm. The fading behavior of $ErAl_3$ should be investigated to mitigate the loss of the grain refiner in the melt. For example, by taking samples from the bottom of the crucible to verify if bifilms indeed sink to the bottom of the crucible and check if Er and/or Eu have nucleated on the bifilms. Research with different addition ratios of Er and Eu would provide more insight into the effect of modification of the microstructure and the formation of intermetallics. Lastly, the modification of the eutectic Si in the base alloy should be investigated since there is no explanation to be found in the current literature for this phenomenon.

7. Appendix

7.1 Head pressure calculation Vacuum mold

In the Vacuum setup, the vacuum generator emulates the metallostatic pressure. To determine the pressure setting on the vacuum regulator, the distance h should be known from Figure 7.1.

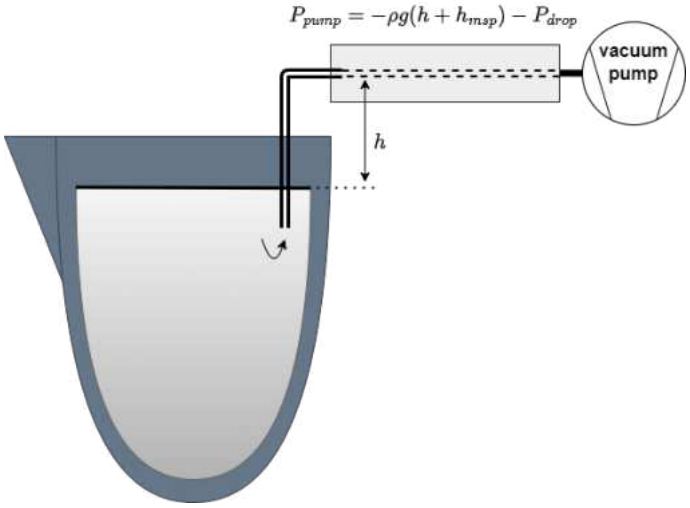

Figure 7.1: Metallostatic pressure calculation Vacuum setup

Moreover, the flow meter, hosing, die and straw also provide resistance to the flow, which creates an additional pressure drop. This can be thought of as the impedance of the electrical system, as the electrical circuit equivalent shows in Figure 7.2. This pressure drop should be compensated and can be measured by installing all the components and applying suction without putting the straw into the melt. The pressure read on the vacuum regulator is the pressure drop in the whole system. This pressure drop should be added to the emulated metastatic pressure to apply the correct partial vacuum.

To calculate the pressure setting on the vacuum regulator the following example is provided: If a 27.5mm metallostatic pressure is desired, $h = 250$mm, assuming $\rho_L = 2550kg/m^3$ [96] and the pressure drop through the system is $P_{drop} = -52kPa$ then:

$$P_{pump} = -\rho_L \cdot g(h+h_{msp}) - P_{drop} = -2400 \cdot 9.81 \cdot (0.25+0.0275) - 52kPa = -58.5kPa \quad (7.1)$$

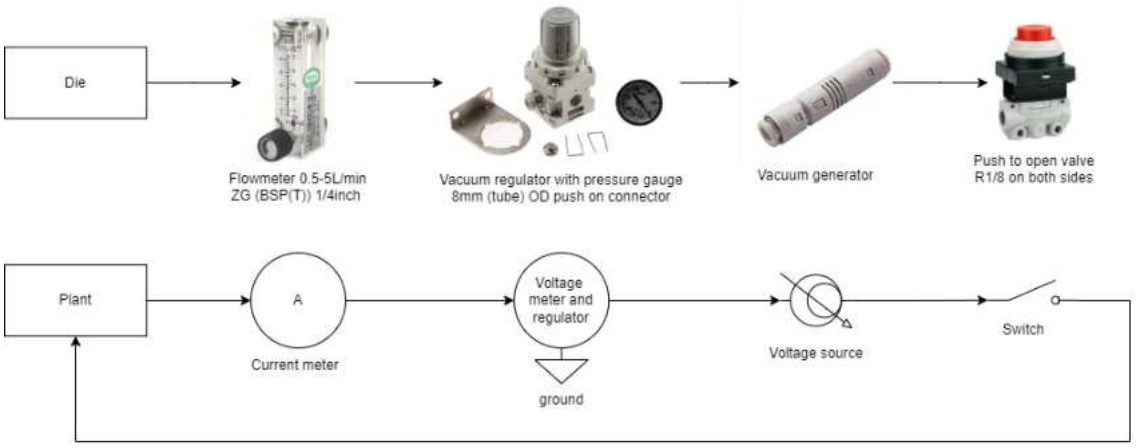

Figure 7.2: Component overview electrical equivalent

7.2 Flow setting calculation

To determine the flow setting on the rotameter, which uses L/min, a small calculation needs to be performed. The flow rate through the flow meter equals the cross-sectional area of the channel, shown in Figure 7.3, multiplied by the maximum flow velocity which is 0.5m/s, as calculated in section 2.5.3.

$$Q = A_{Channel} \cdot V_{flow} = 83.65 \cdot 500 = 25095mm^3/s = 2.51L/min \tag{7.2}$$

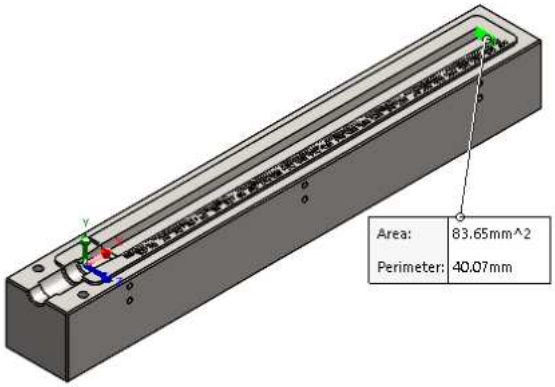

Figure 7.3: Cross-sectional area vacuum mold

This maximum flow velocity should be read on the flow meter with the straw installed, without sucking from the melt.

7.3 Requirements

In this section, the requirements for the fluidity test in a permanent mold gravity casting are discussed.

- The mold must have 1 with a maximum of 4 cavities of different channel thickness, between 6mm and 3mm
- The channel cavities must be horizontally orientated, to ensure constant (metallostatic) pressure in the channel
- The (metallostatic) pressure must be the same within all channel cavities
- The fluidity channels should be filled at the same time
- The ingate temperature should be the same within all channel cavities
- The mold must have venting systems ($\varnothing$ 1mm) within all channel cavities
- The drag must have length indication (1mm increments) to help read fluidity lengths
- The draft angle needs to be 10°C
- The maximum pouring volume must be less than $1L \approx 2.5$kg
- The mold must be able to be manually opened by a single person
- The size of the die must fully fit within a bounding box of 100x800x800mm
- The mold must be able to be heated within ± 3°C in the range of 20°C to 500°C
- The mold must have at least the thermal capacity such that the mold will not heat up more then 10°C during the tests
- Metal flow velocity should be ≤ 0.65m/s to prevent major surface turbulence

7.4 Technical drawings

In this appendix, all the technical drawings can be found of the Radial Quad mold, stopper design, Vacuum mold, isolating pouring basin mold.

7.4.1 Technical drawings Radial Quad mold

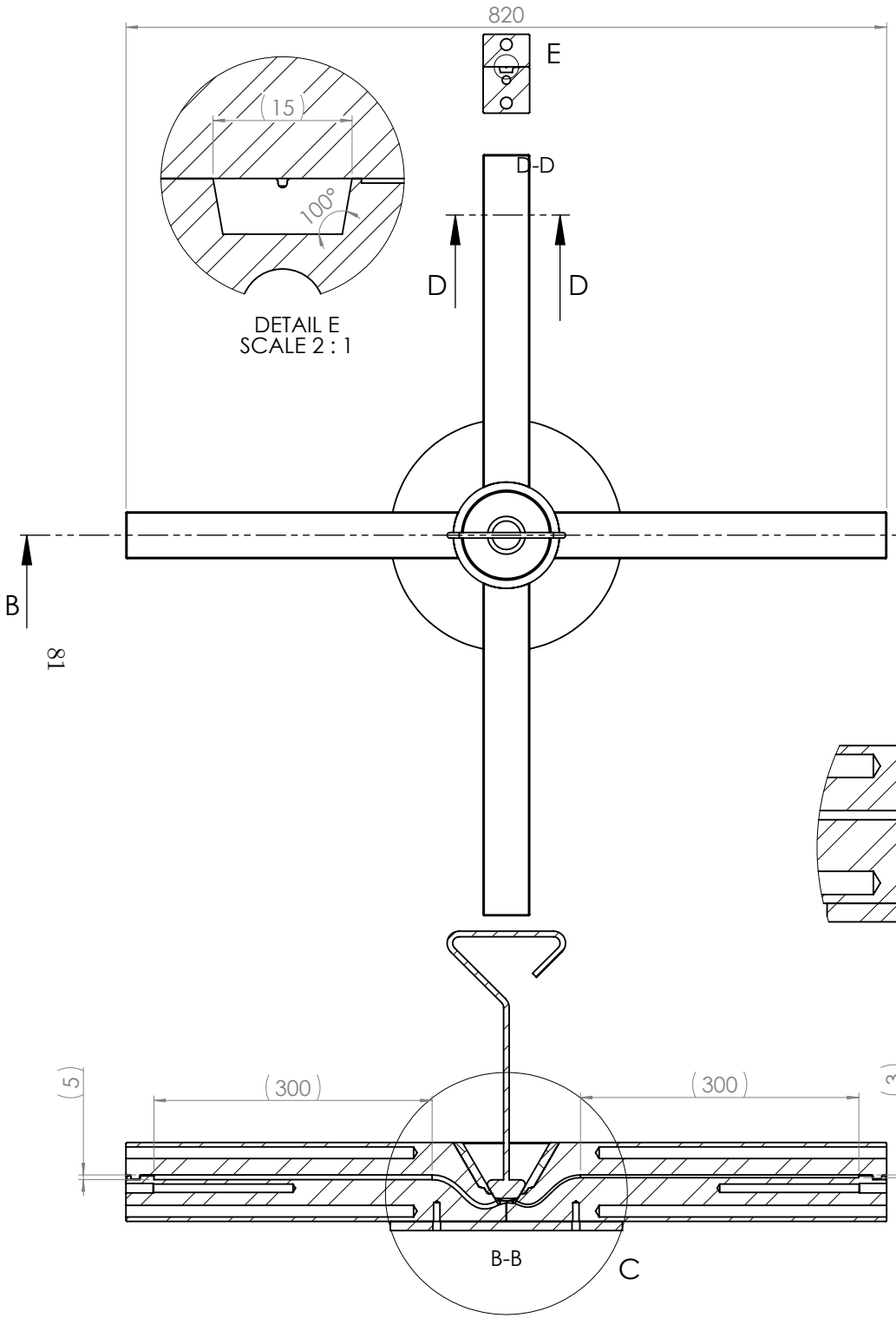

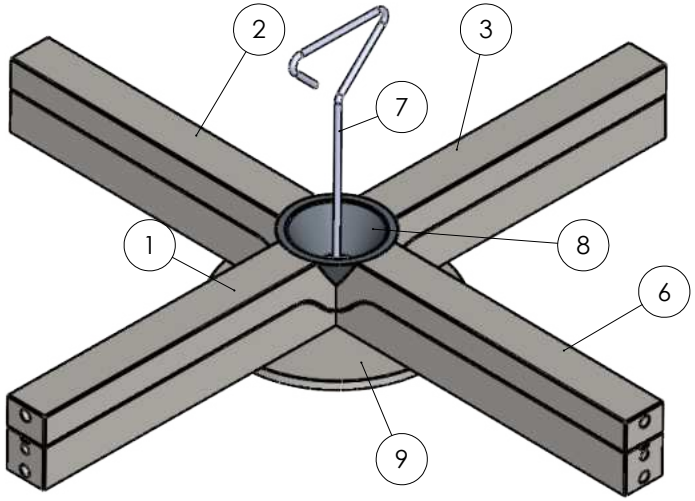

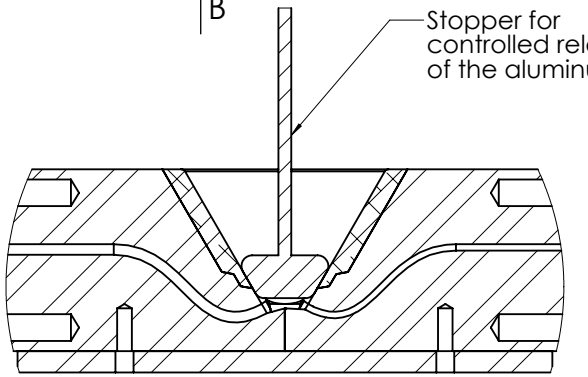

DETAIL C
SCALE 2 : 5

ITEM NO.	PART NUMBER	QTY.
1	ChannelRadialFour	1
2	ChannelRadialFour	1
3	ChannelRadialFour	1
4	PouringBasinTop	1
5	StopperFilterDisk	1
6	ChannelRadialFour	1
7	Stopper	1
8	High precission sleeve	1
9	BottomPlateRadialElaphantHex	1

Use STEP-file for not mentioned dimensions

General tolerances according NEN ISO 2768-mK
Geometrical tolerancess according ISO 1101
Thermal cutting tolerances according ISO 9013-1
Welding tolerances according ISO 13920-BF
Remove sharp edges according NEN ISO 13175
General roughness according DIN ISO 1302
Ra 3,2

Projection

Drawn by	Jan Veenhuis	Date	07/02/2024
Weight	50.95 kg	Scale	1:5

Material

Treatment

Part number

REV.

Drawing number
RadialElaphantHex

Description
Quad Radial Test Setup

A3

DIMENSIONS IN MILLIMETERS

SHEET 1 OF 1

Do not scale drawing

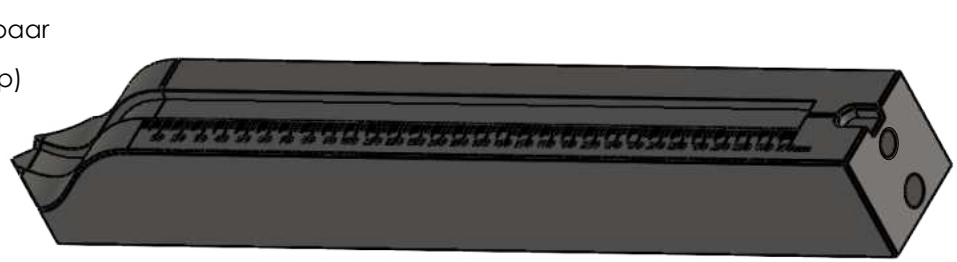

DETAIL F
SCALE 1 : 1

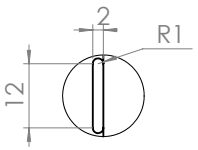

DETAIL E
SCALE 1 : 1

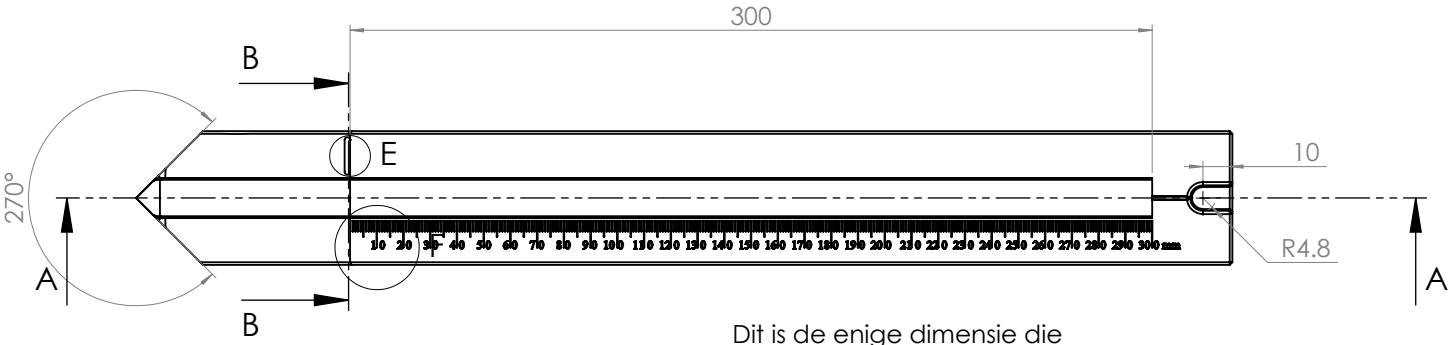

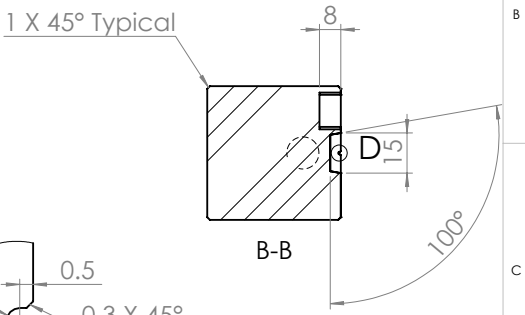

B-B

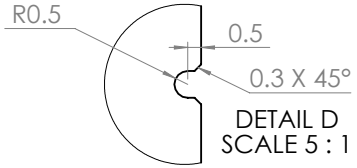

DETAIL D
SCALE 5 : 1

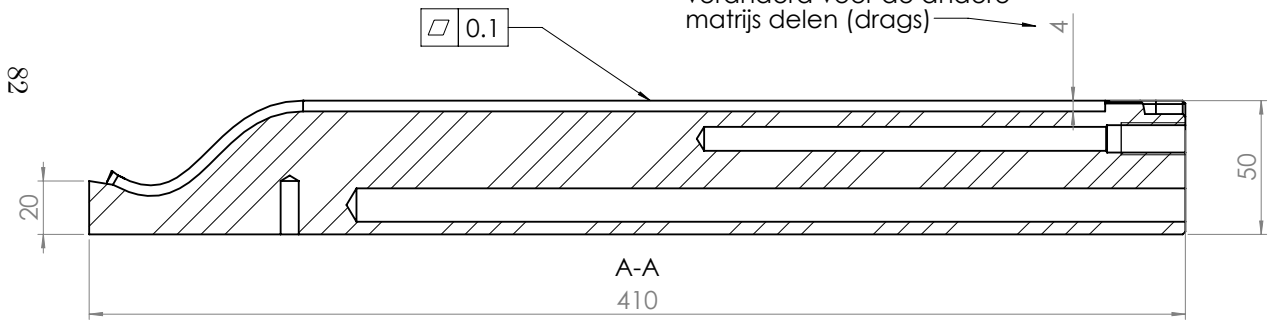

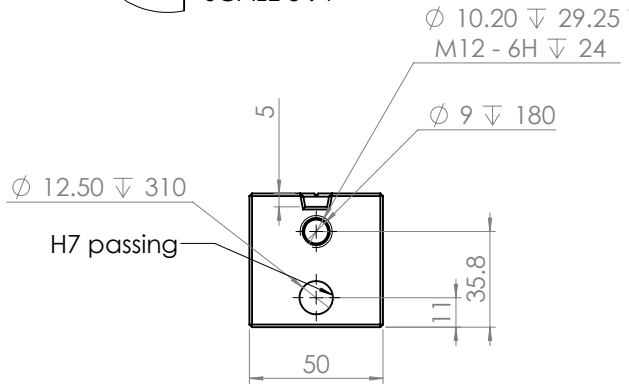

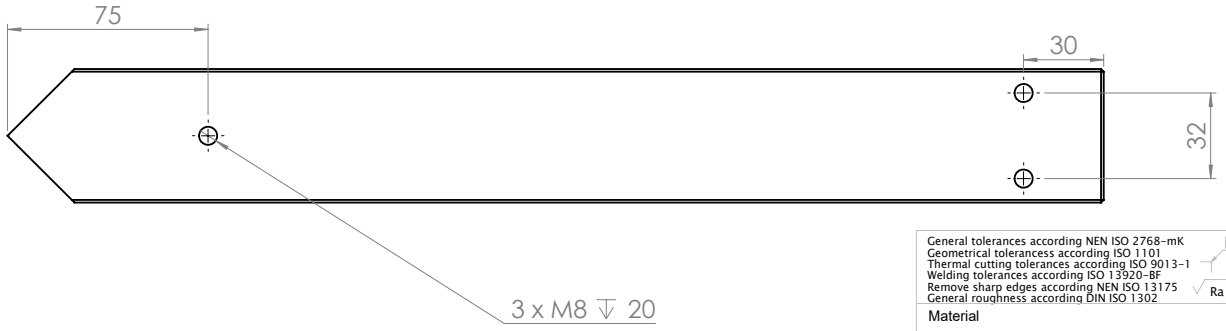

Use STEP-file for not mentioned dimensions

General tolerances according NEN ISO 2768-mK Geometrical tolerancess according ISO 1101 Thermal cutting tolerances according ISO 9013-1 Welding tolerances according ISO 13920-BF Remove sharp edges according NEN ISO 13175 General roughness according DIN ISO 1302 Ra 3,2	Projection	Drawn by	Jan Veenhuis	Date	07/02/2024
		Weight	6.89 kg	Scale	1:2
Material	Treatment	Part number			REV.
1.4401 (X5CrNiMo17-12-2)	Deburring	Drawing number	4mm Drag		
		Description	4mm drag		A3
		DIMENSIONS IN MILLIMETERS		SHEET 1 OF 1	

Do not scale drawing

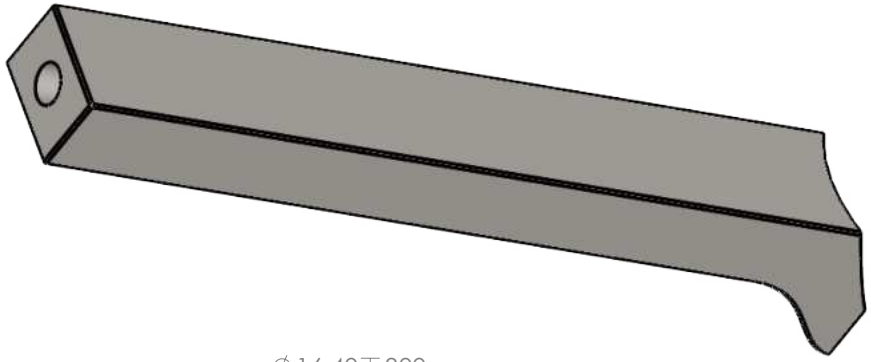

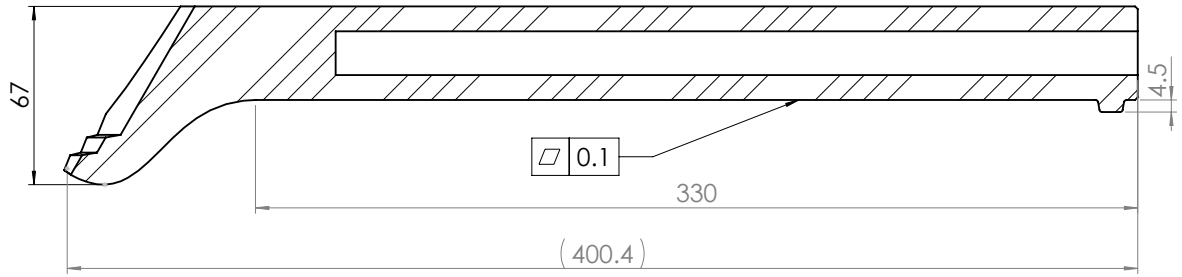

A-A

Use STEP-file for not mentioned dimensions

General tolerances according NEN ISO 2768-mK Geometrical tolerancess according ISO 1101 Thermal cutting tolerances according ISO 9013-1 Welding tolerances according ISO 13920-BF Remove sharp edges according NEN ISO 13175 General roughness according DIN ISO 1302 Ra 3,2	Projection	Drawn by	Jan Veenhuis	Date	
		Weight	4.92 kg	Scale	1:2
Material	Treatment	Part number			REV.
1.4401 (X5CrNiMo17-12-2)	Deburring	Drawing number	4mm Cope		A3
		Description	Cope for all channels		
		DIMENSIONS IN MILLIMETERS		SHEET 1 OF 1	

Do not scale drawing

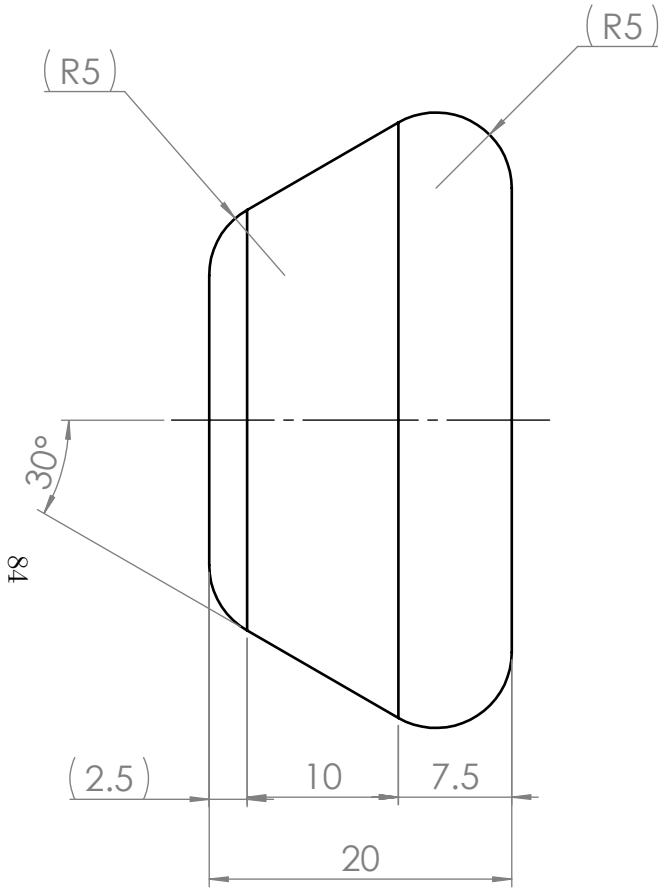

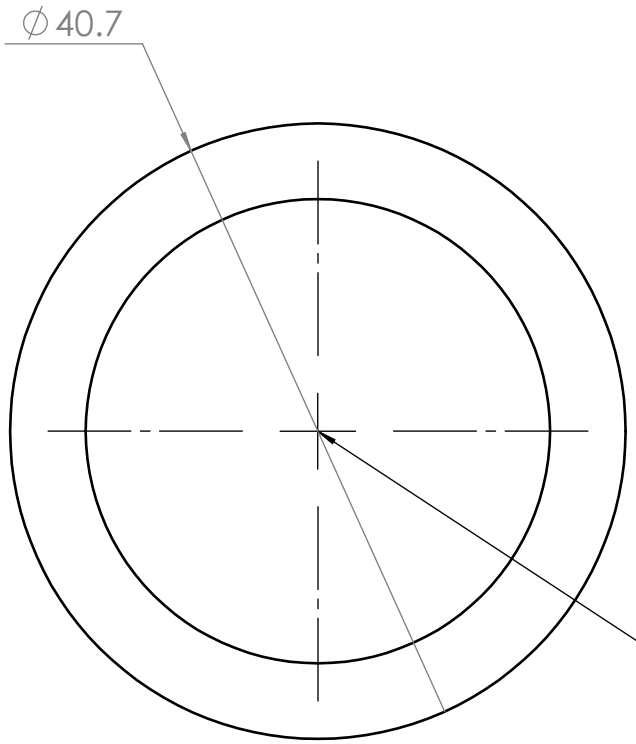

Use STEP-file for not mentioned dimensions

General tolerances according NEN ISO 2768-mK Geometrical tolerancess according ISO 1101 Thermal cutting tolerances according ISO 9013-1 Welding tolerances according ISO 13920-BF Remove sharp edges according NEN ISO 13175 General roughness according DIN ISO 1302 Ra 3,2	Projection	Drawn by	Jan Veenhuis	Date	07/02/2024
		Weight	0.15 kg	Scale	2:1
Material: Plain Carbon Steel	Treatment: Deburring	Part number		REV.	
		Drawing number: Stopper			
		Description: Stopper plug		A4	
		DIMENSIONS IN MILLIMETERS		SHEET 1 OF 1	

Afmetingen zijn indicatief
Het moet gewoon een hendel zijn
die makkelijk te gebruiken is

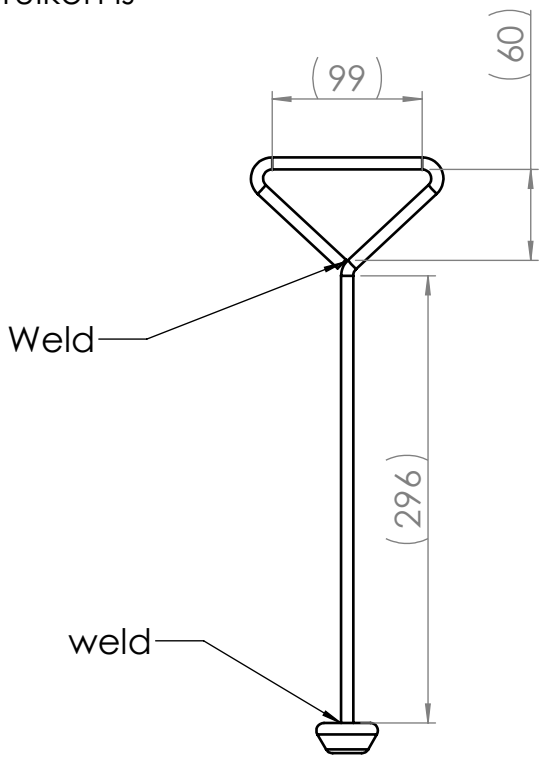

Use STEP-file for not mentioned dimensions

General tolerances according NEN ISO 2768-mK Geometrical tolerancess according ISO 1101 Thermal cutting tolerances according ISO 9013-1 Welding tolerances according ISO 13920-BF Remove sharp edges according NEN ISO 13175 General roughness according DIN ISO 1302 Ra 3,2	Projection	Drawn by	Jan Veenhuis	Date	15/02/2024
		Weight	0.38 kg	Scale	1:5
Material	Treatment welded	Part number			REV.
		Drawing number Stopper			
		Description Stopper with handle			A4
		DIMENSIONS IN MILLIMETERS			SHEET 1 OF 1

7.4.2 Technical drawings of the Vacuum mold

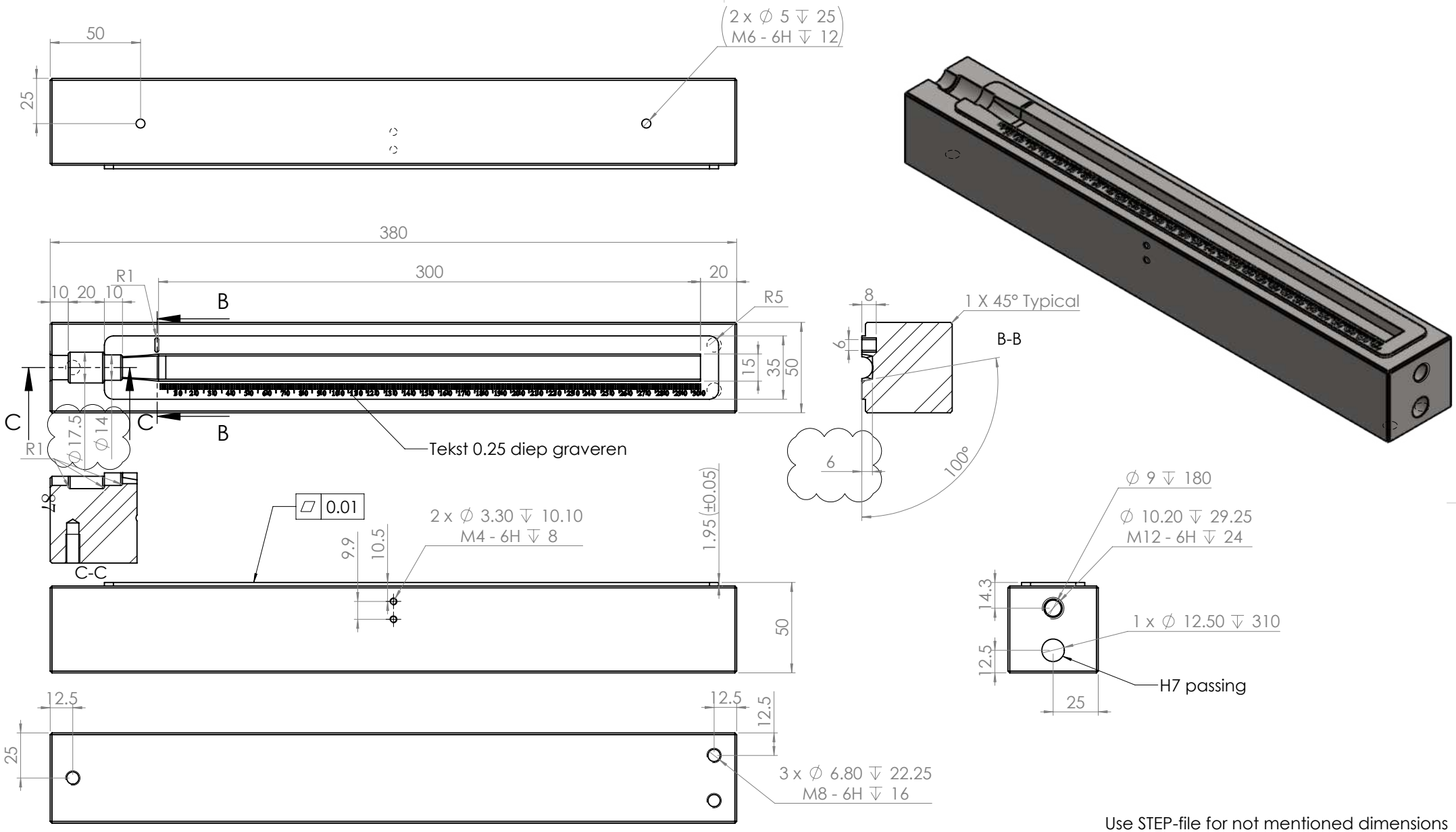

Use STEP-file for not mentioned dimensions

General tolerances according NEN ISO 2768-mK Geometrical tolerancess according ISO 1101 Thermal cutting tolerances according ISO 9013-1 Welding tolerances according ISO 13920-BF Remove sharp edges according NEN ISO 13175 General roughness according DIN ISO 1302 Ra 3,2	Projection	Drawn by	Jan Veenhuis	Date	28/02/2024
		Weight	6.81 kg	Scale	1:2
Material	Treatment	Part number		REV.	
1.4401 (X5CrNiMo17-12-2)	Deburring			1	
		Drawing number	Drag Vacuum		
		Description	Drag vacuum	A3	
		DIMENSIONS IN MILLIMETERS		SHEET 1 OF 1	

Do not scale drawing

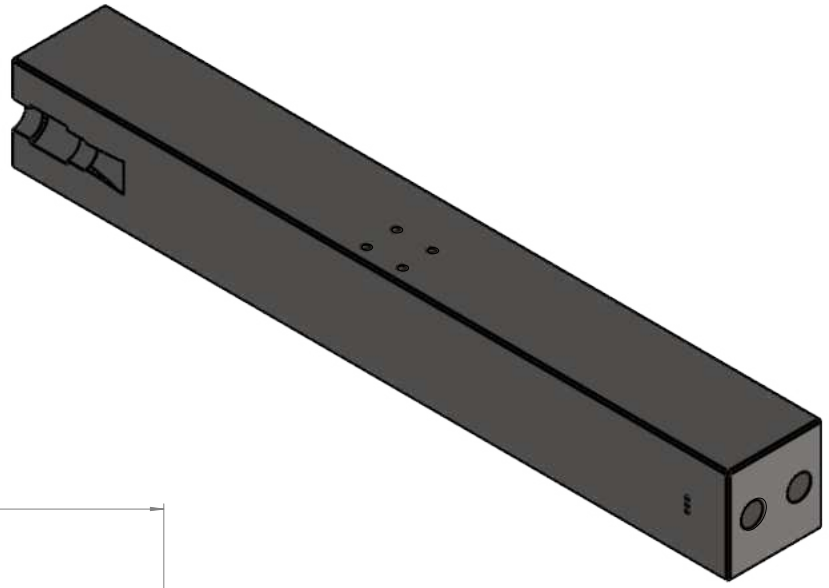

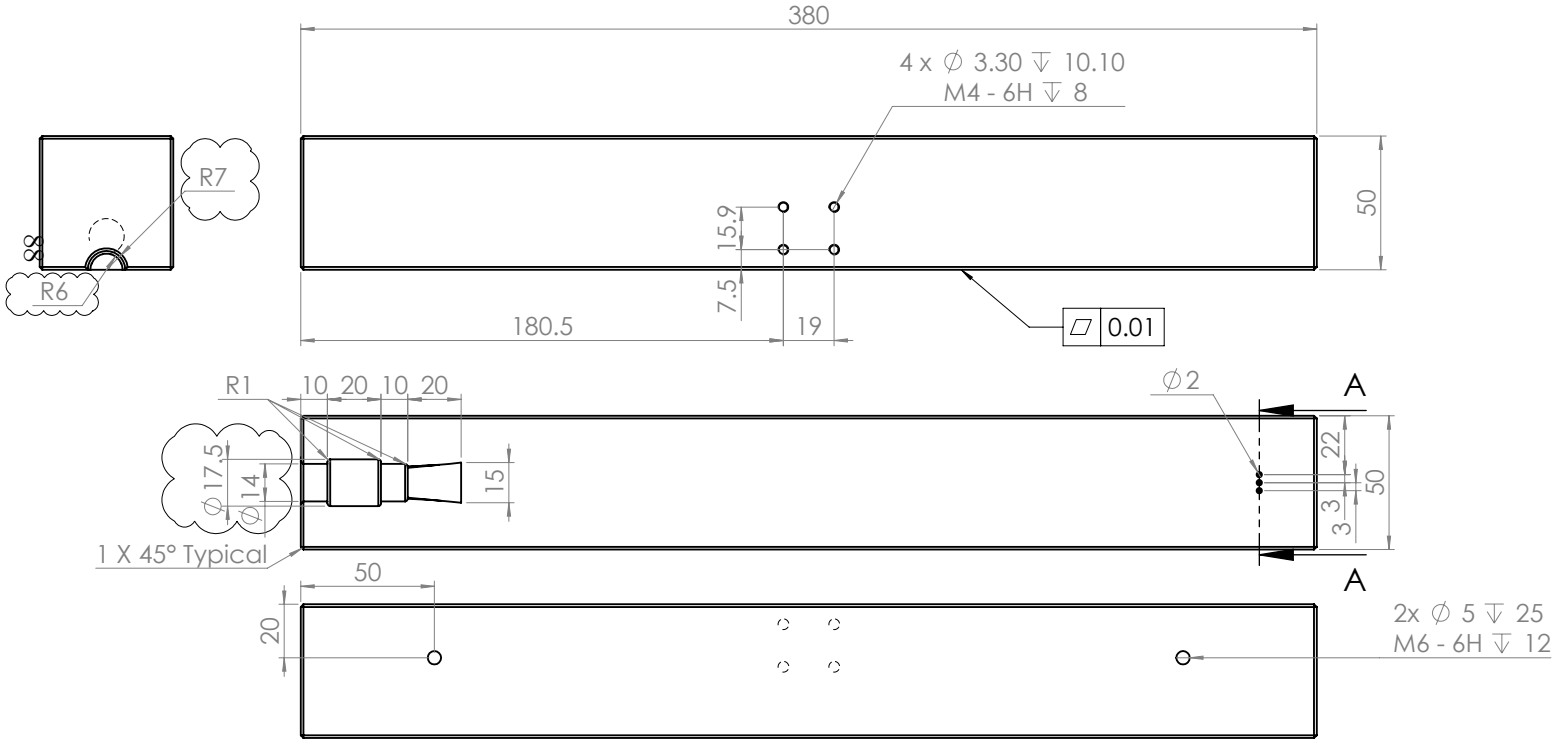

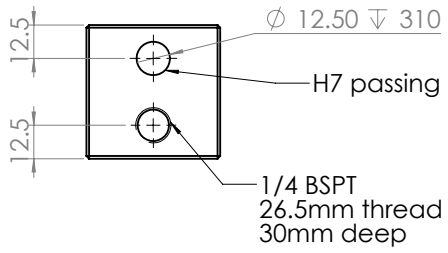

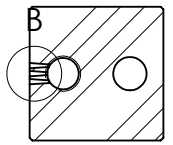

A-A

DETAIL B
SCALE 1 : 1

Use STEP-file for not mentioned dimensions

General tolerances according NEN ISO 2768-mK
Geometrical tolerancess according ISO 1101
Thermal cutting tolerances according ISO 9013-1
Welding tolerances according ISO 13920-BF
Remove sharp edges according NEN ISO 13175
General roughness according DIN ISO 1302
Ra 3,2

Projection

Drawn by	Jan Veenhuis	Date	28/02/2024
Weight	7.21 kg	Scale	1:2

Material	Treatment	Part number	REV.
1.4401 (X5CrNiMo17-12-2)	Deburring		1

Drawing number: Cope Vacuum

Description: Cope Vacuum

A3

DIMENSIONS IN MILLIMETERS

SHEET 1 OF 1

Do not scale drawing

7.4.3 Technical drawings of the isolating pouring basin shooting mold

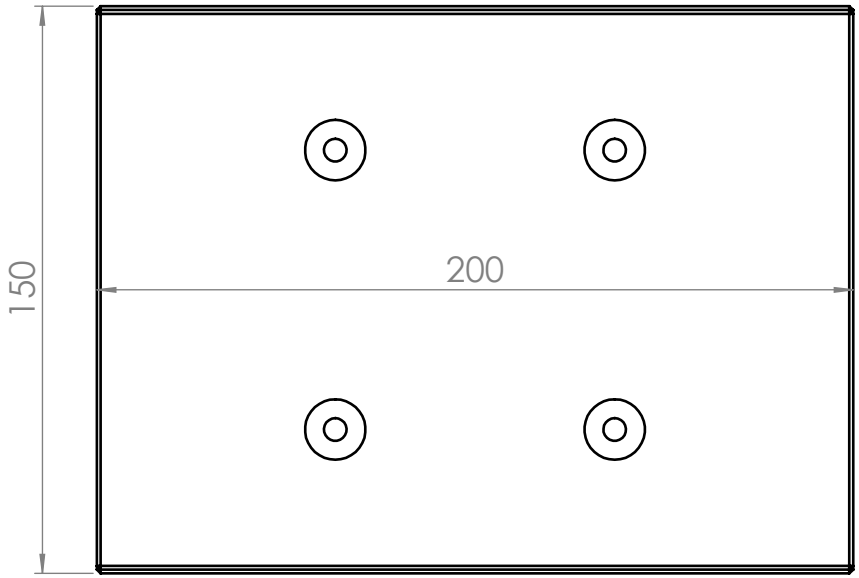

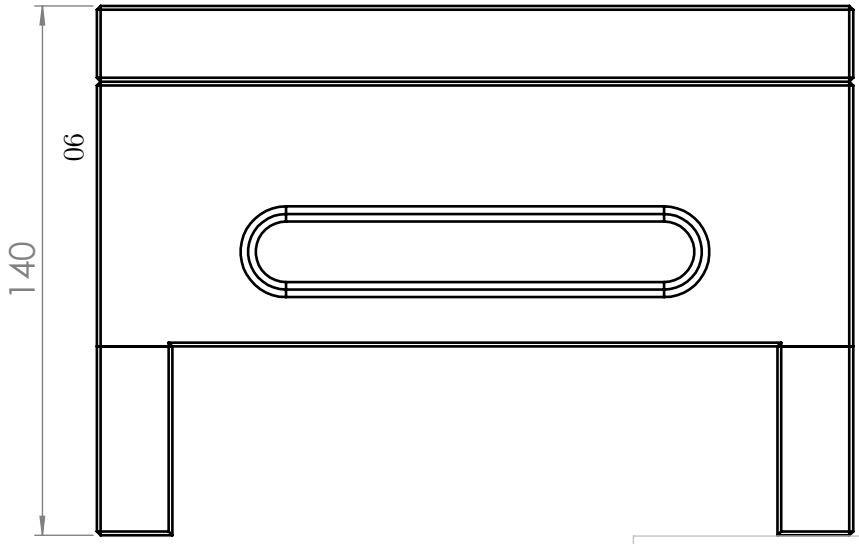

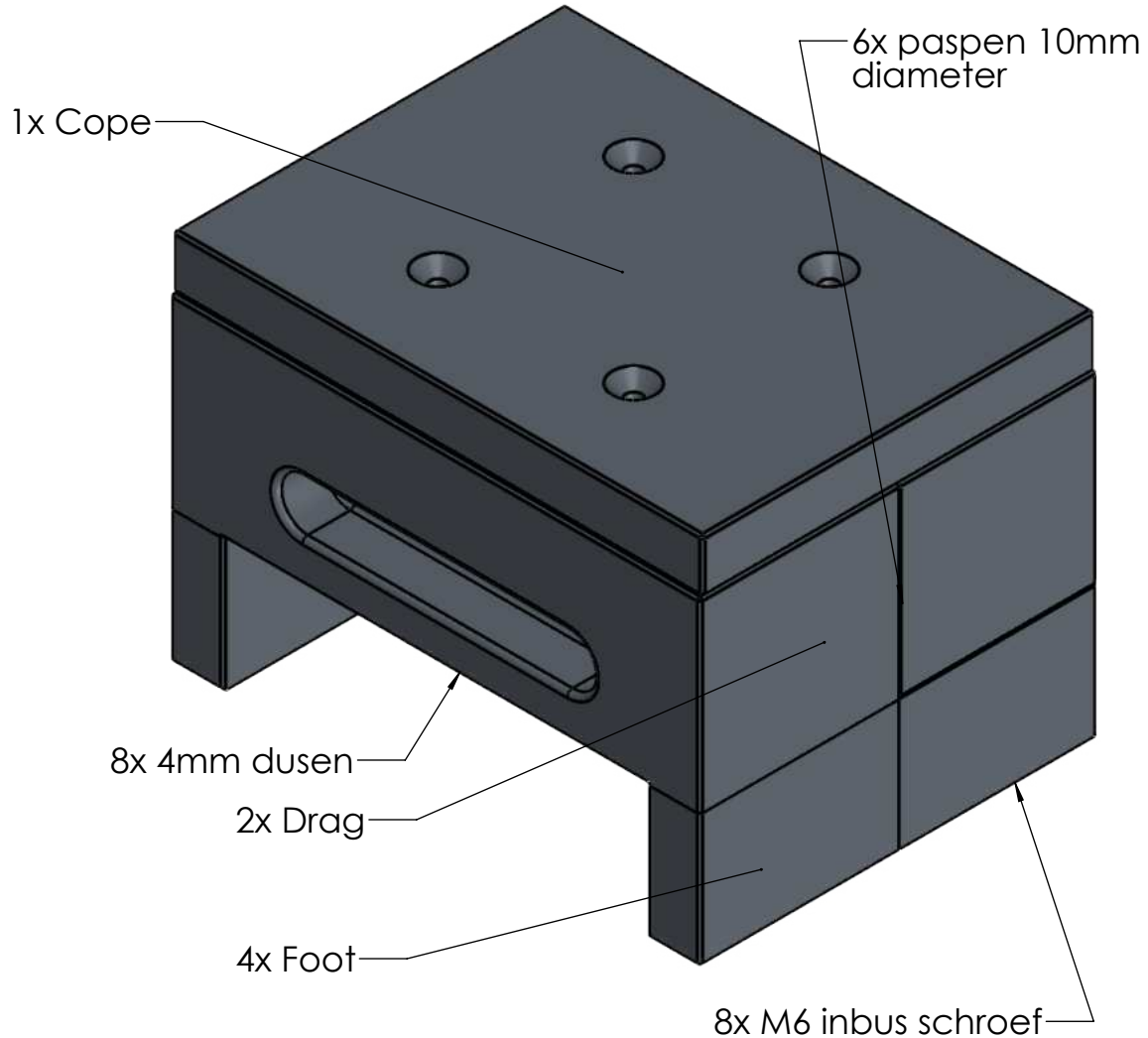

Use STEP-file for not mentioned dimensions

General tolerances according NEN ISO 2768-mK Geometrical tolerancess according ISO 1101 Thermal cutting tolerances according ISO 9013-1 Welding tolerances according ISO 13920-BF Remove sharp edges according NEN ISO 13175 General roughness according DIN ISO 1302 Ra 3,2	Projection	Drawn by	Jan Veenhuis	Date	01/02/2024
		Weight	7.66 kg	Scale	1:2
Material: AW-5083	Treatment: Deburring	Part number		REV.	
		Drawing number: High precission sleeve		A4	
		Description: Mold for isolating sleeve			
		DIMENSIONS IN MILLIMETERS		SHEET 1 OF 1	

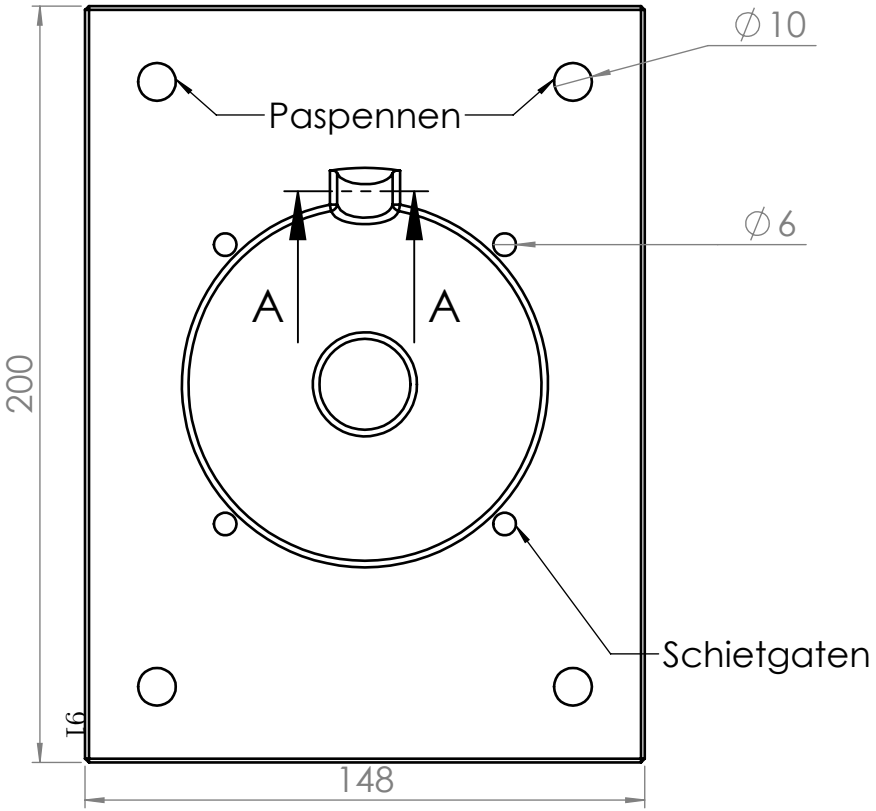

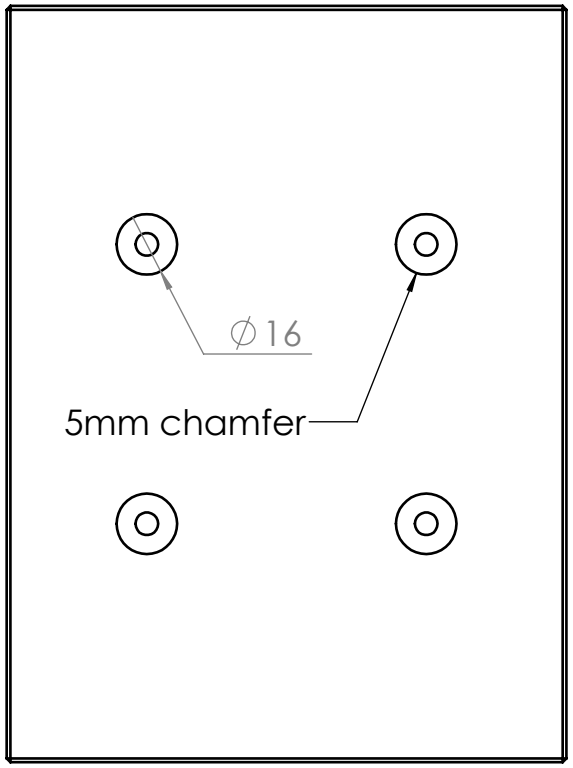

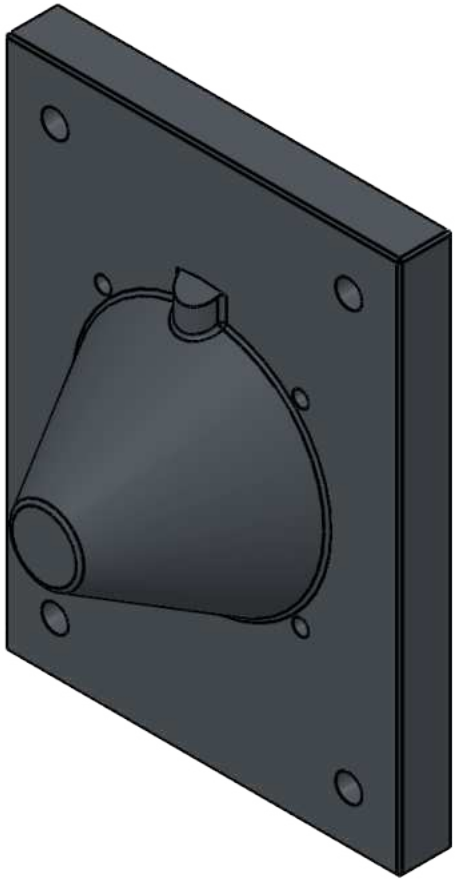

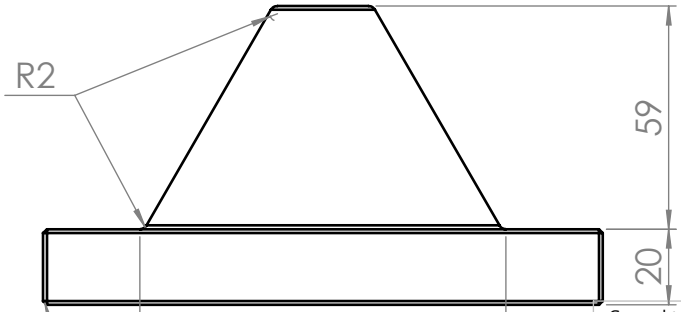

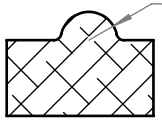

A-A

Use STEP-file for not mentioned dimensions

General tolerances according NEN ISO 2768-mK
Geometrical tolerancess according ISO 1101
Thermal cutting tolerances according ISO 9013-1
Welding tolerances according ISO 13920-BF
Remove sharp edges according NEN ISO 13175
General roughness according DIN ISO 1302
Ra 3,2

Projection

Drawn by	Jan Veenhuis	Date	01/02/2024
Weight	2.07 kg	Scale	1:2

Material	AW-5083
Treatment	Deburring
Part number	
REV.	
Drawing number	Cope
Description	Cope
A4	
DIMENSIONS IN MILLIMETERS	SHEET 1 OF 1

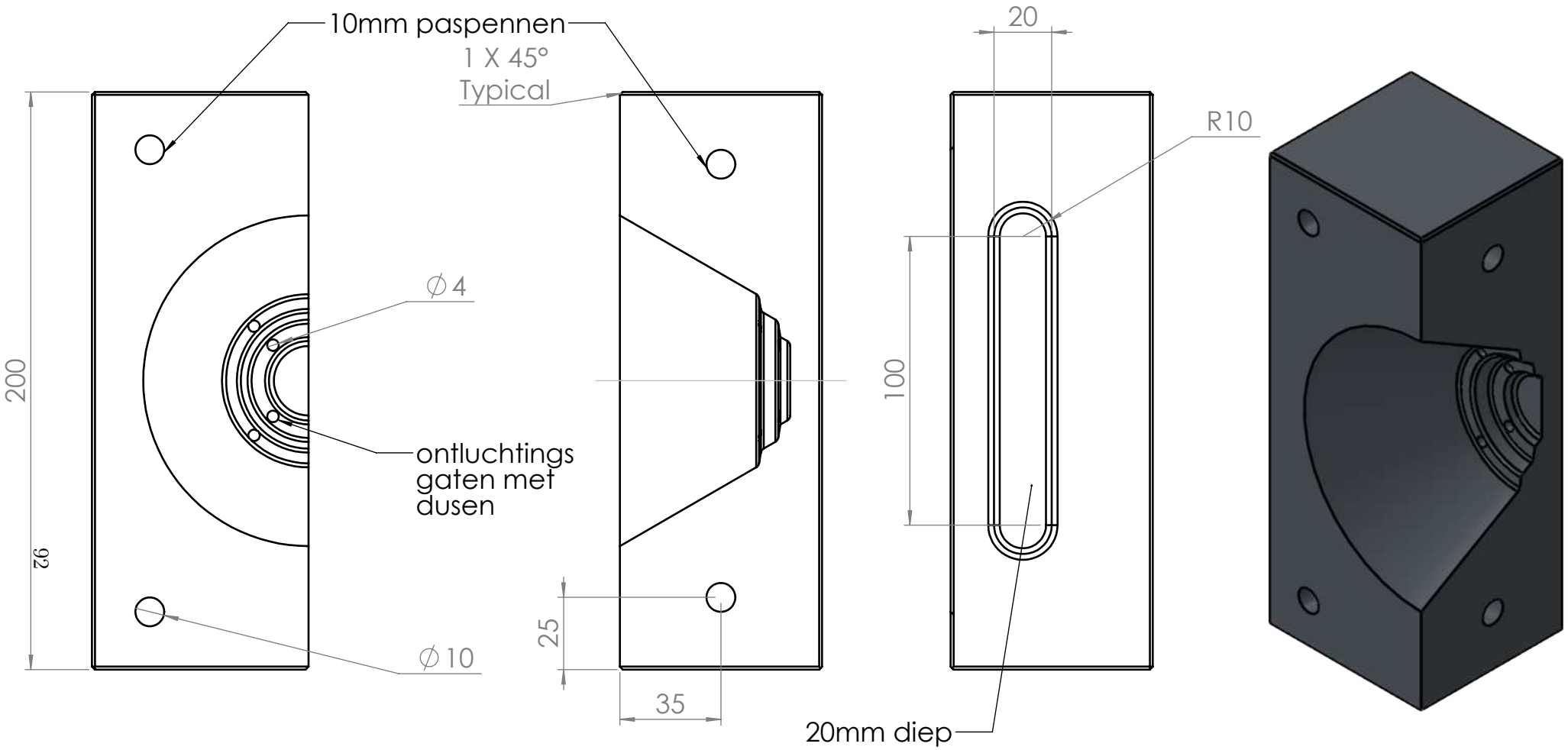

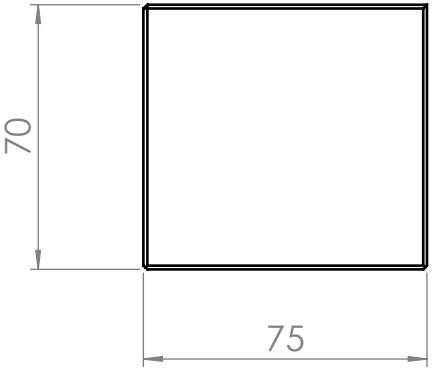

Use STEP-file for not mentioned dimensions

General tolerances according NEN ISO 2768-mK Geometrical tolerancess according ISO 1101 Thermal cutting tolerances according ISO 9013-1 Welding tolerances according ISO 13920-BF Remove sharp edges according NEN ISO 13175 General roughness according DIN ISO 1302 Ra 3,2	Projection	Drawn by	Jan Veenhuis	Date	01/02/2024
		Weight	2.26 kg	Scale	1:2
Material: AW-5083	Treatment: Deburring	Part number		REV.	
		Drawing number: Drag			
		Description: Drag		A4	
		DIMENSIONS IN MILLIMETERS		SHEET 1 OF 1	

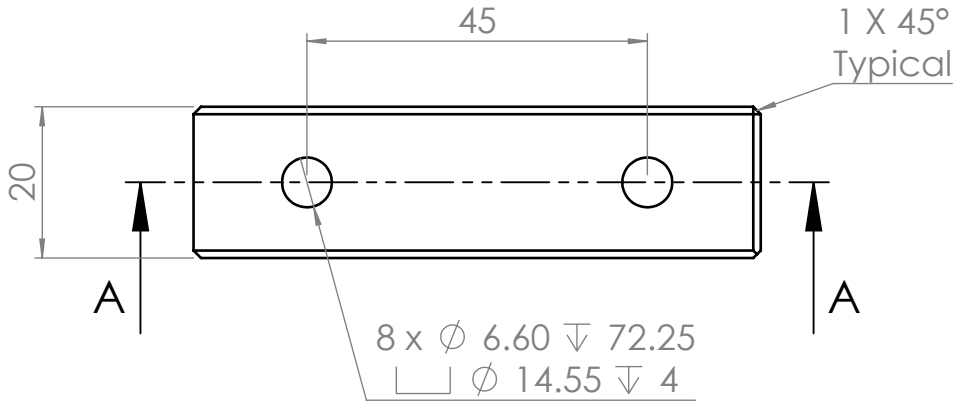

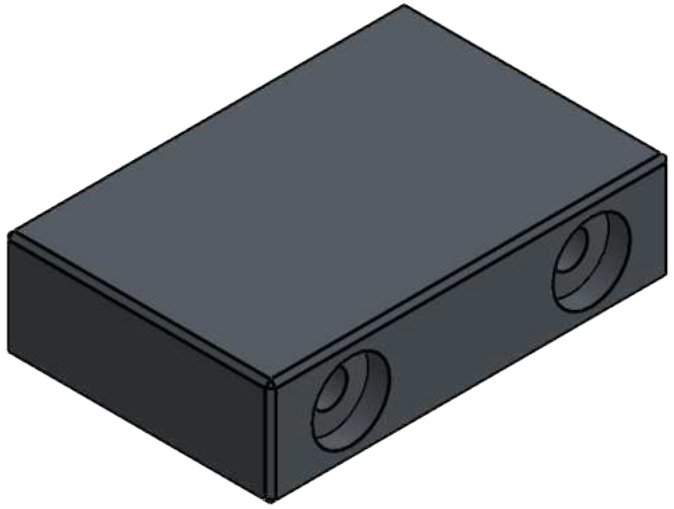

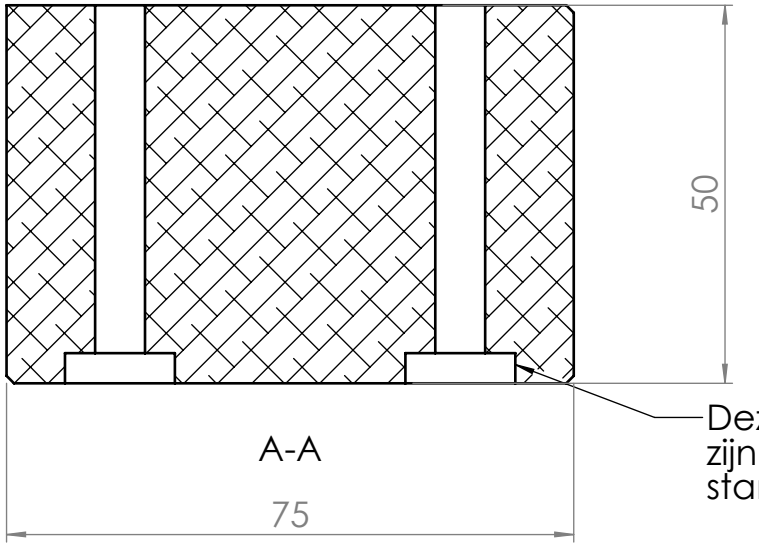

Deze mogen dieper zijn voor een standaard maat bout

Use STEP-file for not mentioned dimensions

General tolerances according NEN ISO 2768-mK Geometrical tolerancess according ISO 1101 Thermal cutting tolerances according ISO 9013-1 Welding tolerances according ISO 13920-BF Remove sharp edges according NEN ISO 13175 General roughness according DIN ISO 1302 Ra 3,2	Projection	Drawn by	Jan Veenhuis	Date	01/02/2024
		Weight	0.19 kg	Scale	1:1
Material: AW-5083	Treatment: Deburring	Part number		REV.	
		Drawing number: Foot			
		Description: Foot		A4	
		DIMENSIONS IN MILLIMETERS		SHEET 1 OF 1	

7.5 Safety equipment

The experiments are carried out with molten aluminum (at +700°C) in the foundry conditions therefore safety is utmost importance when performing these tests. When working in the foundry the protective clothing in Figure 7.4 including work shoes, safety goggles and a hard hat are mandatory.

(a) Protective underwear (b) Foundry jacket and pants

Figure 7.4: Protective foundry clothing

When the raw material is melted in the furnace and/or casting operation is conducted the clothing, in Figure 7.5, should be added to the personal protective equipment (PPE). Which include fire-resistant and reflective gloves, jacket, helmet with neck protection and face shield and foundry boots.

Figure 7.5: Additional melting and casting PPE

7.6 Images for grain size analysis of Barker samples under polarised light

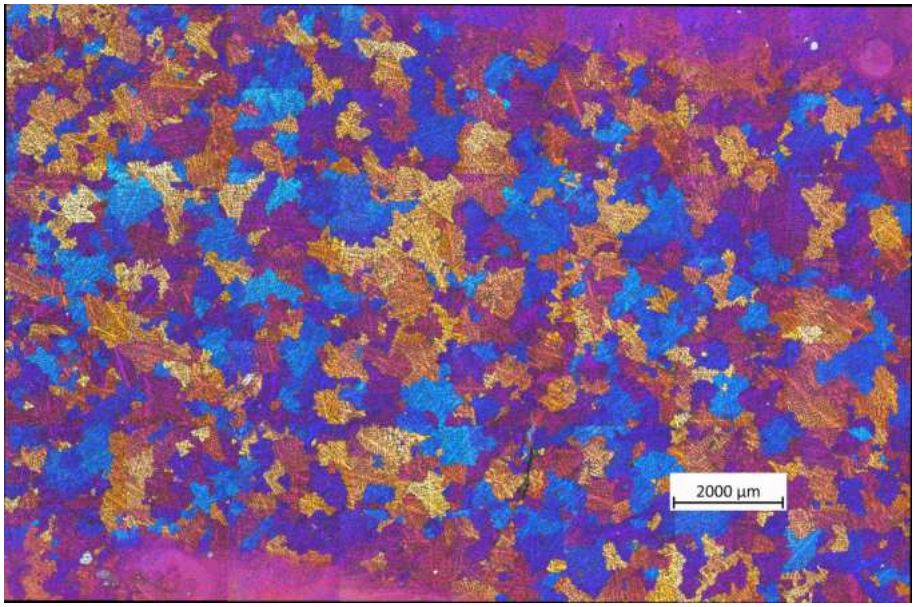

Figure 7.6: Barker sample grain size overview before Er addition

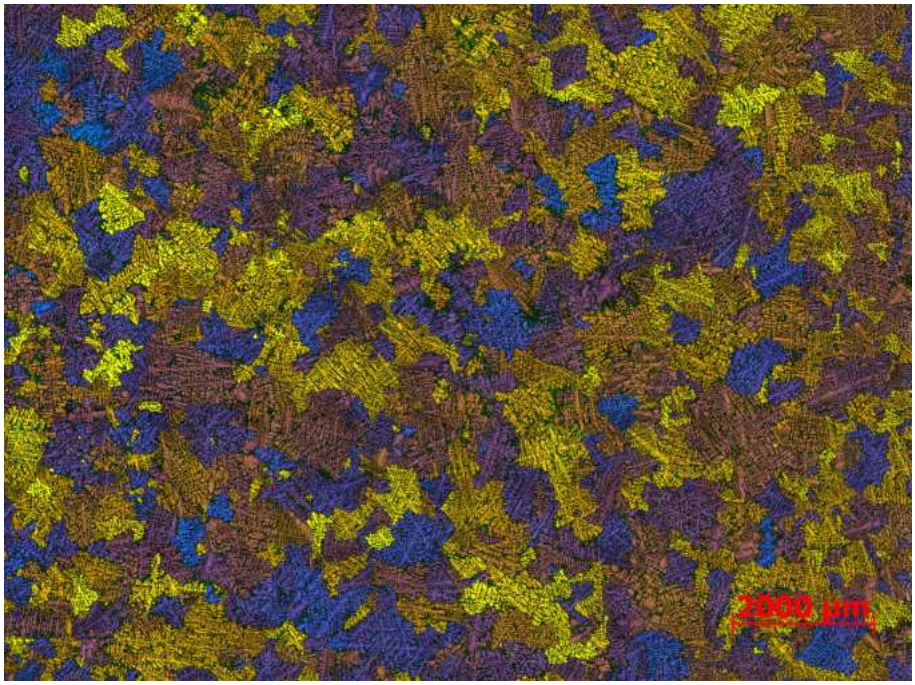

Figure 7.7: Barker sample grain size overview 0.0 base alloy before fluidity trials

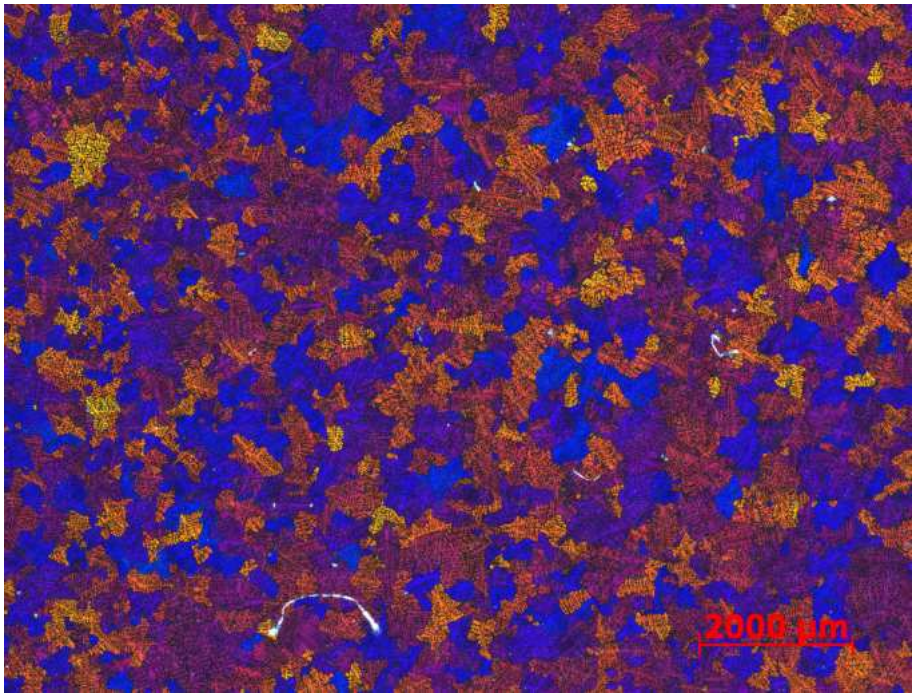

Figure 7.8: Barker sample grain size overview 0.0 base alloy after fluidity trials

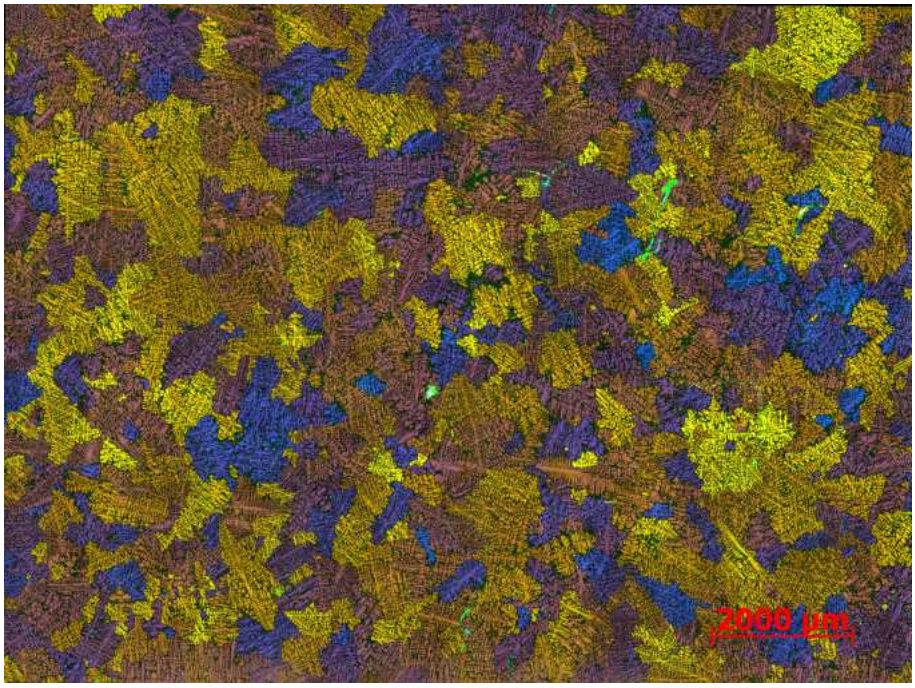

Figure 7.9: Barker sample grain size overview Er addition before fluidity trials

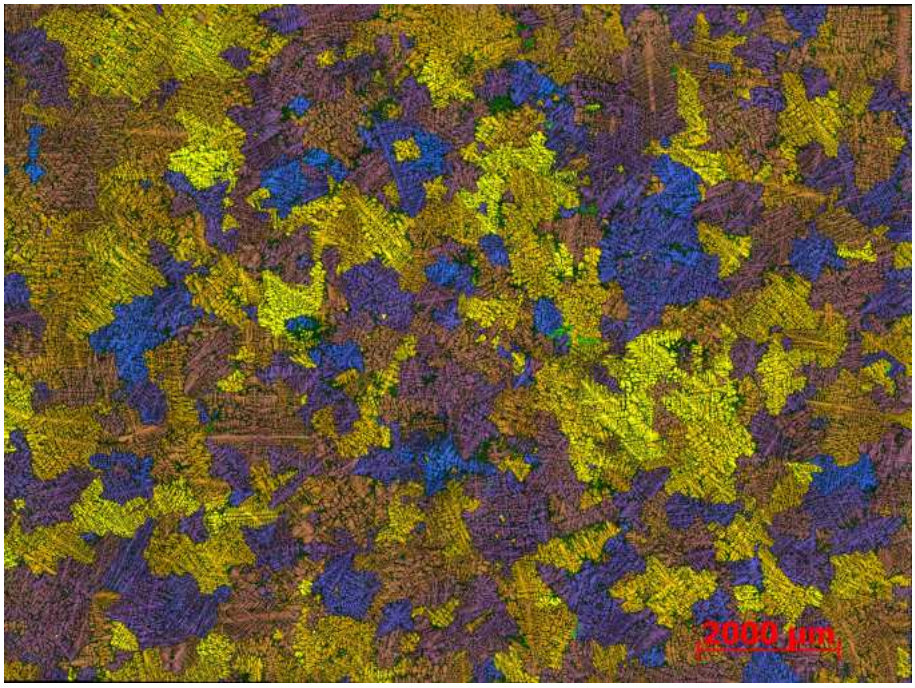

Figure 7.10: Barker sample grain size overview Er addition after fluidity trials

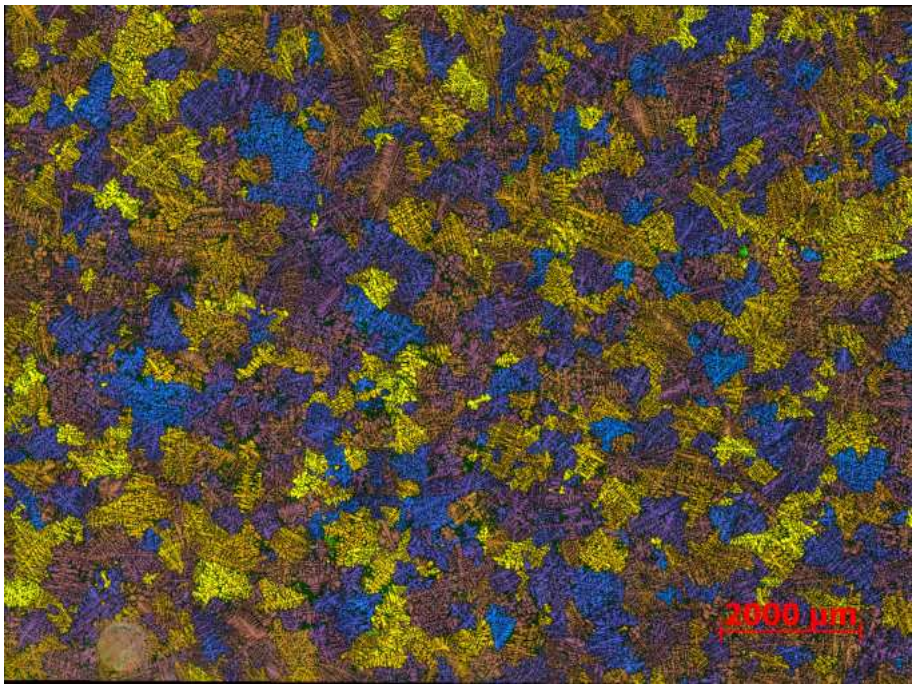

Figure 7.11: Barker sample grain size overview Eu addition before fluidity trials

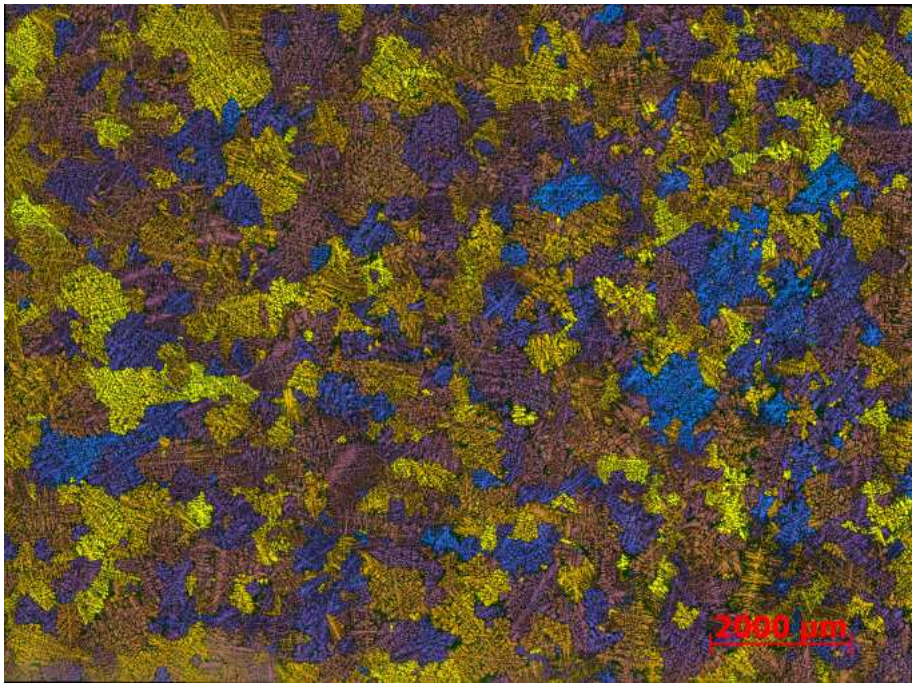

Figure 7.12: Barker sample grain size overview Eu addition after fluidity trials

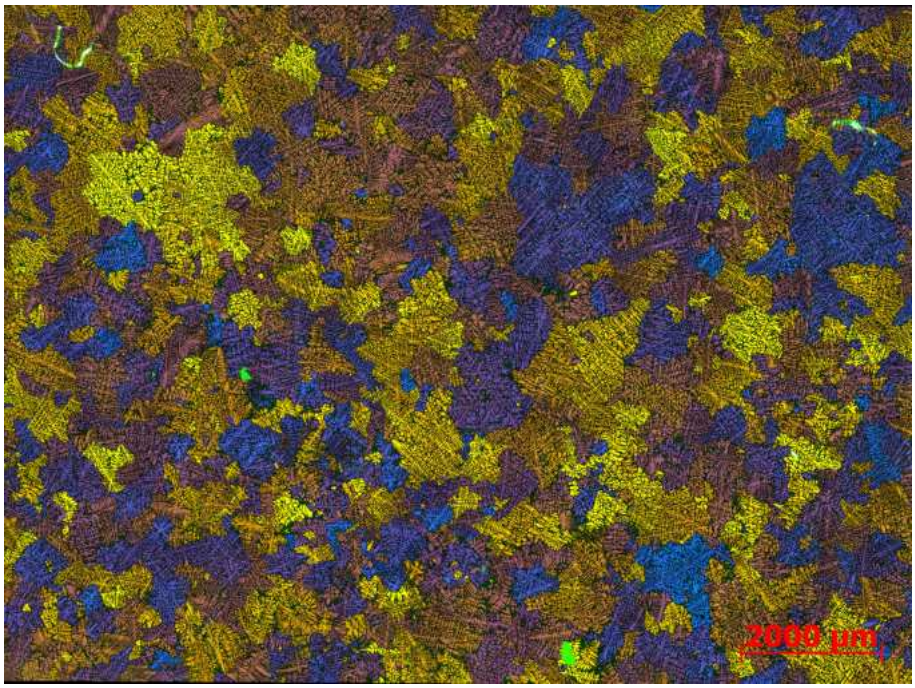

Figure 7.13: Barker sample grain size overview Er + Eu addition before fluidity trials

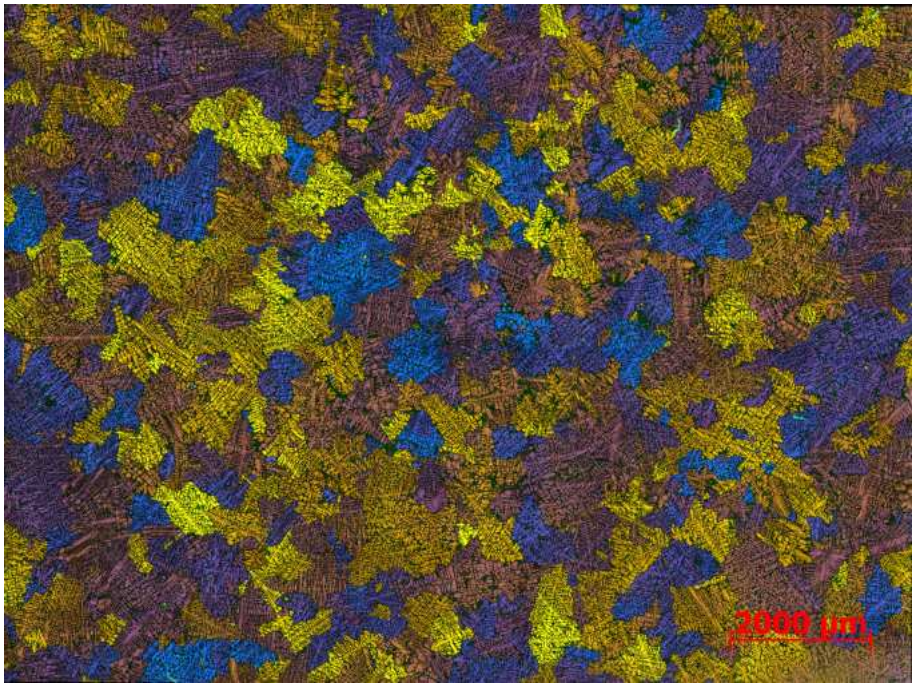

Figure 7.14: Barker sample grain size overview Er + Eu addition after fluidity trials

7.7 Overview images for optical analysis of Barker samples

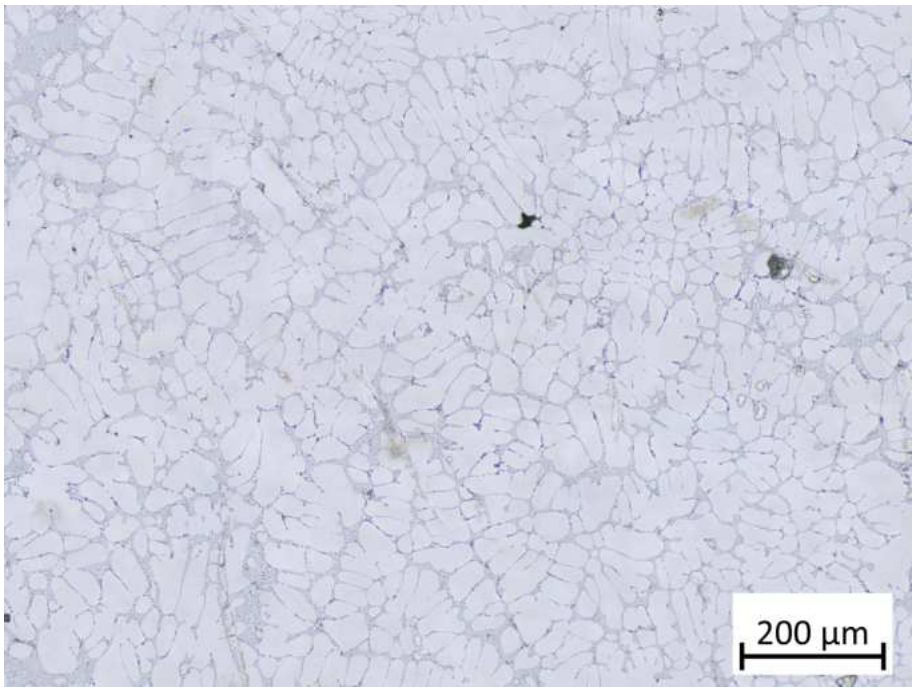

Figure 7.15: Barker sample optical overview 0.0 base alloy before fluidity trials

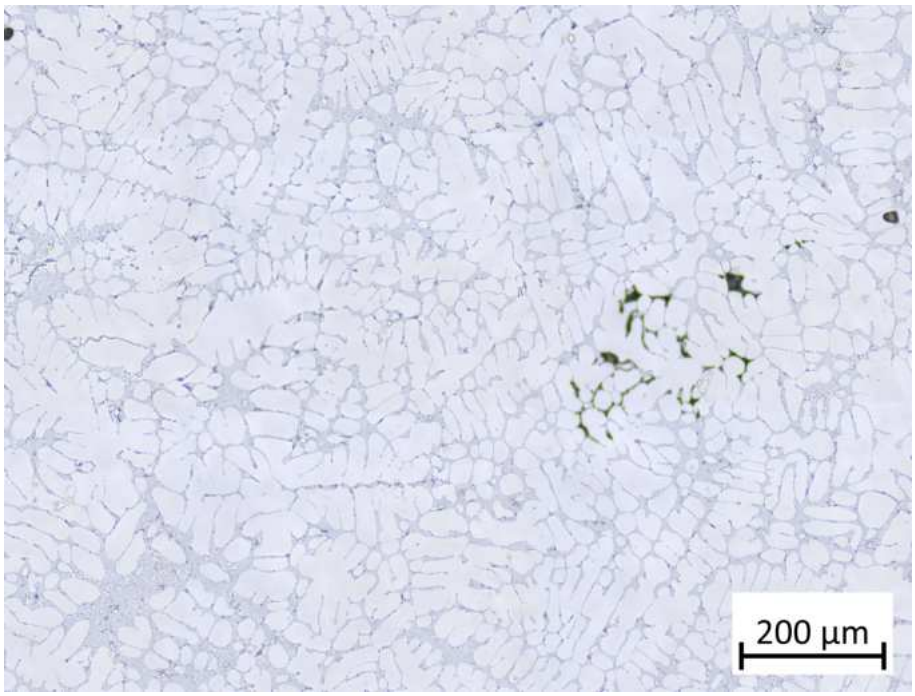

Figure 7.16: Barker sample optical overview 0.0 base alloy after fluidity trials

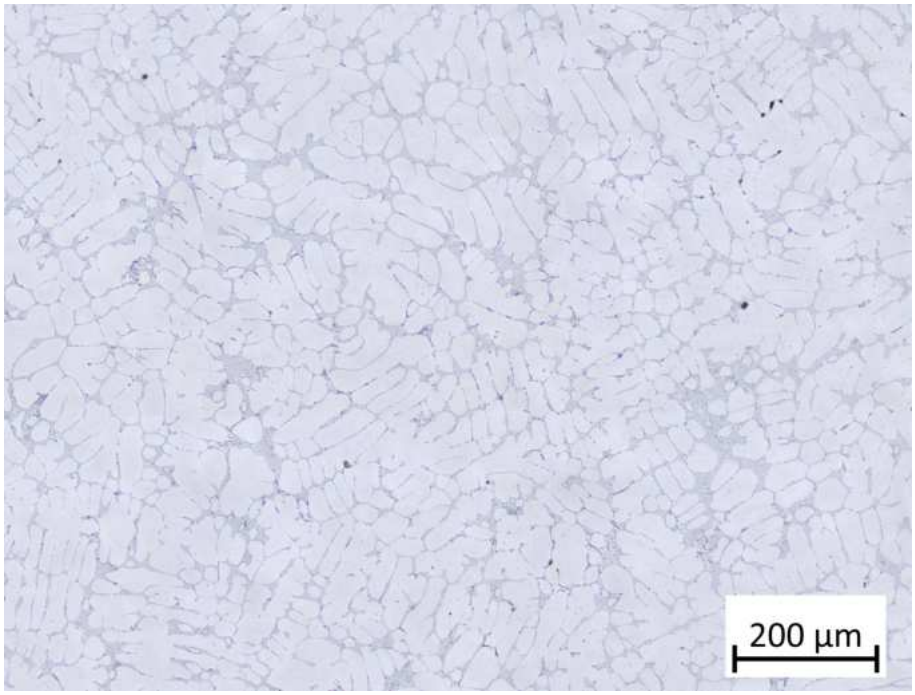

Figure 7.17: Barker sample optical overview Er addition before fluidity trials

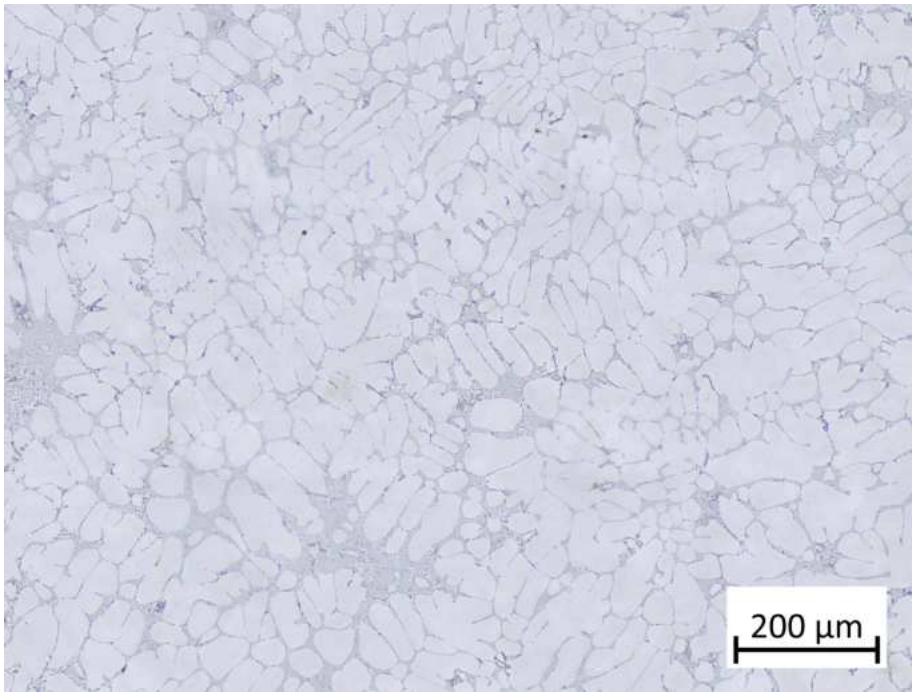

Figure 7.18: Barker sample optical overview Er addition after fluidity trials

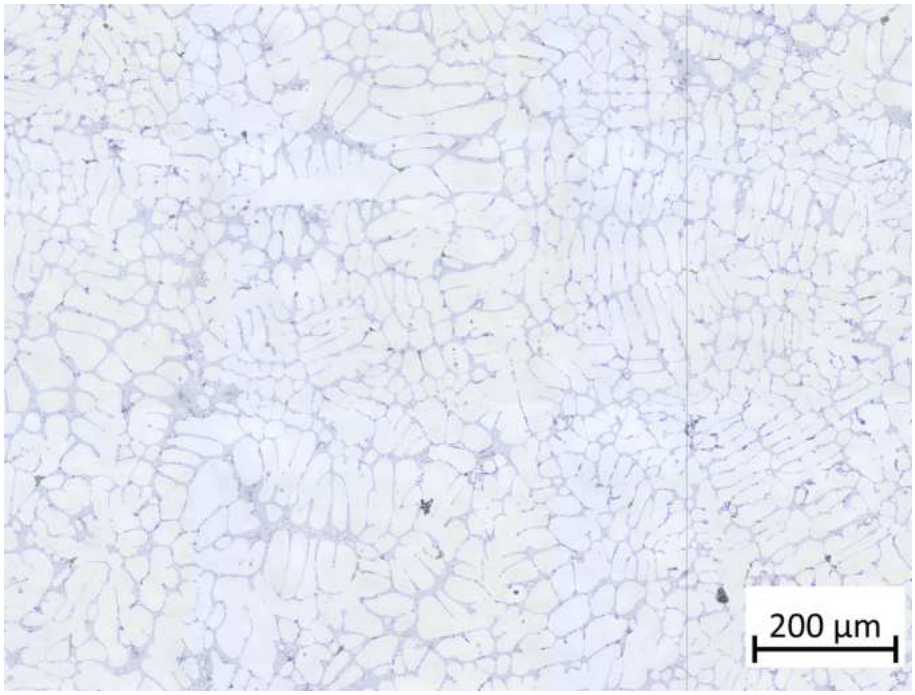

Figure 7.19: Barker sample optical overview Eu addition before fluidity trials

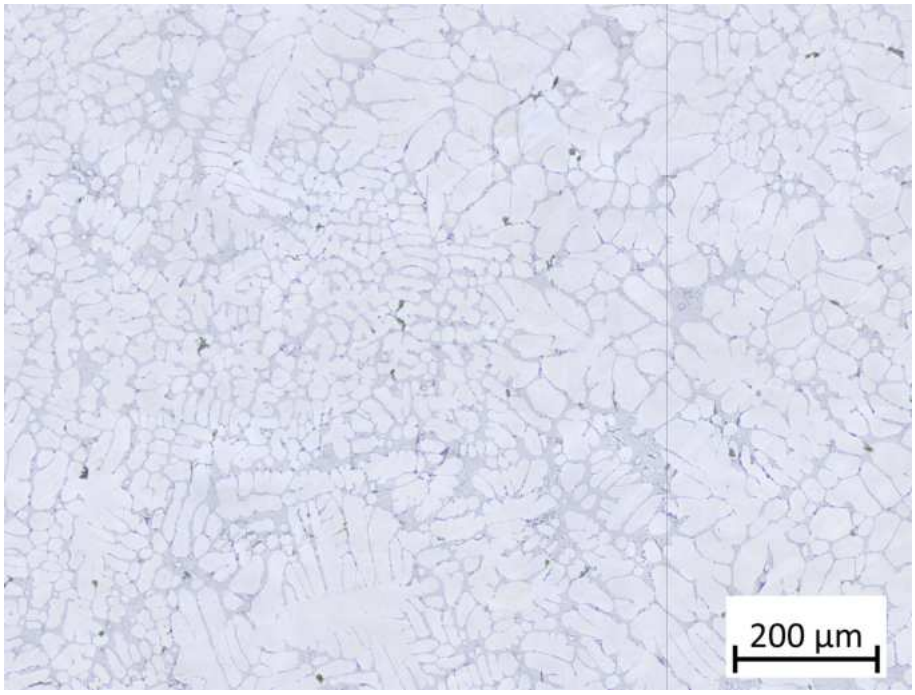

Figure 7.20: Barker sample optical overview Eu addition after fluidity trials

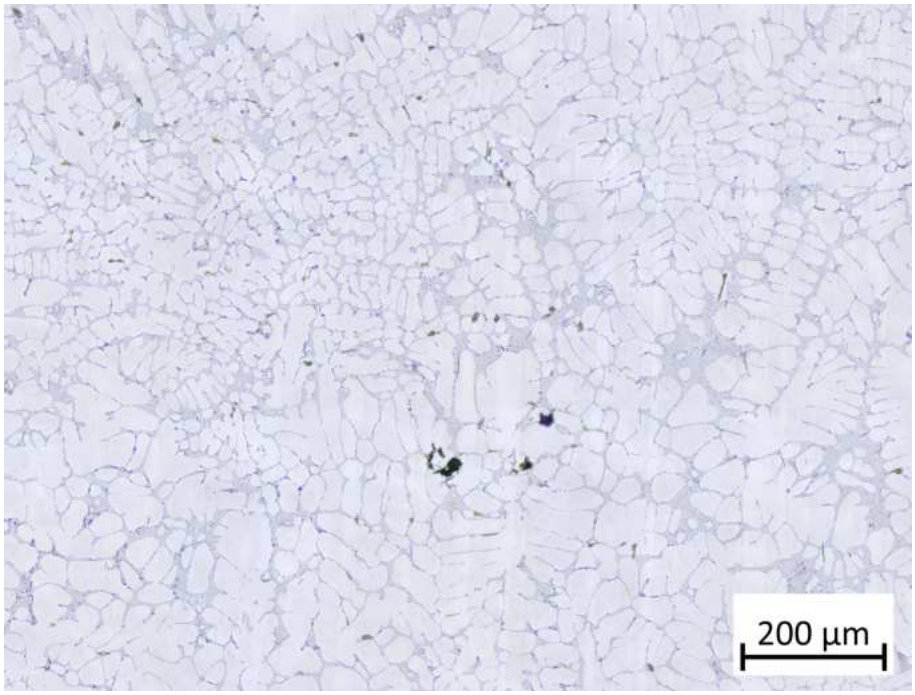

Figure 7.21: Barker sample optical overview Er + Eu addition before fluidity trials

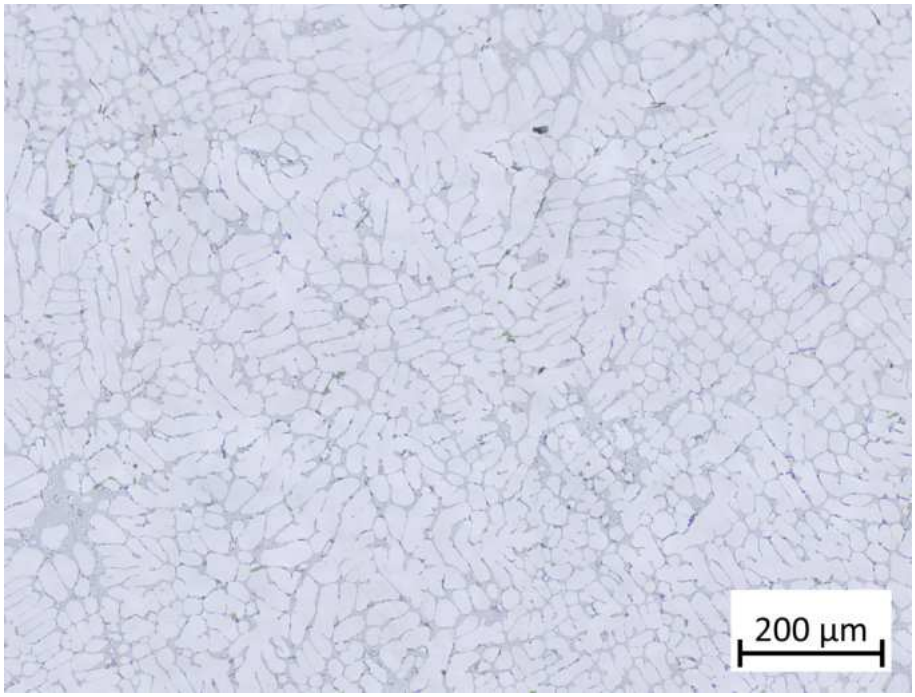

Figure 7.22: Barker sample optical overview Er + Eu addition after fluidity trials

7.8 Cross-sections of channels edged for grain size analysis

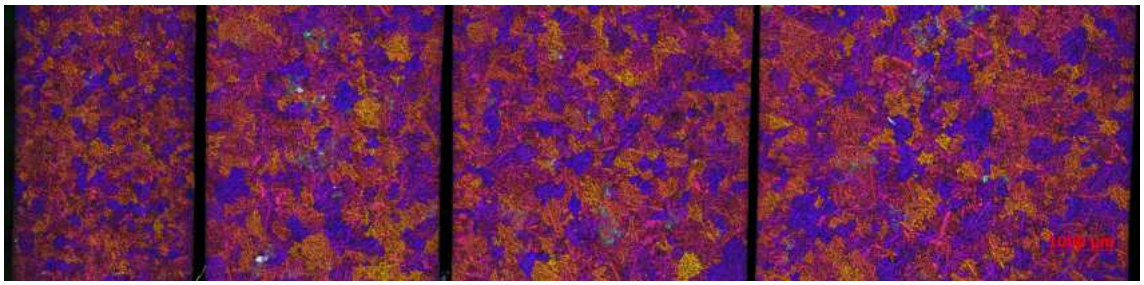

Figure 7.23: Cross-section of channels 0.0 base alloy long under polarised light

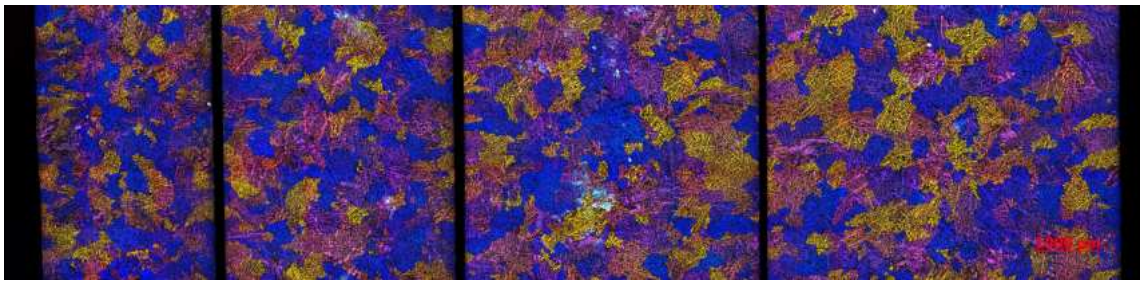

Figure 7.24: Cross-section of channels Er short composition under polarised light

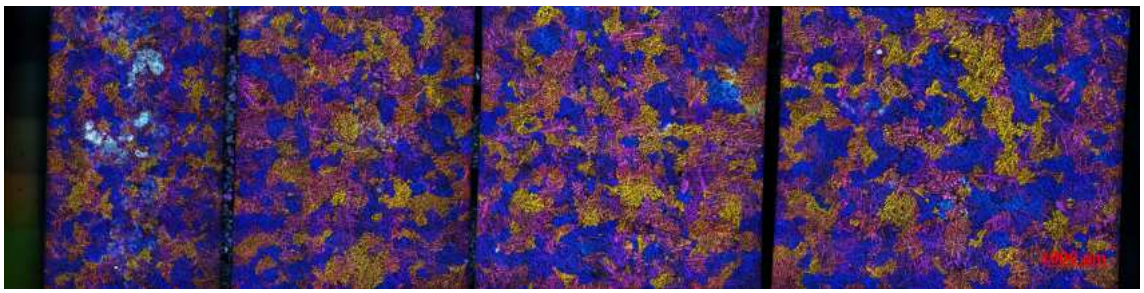

Figure 7.25: Cross-section of channels Eu short composition under polarised light

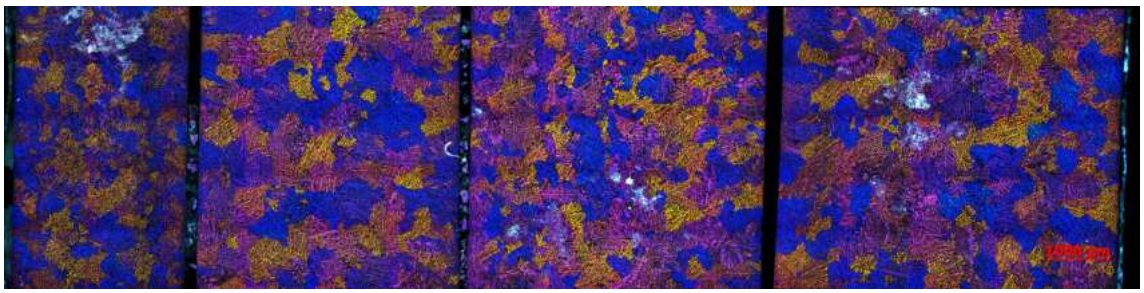

Figure 7.26: Cross-section of channels Er + Eu short composition under polarised light

7.9 Gage R&R filled in worksheets

Appraiser	Replicate Measurements	0.0 Base alloy									
		1	2	3	4	5	6	7	8	9	Averages
Derya	1	124	129	116	143	129	118	146	127	146	
	2	127	134	120	147	133	120	131	130	151	
	3										
	Average	126	131	118	145	131	119	139	128	149	131.81
	Range	3	5	3	4	4	2	15	3	6	
Hayati	1	126	133	119	147	133	120	148	131	149	
	2	127	133	120	147	134	121	148	131	149	
	3										
	Average	126	133	120	147	133	121	148	131	149	134.23
	Range	1	1	1	1	1	0	0	0	1	
Jan	1	126	132	117	148	132	121	149	130	151	
	2	125	131	117	145	132	119	147	129	148	
	3										
	Average	125	131	117	147	132	120	148	130	149	133.28
	Range	1	0	0	3	0	2	2	1	3	
Total	Part Averages	126	132	118	146	132	120	145	130	149	133.107
	Average Range										2.310
	Range Between Part Averages										30.653
	Range Amongst Operators (R_o)										2.421

	m	n	d2
d2 equipm	# replicates	# part x # operators	1.128
d2 Apprai	# operators	1 always	1.912
d2 part-pa	# parts	1 always	3.025
	# parts	9	
	# trials	2	
	#operators	3	

		% of Total Variation
Equipment Variation (EV):	2.0478	19.7%
Appraiser Variation (AV):	1.1708	11.3%
Gauge R&R (GRR):	2.3588	22.7%
Part Variation (PV):	10.1331	97.4%
Total Variation (TV):	10.4041	

Figure 7.27: Gage R&R worksheet of the 0.0 base alloy composition

Appraiser	Replicate Measurements	0.1 Er									
		1	2	3	4	5	6	7	8	9	Averages
Derya	1	108	125	164	120	146	156	147	146	141	
	2	109	126	164	124	147	159	148	152	138	
	3										
	Average	108	126	164	122	147	158	148	149	139	140.01
	Range	0	0	1	3	1	3	1	6	3	
Hayati	1	108	125	164	124	147	159	148	151	139	
	2	109	126	165	124	147	159	149	152	139	
	3										
	Average	108	126	165	124	147	159	149	151	139	140.94
	Range	1	1	0	0	0	1	1	1	0	
Jan	1	107	123	164	123	146	158	147	150	138	
	2	107	125	165	123	146	158	147	149	138	
	3										
	Average	107	124	164	123	146	158	147	150	138	139.62
	Range	0	1	1	0	1	0	0	1	0	
Total	Part Averages	108	125	164	123	147	158	148	150	139	140.189
	Average Range										1.054
	Range Between Part Averages										56.458
	Range Amongst Operators (R_O)										1.313

	m	n	d2
d2 equipm	# replicates	# part x # operators	1.128
d2 Apprais	# operators	1 always	1.912
d2 part-pa	# parts	1 always	3.025
	# parts	9	
	# trials	2	
	#operators	3	

		% of Total Variation
Equipment Variation (EV):	0.9347	5.0%
Appraiser Variation (AV):	0.6504	3.5%
Gauge R&R (GRR):	1.1387	6.1%
Part Variation (PV):	18.6639	99.8%
Total Variation (TV):	18.6986	

Figure 7.28: Gage R&R worksheet of the Er composition

Replicate Measurements	0.2 Eu									
	1	2	3	4	5	6	7	8	9	Averages
1	114	128	119	134	169	132	124	137	129	
2	116	131	121	138	171	134	126	137	130	
3										
Average	115	129	120	136	170	133	125	137	129	132.86
Range	2	3	2	4	2	2	2	0	1	
1	116	130	121	137	171	134	126	137	127	
2	116	130	121	138	171	135	126	138	131	
3										
Average	116	130	121	138	171	135	126	137	129	133.72
Range	0	0	0	1	0	1	1	0	4	
1	114	131	120	138	170	133	125	139	129	
2	115	129	121	138	170	132	125	135	127	
3										
Average	114	130	120	138	170	133	125	137	128	132.88
Range	1	1	1	1	0	0	0	4	2	
Part Averages	115	130	120	137	170	134	125	137	129	133.153
Average Range										1.315
Range Between Part Averages										55.331
Range Amongst Operators (R_o)										0.856

	m	n	d2
d2 equipment	# replicate	# part x # operators	1.128
d2 Appraiser	# operato	1 always	1.912
d2 part-part	# parts	1 always	3.025
	# parts	9	
	# trials	2	
	#operator	3	

		% of Total Variation
Equipment Variation (EV):	1.1662	6.4%
Appraiser Variation (AV):	0.3537	1.9%
Gauge R&R (GRR):	1.2186	6.6%
Part Variation (PV):	18.2911	99.8%
Total Variation (TV):	18.3316	

Figure 7.29: Gage R&R worksheet of the Eu composition

Appraiser	Replicate Measurements	0.1 Er + 0.2 Eu									
		1	2	3	4	5	6	7	8	9	Averages
Derya	1	134	119	148	123	143	151	155	142	137	
	2	144	122	150	128	145	153	154	146	141	
	3										
	Average	139	121	149	125	144	152	154	144	139	140.76
	Range	10	3	2	5	2	2	1	4	4	
Hayati	1	139	122	151	128	145	152	156	145	140	
	2	139	122	152	128	145	153	157	144	141	
	3										
	Average	139	122	151	128	145	152	157	145	141	142.21
	Range	1	0	1	0	1	1	1	1	0	
Jan	1	138	122	150	124	146	154	156	145	148	
	2	138	121	149	127	144	151	154	144	139	
	3										
	Average	138	122	149	126	145	153	155	144	144	141.68
	Range	0	1	0	4	2	4	2	1	9	
Total	Part Averages	139	122	150	126	144	152	155	144	141	141.552
	Average Range										2.239
	Range Between Part Averages										33.783
	Range Amongst Operators (R_o)										1.449

	m	n	d2
d2 equipm	# replicates	# part x # operators	1.128
d2 Apprais	# operators	1 always	1.912
d2 part-pa	# parts	1 always	3.025
	# parts	9	
	# trials	2	
	#operators	3	

		% of Total Variation
Equipment Variation (EV):	1.9848	17.5%
Appraiser Variation (AV):	0.5963	5.2%
Gauge R&R (GRR):	2.0725	18.2%
Part Variation (PV):	11.1680	98.3%
Total Variation (TV):	11.3587	

Figure 7.30: Gage R&R worksheet of the Er + Eu composition

Bibliography

[1] William B. Frank, Warren E. Haupin, Helmut Vogt, Marshall Bruno, Jomar Thonstad, Robert K. Dawless, Halvor Kvande, and Oyebode A. Taiwo. Aluminum. *Ullmann's Encyclopedia of Industrial Chemistry*, 7 2009.

[2] A. Heidarzadeh, M. Emamy, A. Rahimzadeh, R. Soufi, D. Sohrabi Baba Heidary, and Sh Nasibi. The effect of copper addition on the fluidity and viscosity of an Al-Mg-Si alloy. *Journal of Materials Engineering and Performance*, 23(2):469–476, 2 2014.

[3] WC Harrigan and S Ochiai. *Handbook of metallic composites.* Marcel Dekker, New York, 1994.

[4] D. Qiu, J. A. Taylor, M. X. Zhang, and P. M. Kelly. A mechanism for the poisoning effect of silicon on the grain refinement of Al–Si alloys. *Acta Materialia*, 55(4):1447–1456, 2 2007.

[5] Liming Lu, K. Nogita, and A. K. Dahle. Combining Sr and Na additions in hypoeutectic Al–Si foundry alloys. *Materials Science and Engineering: A*, 399(1-2):244–253, 6 2005.

[6] Rare earth prices in February 2020 | Institute for Rare Earths and Metals.

[7] Ali Mazahery, Mahdi Habibnejad-korayem, and Kifah Takrouri. Performance of europium in microstructural modification of high strength lightweight aluminum components. *International Journal of Lightweight Materials and Manufacture*, 2(3):250–254, 9 2019.

[8] Hayati Sahin and Derya Dispinar. Effect of Rare Earth Elements Erbium and Europium Addition on Microstructure and Mechanical Properties of A356 (Al–7Si–0.3Mg) Alloy. *International Journal of Metalcasting*, 17(4):2612–2621, 10 2023.

[9] Z. M. Shi, Q. Wang, G. Zhao, and R. Y. Zhang. Effects of erbium modification on the microstructure and mechanical properties of A356 aluminum alloys. *Materials Science and Engineering: A*, 626:102–107, 2 2015.

[10] Complete Casting Handbook: Metal Casting Processes, Metallurgy, Techniques ... - John Campbell - Google Books.

[11] M. Sabatino and L. Arnberg. A review on the fluidity of al based alloys. *Metallurgical Science and Tecnology*, 2013.

[12] Murat Çolak, Ramazan Kayikci, and Derya Dispinar. Influence of Different Cross Sections on Fluidity Characteristics of A356. *Transactions of the Indian Institute of Metals*, 68(2):275–281, 4 2015.

[13] D. Dispinar and J. Campbell. Critical assessment of reduced pressure test. Part 1: Porosity phenomena. *International Journal of Cast Metals Research*, 17(5):280–286, 2004.

[14] Young Dong Kwon and Zin Hyoung Lee. The effect of grain refining and oxide inclusion on the fluidity of Al–4.5Cu–0.6Mn and A356 alloys. *Materials Science and Engineering: A*, 360(1-2):372–376, 11 2003.

[15] J. D. Robson, O. Engler, C. Sigli, A. Deschamps, and W. J. Poole. Advances in Microstructural Understanding of Wrought Aluminum Alloys. *Metallurgical and Materials Transactions A: Physical Metallurgy and Materials Science*, 51(9):4377–4389, 9 2020.

[16] Matmatch. Cast vs. Wrought Aluminium - Matmatch.

[17] John Dwight. Aluminium Design and Construction - John Dwight - Google Books, 1998.

[18] J. Gilbert Kaufman and Elwin L. Rooy. Aluminum Casting Alloys. *Aluminum Alloy Castings*, pages 7–20, 12 2004.

[19] PK Tawele, LP Raut International Journal of Advanced Research, and undefined 2015. Warpage in casting: a Review. *researchgate.net*, 2(4):2394–2444, 2015.

[20] MRT castings. Low & High Pressure Diecasting | Choosing a Pressure Casting.

[21] Adrian P. Mouritz. *Introduction to Aerospace Materials*. Elsevier Inc., 5 2012.

[22] Open University. Gravity die casting | OpenLearn - Open University, 11 2017.

[23] M. T. Murray and M. Murray. High pressure die casting of aluminium and its alloys. *Fundamentals of Aluminium Metallurgy: Production, Processing and Applications*, pages 217–261, 2010.

[24] Helder Nunes, Omid Emadinia, Manuel F. Vieira, Ana Reis, Helder Nunes, Omid Emadinia, Manuel F. Vieira, and Ana Reis. Low- and High-Pressure Casting Aluminum Alloys: A Review. *Recent Advancements in Aluminum Alloys*, 2 2023.

[25] Kurtz Ersa Magazine. Low-pressure vs. high-pressure die casting, 7 2016.

[26] F. Bonollo, J. Urban, B. Bonatto, and M. Botter. Gravity and low pressure die casting of aluminium alloys: a technical and economical benchmark. *La Metallurgia Italiana*, 6 2005.

[27] Casting: An Analytical Approach - Alexandre Reikher, Michael R. Barkhudarov - Google Books.

[28] Marisa Di Sabatino and Lars Arnberg. Castability of aluminium alloys. *Transactions of the Indian Institute of Metals*, 62(4-5):321–325, 2009.

[29] John Campbell. Complete Casting Handbook : Metal Casting Processes, Techniques and Design. page 1242, 2011.

[30] Christoph Beckermann. Macrosegregation. *Casting*, pages 348–352, 12 2008.

[31] Melek Durmuş, Derya Dispinar, Mehmet Gavgali, Emin Uslu, and Murat Çolak. Evaluation of Fe Content on the Fluidity of A356 Aluminum Alloy by New Fluidity Index. *International Journal of Metalcasting*, pages 1–15, 7 2024.

[32] K. R. Ravi, R. M. Pillai, K. R. Amaranathan, B. C. Pai, and M. Chakraborty. Fluidity of aluminum alloys and composites: A review. *Journal of Alloys and Compounds*, 456(1-2):201–210, 5 2008.

[33] Richard Pastirčák and Denis Martinec. Simulation Fluidity Test for Semisolid Squeeze Casting. *MATEC Web of Conferences*, 328:02006, 2020.

[34] M C Flemings, E Niyama, and H F Taylor. Fluidity of Aluminum Alloys: An experimental and quantitative evaluation. *AFS Trans*, 69:625, 1961.

[35] Chvorinov: Theorie der Erstarrung von Gussstücken - Google Scholar.

[36] EN Pan and KY Liao. Study on flowability of EPC A356 Al alloy. *AFS Trans.*, 106:233–242, 1998.

[37] D. J. Lloyd. Particle reinforced aluminium and magnesium matrix composites. *https://doi.org/10.1179/imr.1994.39.1.1*, 39(1):1–23, 1 1994.

[38] Stefano. Odorizzi and Franco. Bonollo. Numerical Simulation of Foundry Processes. pages 1–264, 2023.

[39] V. E. Bazhenov, A. V. Petrova, and A. V. Koltygin. Simulation of Fluidity and Misrun Prediction for the Casting of 356.0 Aluminum Alloy into Sand Molds. *International Journal of Metalcasting*, 12(3):514–522, 7 2018.

[40] Marisa Di Sabatino. Fluidity of Aluminium Foundry Alloys. 2005.

[41] A K Dahel, L Baeckrund, and L Arnberg. Castability of Aluminum foundry alloys. *Final report for AFS*, 1997.

[42] J. Campbell. Review of fluidity concepts in casting. *Cast Metals*, 7(4):227–237, 1 1995.

[43] A K Dahle, S Karlsen, and L Arnberg. Effect of grain refinement on the fluidity of some binary Al—Cu and Al—Mg alloys. *International Journal of Cast Metals Research*, 9(2):103–112, 1996.

[44] G Lang. Casting properties and Surface Tension of Aluminum and Binary Aluminum Alloys. Pt. 1. Fluidity. *Aluminium*, 48(10):664–672, 1972.

[45] D K Dwivedi, Ashok Sharma, and T V Rajan. Methods to improve the structure and properties of cast Al-Si base alloys. *Institution of Engineers, India*, 83:46, 2002.

[46] K. Sunitha and K. Gurusami. Study of Al-Si alloys grain refinement by inoculation. *Materials Today: Proceedings*, 43:1825–1829, 1 2021.

[47] Joanna Bojarska, Patrycja Złoty, and Wojciech M. Wolf. Life cycle assessment as tool for realization of sustainable development goals-towards sustainable future of the world: Mini review. *Acta Innovations*, 38:49–61, 3 2021.

[48] C. Limmaneevichitr and W. Eidhed. Fading mechanism of grain refinement of aluminum–silicon alloy with Al–Ti–B grain refiners. *Materials Science and Engineering: A*, 349(1-2):197–206, 5 2003.

[49] Wattanachai Prukkanon, Nakorn Srisukhumbowornchai, and Chaowalit Limmaneevichitr. Influence of Sc modification on the fluidity of an A356 aluminum alloy. *Journal of Alloys and Compounds*, 487(1-2):453–457, 11 2009.

[50] V. E. Bazhenov, I. I. Baranov, A. Yu Titov, A. V. Sannikov, D. Yu Ozherelkov, A. A. Lyskovich, A. V. Koltygin, and V. D. Belov. Effect of Ti, Sr, and B Addition on the Fluidity of A356.2 Grade Aluminum Alloy. *Russian Journal of Non-Ferrous Metals*, 63(5):526–536, 10 2022.

[51] A L Greer. Grain Refinement, Manufacturing High Integrity Aluminium and Magnesium Castings. *International Summer School, Worcester Polytechnic Institute*, 2003.

[52] Sathyapal Hegde and K. Narayan Prabhu. Modification of eutectic silicon in Al-Si alloys. *Journal of Materials Science*, 43(9):3009–3027, 5 2008.

[53] A. K. Dahle, K. Nogita, S. D. McDonald, C. Dinnis, and L. Lu. Eutectic modification and microstructure development in Al–Si Alloys. *Materials Science and Engineering: A*, 413-414:243–248, 12 2005.

[54] Feng Mao, Yongfeng Qiao, Po Zhang, Liming Ou, Chong Chen, Cheng Zhang, and Yu Wang. Modification Mechanism of Rare Earth Eu on Eutectic Si in Hypoeutectic Al-Si Alloy. *International Journal of Metalcasting*, 16(2):634–645, 4 2022.

[55] John Campbell. The Modification Of Al-Si Casting Alloys: Important Practical And Theoretical Aspects. *International journal of metalcasting*, 3:65–67, 4 2009.

[56] Kazuhiro Nogita, Stuart D. McDonald, and Arne K. Dahle. Eutectic Modification of Al-Si Alloys with Rare Earth Metals. *MATERIALS TRANSACTIONS*, 45(2):323–326, 2004.

[57] Francois R. Mollard, Merton C. Flemings, and Eisuke F. Niyama. Aluminum Fluidity in Casting. *JOM 1987 39:11*, 39(11):34–34, 10 2012.

[58] Desmond E.P. Klenam, Joseph E. Oghenevweta, and Winston O. Soboyejo. Fracture and Toughening of Intermetallics. *Comprehensive Structural Integrity*, pages 102–139, 1 2023.

[59] E. Taghaddos, M. M. Hejazi, R. Taghiabadi, and S. G. Shabestari. Effect of iron-intermetallics on the fluidity of 413 aluminum alloy. *Journal of Alloys and Compounds*, 468(1-2):539–545, 1 2009.

[60] Reza Vatankhah Barenji. Casting fluidity, viscosity, microstructure and tensile properties of aluminum matrix composites with different Mg2Si contents. *Rare Metals*, 41(8):2767–2776, 8 2022.

[61] Stanislav Naboychenko Oleg D Neikov, N. A. Yefimov. Handbook of Non-Ferrous Metal Powders: Technologies and Applications - Oleg D Neikov, N. A. Yefimov, Stanislav Naboychenko - Google Books, 2009.

[62] Brian A Dewhirst. *Castability Control in Metal Casting via Fluidity Measures: Application of Error Analysis to Variations in Fluidity Testing*. PhD thesis, Worcester Polytechnic Institute, 2008.

[63] A. T. Dinsdale and P. N. Quested. The viscosity of aluminium and its alloys - A review of data and models. *Journal of Materials Science*, 39(24):7221–7228, 12 2004.

[64] P. D. Ingle and B. E. Narkhede. A Literature Survey Of Methods To Study And Analyze The Gating System Design For Its Effect On Casting Quality. *Materials Today: Proceedings*, 5(2):5421–5429, 1 2018.

[65] 10 Concepts for a Successful Die Casting Design.

[66] M. C. Flemings. Solidification processing. *Metallurgical Transactions*, 5(10):2121–2134, 10 1974.

[67] Samuel L. Manzello, Jiann C. Yang, and Thomas G. Cleary. On the interaction of a liquid droplet with a pool of hot cooking oil. *Fire Safety Journal*, 38(7):651–659, 11 2003.

[68] Joel T. Clemmer, Flint Pierce, Thomas C. O'Connor, Thomas D. Nevins, Elizabeth M.C. Jones, Jeremy B. Lechman, and John Tencer. A hybrid smoothed-particle hydrodynamics model of oxide skins on molten aluminum. *Applied Mathematical Modelling*, 130:310–326, 6 2024.

[69] W. Kahl and E. Fromm. Examination of the Strength of Oxide Skins on Aluminum Alloy Melts. *Metallurgical Transactions B*, 16(1):47–51, 12 1985.

[70] Axel Kolsgaard. *Casting characteristics of SiC particulate reinforced AlSi7Mg aluminium matrix composites*. NTH, 1993.

[71] R Gopalan, NK Prabhu Materials Science Technology, , and undefined 2011. Oxide bifilms in aluminium alloy castings–a review. *Taylor & FrancisR Gopalan, NK PrabhuMaterials Science and Technology, 2011•Taylor & Francis*, 27(12):1757–1769, 2011.

[72] M DROUZY, JACOB S, and RICHARD M. INTERPRETATION OF TENSILE RESULTS BY MEANS OF QUALITY INDEX AND PROBABLE YIELD STRENGTH:APLICATION TO AL-SI7 MG FOUNDRY ALLOYS. *INTERPRETATION OF TENSILE RESULTS BY MEANS OF QUALITY INDEX AND PROBABLE YIELD STRENGTH:APLICATION TO AL-SI7 MG FOUNDRY ALLOYS*, 1980.

[73] Eray Erzi, Özen Gürsoy, Çağlar Yüksel, Murat Colak, and Derya Dispinar. Determination of Acceptable Quality Limit for Casting of A356 Aluminium Alloy: Supplier's Quality Index (SQI). *Metals 2019, Vol. 9, Page 957*, 9(9):957, 8 2019.

[74] Muhammet Uludağ, Remzi Çetin, Derya Dişpinar, and Murat Tiryakioğlu. On the Interpretation of Melt Quality Assessment of A356 Aluminum Alloy by the Reduced Pressure Test: The Bifilm Index and Its Physical Meaning. *International Journal of Metalcasting*, 12(4):853–860, 10 2018.

[75] Giulio Timelli and Daniele Caliari. Effect of Superheat and Oxide Inclusions on the Fluidity of A356 Alloy. *Materials Science Forum*, 884:71–80, 2017.

[76] Gábor Gyarmati, György Fegyverneki, Monika Tokár, and Tamás Mende. The Effects of Rotary Degassing Treatments on the Melt Quality of an Al–Si Casting Alloy. *International Journal of Metalcasting*, 15(1):141–151, 1 2021.

[77] Gabrielle Gaustad, Elsa Olivetti, and Randolph Kirchain. Improving aluminum recycling: A survey of sorting and impurity removal technologies. *Resources, Conservation and Recycling*, 58:79–87, 1 2012.

[78] Srinivasa Rao Pulivarti and Anil Kumar Birru. Fluidity of A206 Cast Alloy with and Without Scrap Addition Using Thin Cross-Sectional Fluidity Test: A Comparison. *Lecture Notes on Multidisciplinary Industrial Engineering*, Part F163:517–525, 2019.

[79] Xin Wu and Qiang Han. Thermal conductivity of monolayer hexagonal boron nitride: From defective to amorphous. *Computational Materials Science*, 184:109938, 11 2020.

[80] L Cepova, A Kovacikova, R Cep, P Klaput Measurement Science ..., and undefined 2018. Measurement system analyses–Gauge repeatability and reproducibility methods. *sciendo.comL Cepova, A Kovacikova, R Cep, P Klaput, O MizeraMeasurement Science Review, 2018•sciendo.com*, 18(1):20–27, 2 2018.

[81] C Peeratatsuwan, P Pandee, U Patakham Journal of Rare ..., and undefined 2022. Microstructure and rheological properties of a semisolid A356 alloy with erbium addition. *Elsevier*.

[82] J F Nie, A J Morton, B C Muddle, Z R Nie, J B Fu, J X Zou, T N Jin, J J Yang, G F Xu, H Q Ruan, and T Y Zuo. Advanced aluminum alloys containing rare-earth erbium. *icaa-conference.netZR Nie, JB Fu, JX Zou, TN Jin, JJ Yang, GF Xu, HQ Ruan, TY ZuoMaterials forum, 2004•icaa-conference.net*, page 197, 2004.

[83] R. Ahmad, N. A. Wahab, S. Hasan, Z. Harun, M. M. Rahman, and N. R. Shahizan. Effect of Erbium Addition on the Microstructure and Mechanical Properties of Aluminium Alloy. *Key Engineering Materials*, 796:62–66, 2019.

[84] Jiehua Li, Fredrik Hage, Manfred Wiessner, Lorenz Romaner, Daniel Scheiber, Bernhard Sartory, Quentin Ramasse, and Peter Schumacher. The roles of Eu during the growth of eutectic Si in Al-Si alloys. *Scientific Reports 2015 5:1*, 5(1):1–10, 9 2015.

[85] Ren Guo Guan and Di Tie. A Review on Grain Refinement of Aluminum Alloys: Progresses, Challenges and Prospects. *Acta Metallurgica Sinica (English Letters) 2017 30:5*, 30(5):409–432, 3 2017.

[86] John Campbell. An overview of the effects of bifilms on the structure and properties of cast alloys. *Metallurgical and Materials Transactions B: Process Metallurgy and Materials Processing Science*, 37(6):857–863, 12 2006.

[87] M. A. Easton and D. H. StJohn. Improved prediction of the grain size of aluminum alloys that includes the effect of cooling rate. *Materials Science and Engineering: A*, 486(1-2):8–13, 7 2008.

[88] T Tunçay Acta Physica Polonica A and undefined 2017. The effect of modification and grain refining on the microstructure and mechanical properties of A356 alloy. *bibliotekanauki.plT TunçayActa Physica Polonica A, 2017•bibliotekanauki.pl*, 2017.

[89] DE Groteke, QC Designs, et al. Influence of SNIF treatment on characteristics of aluminum foundry alloys, 1985.

[90] J. H. Li, T. H. Ludwig, B. Oberdorfer, and P. Schumacher. Solidification behaviour of Al–Si based alloys with controlled additions of Eu and P. *International Journal of Cast Metals Research*, 31(6):319–331, 11 2018.

[91] R. Raiszadeh and W. D. Griffiths. A semi-empirical mathematical model to estimate the duration of the atmosphere within a double oxide film defect in pure aluminum alloy. *Metallurgical and Materials Transactions B: Process Metallurgy and Materials Processing Science*, 39(2):298–303, 4 2008.

[92] J. Campbell. Entrainment defects. *Materials Science and Technology*, 22(2):127–145, 2 2006.

[93] Gábor Gyarmati, Levente Bogoly, Marcin Stawarz, György Fegyverneki, Zoltán Kéri, Monika Tokár, and Tamás Mende. Grain Refiner Settling and Its Effect on the Melt Quality of Aluminum Casting Alloys. *Materials 2022, Vol. 15, Page 7679*, 15(21):7679, 11 2022.

[94] Gábor Gyarmati, György Fegyverneki, Tamás Mende, and Mónika Tokár. The Effect of Fluxes on the Melt Quality of AlSi7MgCu Alloy. *International Journal of Engineering and Management Sciences*, 4(1):372–380, 3 2019.

[95] D. Dispinar, S. Akhtar, A. Nordmark, M. Di Sabatino, and L. Arnberg. Degassing, hydrogen and porosity phenomena in A356. *Materials Science and Engineering: A*, 527(16-17):3719–3725, 6 2010.

[96] Jia hua LIN, Hai dong ZHAO, and Jia min HUANG. Spatial interfacial heat transfer and surface characteristics during gravity casting of A356 alloy. *Transactions of Nonferrous Metals Society of China (English Edition)*, 29(1):43–50, 1 2019.